THE ROLE OF MUCOLIPIN-1 IN PATHOGENESIS OF THE LYSOSOMAL STORAGE DISEASE MUCOLIPIDOSIS TYPE IV

by

Mark Thomas Miedel

B.S. in Cell and Developmental Biology, Pennsylvania State University, 2002

Submitted to the Graduate Faculty of

The School of Medicine in partial fulfillment

of the requirements for the degree of

Doctor of Philosophy

University of Pittsburgh

2008

UNIVERSITY OF PITTSBURGH

SCHOOL OF MEDICINE

This dissertation was presented

by

Mark Thomas Miedel

It was defended on

August 27, 2008

and approved by

Kirill Kiselyov Ph.D., Department of Biological Sciences

Tom Kleyman, MD, Department of Medicine, Renal-Electrolyte Division

Linton Traub, Ph.D., Cell Biology and Physiology

Committee Chair: Dan Devor, Ph.D., Cell Biology and Physiology

Dissertation Advisor: Ora Weisz, Ph.D., Department of Medicine, Renal-Electrolyte Division

THE ROLE OF MUCOLIPIN-1 IN PATHOGENESIS OF THE LYSOSOMAL STORAGE DISEASE MUCOLIPIDOSIS TYPE IV

Mark Thomas Miedel, Ph.D.

University of Pittsburgh, 2008

Lysosomal storage diseases (LSDs) are a group of inherited disorders that are caused by the defective activity of lysosomal proteins, resulting in the intracellular accumulation of undigested lysosomal metabolites. Mucolipidosis type IV (MLIV) is a neurodegenerative, recessive disease that results in the accumulation of undigested material in most tissue types. MLIV is caused by mutations in the *MCOLN1* gene, encoding the transient receptor potential (TRP) cation channel family member mucolipin-1 (TRP-ML1). While previous work has provided insight into the role of this protein in progression of MLIV, a detailed knowledge of TRP-ML1 function and subsequent role in MLIV pathogenesis remains unclear. The aim of this project was to gain a better understanding of TRP-ML1 function and to provide further insight into the molecular mechanisms behind MLIV pathogenesis.

Since TRP-ML1 is lysosomally localized and is subject to proteolysis, I wanted to first examine the trafficking and characterize the processing of this protein. TRP-ML1 undergoes cleavage within its first extracellular loop during its biosynthetic delivery to lysosomes. The lysosomal delivery of TRP-ML1 is impaired by depletion of the Adaptor Protein (AP) complex AP-1, while proteolysis remains unaffected in cells lacking AP-1, indicating that cleavage may occur in a pre-lysosomal compartment.

Current models of MLIV pathogenesis suggest that TRP-ML1 directly regulates the postendocytic membrane trafficking by mediating interactions between late endosomes and lysosomes. Acute down-regulation of TRP-ML1 reveals that the lysosomal delivery and degradation of various markers is unperturbed, arguing against this model for MLIV pathogenesis. However, LDL-derived cholesterol ester hydrolysis in MLIV fibroblasts was found to be selectively impaired, suggesting that loss of TRP-ML1 alters lysosomal hydrolytic activity and has a cumulative effect on lysosome function.

My findings support a role for TRP-ML1 in maintenance of the ionic balance that is critical for proper lysosome function. This work is significant because it shifts focus away from the concept that TRP-ML1 only functions to regulate specific membrane trafficking events along the endocytic pathway. These results contribute to a more complete understanding of the physiological role of TRP-ML1 and broaden current understanding of MLIV progression, providing the basis for potential therapeutic treatment strategies.

TABLE OF CONTENTS

LIST OF TABLES

LIST OF FIGURES

PREFACE

This work would not have been possible without the guidance and support of many people. First, I would like to thank my thesis advisor, Dr. Ora Weisz. I will always remember the conversation that we had on my last day as a summer undergraduate researcher in her lab. Ora asked me what I thought about my first real hands-on research experience. I remember that my answer was that my 'project' did not seem like work at all. That was probably the first time that I realized I had a plan for myself. I would like to thank her for providing that environment for me to grow in. Ora's patience and guidance has allowed me to progress and develop as a scientist and a person. I will always be grateful and I hope that our paths will cross in the future.

I would like to thank all the members of the Weisz lab, both past and present. Jennifer, thank you for helping me start out in the lab, especially during my time as an undergraduate here. You helped to make complicated things seem easier to do, and much more fun. Kelly and Beth, thank you both for being wonderful examples of hard work and dedication. You have taught me more than most anyone here. I would also especially like to thank my comrade Chris. It was always so much easier to go through this process knowing that there was someone else right there going through the same thing. Our time and work together has been so rewarding.

I would also like to thank the members of my thesis committee: Dr. Devor, Dr. Traub, Dr. Kleyman, and Dr. Kiselyov. You have all provided me with such excellent support, advice, and criticism. I would especially like to thank Dr. Kiselyov's group for introducing me to the world of TRP-ML1. Learning how to collaborate in a scientific setting was one of the most valuable skills I acquired while here.

I would also like to thank my family and friends for their support and encouragement. To my parents, thank you for always putting my education first, and sacrificing so much to do so. That has always motivated me. I love you both very much. To my sister Mary, it has been wonderful to watch you bloom into such a wonderful person and overcome so much. You have made me want to work as hard as you.

I would like to especially dedicate this work to my cousin Timothy. You are why I became interested in research in the first place.

Finally, I would like to thank Sarah. I couldn't have accomplished any of this without your unconditional love and support. My life got better when you came into it. Thank you for always believing in me. Thank you for being so patient and unselfish. Thank you for always making sure that I had lunch. I love you.

1.0 INTRODUCTION

1.1 OVERVIEW

Mucolipidosis type IV (MLIV) is an autosomal recessive lysosomal storage disorder (LSD) characterized by developmental delays and psychomotor retardation, impaired gastric function, and ophthalmologic abnormalities (5, 227). At the cellular level, MLIV is characterized by the lysosomal accumulation of sphingolipids, phospholipids, cholesterol, and other gangliosides in all tissue types (8, 15, 16, 105, 207, 272). MLIV has a similar cellular phenotype when compared to other mucolipidoses. However, storage in other mucolipidoses results from improper targeting and/or activity of lysosomal hydrolases (131, 148). In contrast, MLIV is caused by mutations in the *MCOLN1* gene which codes for the transient receptor potential (TRP) channel family member mucolipin-1 (TRP-ML1) (12, 19).

Approximately two dozen disease causing mutations have been identified in the *MCOLN1* gene (1, 227). TRP-ML1 is localized to late endocytic structures including late endosomes and lysosomes (156, 202). Since mutations in this protein result in abnormal lipid accumulation and no definitive defects in lysosomal enzyme activity have been identified, it is suggested that TRP-ML1 regulates lipid transport along the endocytic pathway (14, 44). Therefore, the essential question regarding MLIV

pathogenesis is to determine how mutations in an intracellular ion channel result in endocytic abnormalities. It is disputed whether TRP-ML1 functions to regulate membrane trafficking involved in lipid transport, or in the maintenance of the proper lysosomal ionic microenvironment required for efficient lipid metabolism.

Endocytosis is a complex process involving numerous transport intermediates and membrane interactions. Fission and fusion between membrane-bound carriers and organelles is regulated in part by fluxes in lumenal Ca^{2+} concentration (200, 239), while the trafficking and activity of hydrolases depends on the acidic environment maintained within these compartments (194, 264, 265). This dependence on ions highlights the significant role that channels have in the coordination of events along the endocytic pathway.

Currently, there is not a clear model of how MLIV pathogenesis occurs. Moreover, how ion channels modulate lipid trafficking and metabolism is uncertain. Thus, the major goal of this dissertation was to characterize how TRP-ML1 functions along the endocytic pathway and to provide insight into the molecular mechanisms behind MLIV pathogenesis (Chapters 2-3). A more complete model of TRP-ML1 function will facilitate development of potential therapeutic treatments for MLIV and will result in a better understanding of lysosome function by determining the overall mode of disease pathogenesis. The following Introduction will discuss: general features of lysosome function and lysosomal storage diseases, mechanisms of intracellular lipid and protein transport, characterization of MLIV and TRP-ML1, and proposed models of MLIV pathogenesis.

1.2 LYSOSOMES AND LYSOSOMAL TRANSPORT

A defining feature of the eukaryotic cell is that it is divided into various compartments that are separated by membranes. The cell is separated from the external environment by the presence of the plasma membrane and specific intracellular microenvironments are maintained by the presence of membrane-limited organelles. Lysosomes (Greek for 'digestive body') were first identified by Christian de Duve and colleagues in 1955 (59). They are defined as hydrolase-rich, acidic organelles that lack mannose 6-phosphate receptors (MPRs) (56, 168). Lysosomes were originally described as an endpoint for intracellular pathways in which proteins and lipids from the endocytic, autophagic, and biosynthetic pathways are degraded and recycled (68, 130). It is apparent that lysosomes have a more dynamic role in physiological processes including down-regulation of cell surface receptors, autophagy, release of endocytosed nutrients, inactivation of pathogenic organisms, MHC class II antigen presentation, and plasma membrane repair (177). This view is also evidenced by observations describing direct interactions between lysosomes and late endosomes (137, 151, 152, 154) and by the identification of specialized organelles termed 'secretory lysosomes', modified lysosomes that undergo regulated exocytic secretion in response to external stimuli (235).

Due to multiple cellular functions and variations in intralumenal content, the morphology of lysosomes is heterogeneous. Their size is variable ranging from 0.5 µm to upwards of 2 µm. They are composed of a single limiting external membrane and can contain numerous intralumenal vesicles. The lysosomal membrane is primarily composed of cholesterol, phospholipids, proteins, and the abundant presence of

carbohydrate moieties. Proteomic analysis has identified over 150 lysosome-associated proteins including 50-60 soluble enzymes (9, 10, 114, 219) including proteases, lipases, nucleases, and polysaccharidases (130).

1.2.1 Intracellular targeting of lysosomal proteins

Interactions between various intracellular compartments take place because of an intricate network of vesicular transport carriers, each maintaining specific protein and lipid compositions. Membrane trafficking is a multi-step process that involves specific vesicle coat assembly and cargo selection, vesicle budding and movement along cytoskeletal tracks, contact and fusion with target membranes, and cargo unloading where trafficking components are recycled for re-use (24, 167). Trafficking events can be divided into two interconnected categories: biosynthetic (secretory) transport and endocytic transport (88). An overview of these pathways is highlighted in Figure 1.1.

In the biosynthetic pathway, newly synthesized proteins, carbohydrates, and lipids are transported through the endoplasmic reticulum (ER) and Golgi complex. Anterograde and retrograde trafficking of biosynthetic cargo is facilitated by COPII (coat protein complex) and COPI coats, respectively. The folding and post-translational modification of newly synthesized proteins also occurs during these steps. From the TGN (*trans*-Golgi network), cargo is directed either to the cell surface or to the endosomal-lysosomal system (88, 101). The biosynthetic transport of both soluble and transmembrane lysosomal proteins is discussed in detail below (1.2.1.1).

Small molecules such as ions, carbohydrates, and amino acids can cross the plasma membrane through specific ion channels or transporters. However, larger

macromolecules require the process of endocytosis in which transport vesicles derived from the plasma membrane are trafficked through the endosomal-lysosomal system. Endocytosis is essential for the transport of cellular lipid and protein components. Four mechanisms describing these processes have been detailed: phagocytosis and pinocytosis, clathrin-mediated endocytosis, caveolae-mediated endocytosis, and clathrin- and caveolae-independent endocytosis (88, 160, 175). General features of endocytic delivery to lysosomes are highlighted in section 1.2.1.2 while the role of organelle acidification and Ca^{2+} in this process is discussed in section 1.2.1.3.

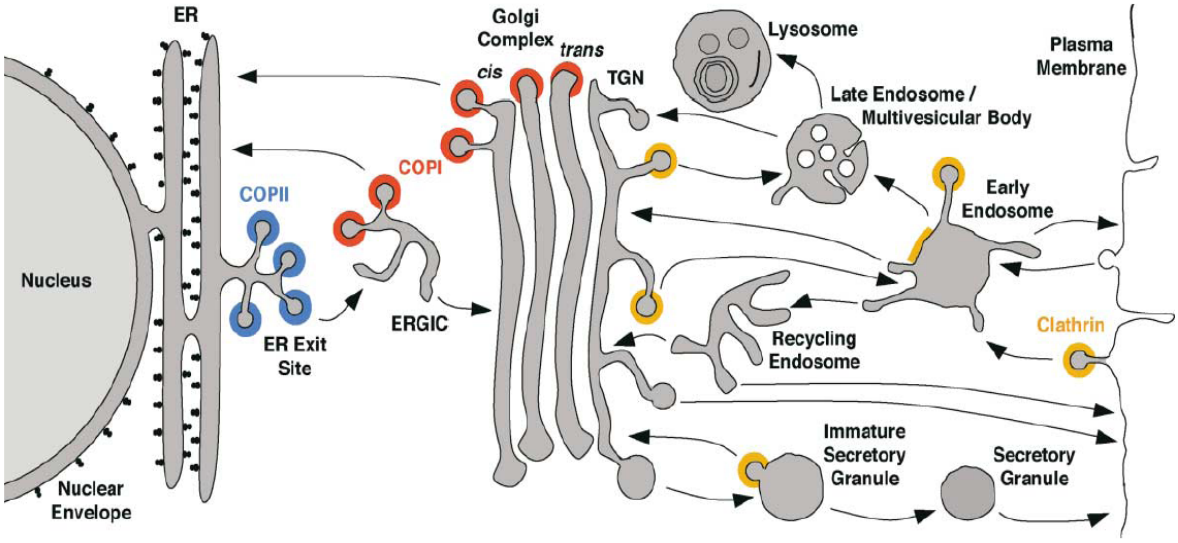

Figure 1.1 Major pathways of intracellular transport.
Schematic representation of the major pathways involved in membrane trafficking. Arrows in this diagram represent known or presumed intracellular transport routes. The coat complexes depicted are COPII (blue), COPI (red), and clathrin (gold). Endocytic carriers and subcellular organelles are labeled as indicated. TGN; *trans*-Golgi network, COP; coat protein complex, ER; endoplasmic reticulum, ERGIC; ER-Golgi intermediate compartment. Figure modified from Bonifacino, J.S. and Glick, B.S. (2004) (24).

1.2.1.1 Biosynthetic transport of lysosomal proteins

Targeting of most soluble lysosomal proteins depends on the mannose 6-phosphate (M6P) residues that are attached to them in the Golgi complex, and the subsequent recognition of this signal by the mannose 6-phosphate receptors (MPRs) located in the TGN (128). Two MPRs have been described, the larger 300 kDa cation-independent MPR (CI-MPR), and the smaller 46 kDa cation-dependent (CD-MPR) (55, 56, 213, 229). From the TGN, MPRs with bound lysosomal enzymes are packaged into clathrin-coated vesicles (CCVs) where they are subsequently delivered to early endosomes (129, 142). This incorporation of hydrolases into CCVs is facilitated by interactions between the AP-1 complex and the Golgi localized, gamma adaptin ear homologous, ADP-ribosylation factor binding proteins (GGAs) (141, 277). In particular, MPR incorporation is mediated by a di-leucine-based motif located in the cytoplasmic tail that is recognized by GGA proteins (78, 277). After delivery to early endosomes, the acidic pH of this compartment facilitates dissociation of MPR from lysosomal enzymes. From here, enzymes are transported to the lysosome while MPRs recycle back to the TGN (65, 163). It is suggested both AP-1 and AP-3 function in MPR trafficking and retrieval from endosomes (141, 163). However, a fraction of the CI-MPR is found at the plasma membrane where it directs missorted M6P-tagged enzymes into the endocytic pathway (77).

Targeting of lysosomal transmembrane proteins is more complex and diverse compared to biosynthetic transport of soluble lysosomal enzymes. This process is mediated by short sequences of amino acids present within the cytosolic domain of a transmembrane protein (27). The specific motifs that facilitate this transport can be

variable, but are usually comprised of 4-7 residues of which 2 or 3 critical residues are of a bulky, hydrophobic nature. Tyrosine-based motifs were the first to be described, and are composed of either NPXY or YXXØ consensus sequence (where N is asparagine, P is proline, X is any amino acid, Y is tyrosine, and Ø is any bulky hydrophobic residue). The Y residue is essential for recognition of the motif while the X residues are often acidic, and a glycine often precedes the critical Y residue. Dileucine-based motifs constitute the second class of lysosomal transmembrane sorting signals and can be categorized into two distinct classes: [D/E]xxxL[L/I] and DxxLL. These signals conform to the consensus LL or LI, and mutation of either of these first critical leucine residues impairs transport ability almost entirely. Additionally, an acidic residue preceding the first leucine residue (at position -4) is also important in[D/E]xxxL[L/I] motifs (27, 215). In DxxLL motifs the requirement for D and LL are strict and do not tolerate substitution. The D residue is generally found within a cluster of acidic residues.

Both tyrosine- and dileucine-based signals are recognized by cytoplasmic coat proteins that associate with the cytosolic face of the membrane. YXXØ and LL/LI are recognized by the clathrin-associated AP complexes (AP-1, AP-2, AP-3, and AP-4) that facilitate CCV incorporation (23, 61, 246). Most notably, AP-1 and AP-3 have been implicated in the transport of lysosomal transmembrane proteins along this pathway (21, 43, 140, 212). Targeting of lysosomal transmembrane proteins can occur via two distinct paths *en route* to lysosomes. The first is the entirely intracellular ‘direct route,’ that does not require passage through the plasma membrane. Alternatively, the ‘indirect route’ involves passage through the plasma membrane and subsequent AP-2-

dependent internalization before re-entry into the endosomal system and transit to lysosomes (27, 212).

It should also be noted that some dileucine motifs are recognized by the GGAs, thus lysosomal delivery of some lysosomal membrane proteins is GGA-mediated (27, 78, 277). Finally, lysosomal targeting may also be achieved through the ubiquitination of cytosolic lysine residues as this modification may serve as a signal for lysosomal sorting at numerous points in the endosomal-lysosomal system (18, 27, 28, 238). Chapter 2 describes the lysosomal targeting of TRP-ML1.

1.2.1.2 Endocytic transport to lysosomes

Endocytosis is divided into four main types according to how cargo is internalized. Chapter 3 will examine the role of TRP-ML1 in the regulation of endocytic trafficking of various protein and lipid markers. Therefore, this section highlights features of clathrin- and caveolae-dependent endocytic pathways.

Clathrin-mediated internalization is the best characterized of the endocytic pathways. Clathrin-dependent endocytosis is essential for numerous cellular functions including nutrient uptake, cell signaling, and tissue/organ development (63, 165, 175). The hallmark feature of this process is the formation and budding of the clathrin-coated vesicle. CCVs are dynamic structures that undergo exchange of coat protein components as they form, allowing for the rapid production of multiple vesicles (25). Clathrin-mediated endocytosis is divided into three key steps: CCV assembly and formation, CCV invagination, and CCV budding (32, 53, 90, 193) (Figure 1.2). This process is mediated by interactions of adaptor proteins with the plasma membrane and

clathrin as well as with accessory proteins and phosphoinositides (92, 251). CCVs are composed of clathrin triskelions that are assembled into a lattice structure, and are accompanied by the heterotetrameric AP-2 complex (52). Fission of CCVs is mediated by the GTPase dynamin, leading to subsequent release of the vesicle (97, 98). Various scaffolding proteins composed of multiple interaction domains allow for protein and lipid interaction, and serve to connect the endocytic machinery to the actin cytoskeleton (79). Additionally, this pathway is regulated by numerous mechanisms including phosphorylation, receptor signaling activity, and lipid modification (175).

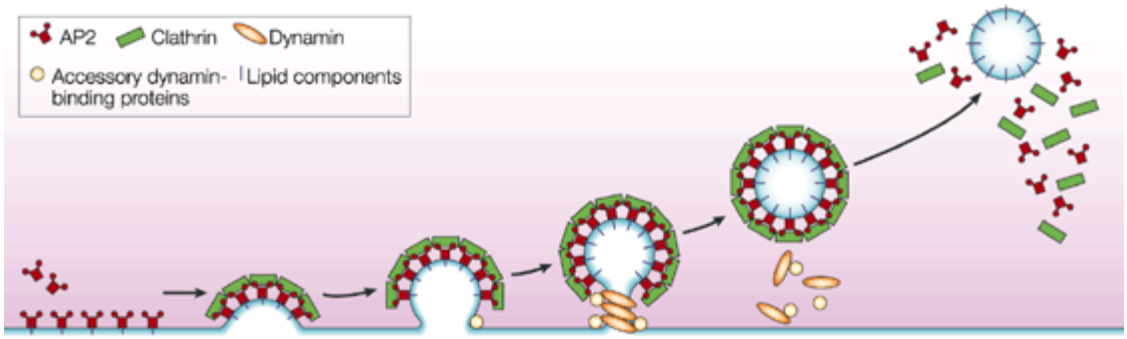

Figure 1.2 Clathrin-mediated vesicle formation.

This figure depicts the mechanisms that are involved in clathrin-mediated vesicle formation and budding from the plasma membrane. Clathrin coated vesicle (CCV) formation is driven by the assembly of clathrin (green) into lattices. Clathrin is recruited to the plasma membrane by AP-2 complex (red) whose membrane association is dependent on interactions with phosphoinositides, protein-protein interactions, and specific sorting signals present in the cytosolic tails of receptors and/or cargo molecules. The formation of an invaginated pit, and its subsequent detachment from the plasma membrane requires the GTPase dynamin (orange) which is targeted to the neck of CCVs where it facilitates vesicle fission (budding). Following release from the plasma membrane, CCV components rapidly uncoat and are returned to the cytosol. Figure adapted from Gundelfinger, ED, Kessels, MM, and Qualmann, B (2003) (90).

Caveolae are flask-shaped plasma membrane invaginations that are the defining feature of caveolae-mediated transport (139, 182). Caveolae are enriched in cholesterol and sphingolipids (lipid raft components), with their primary structural component being the integral membrane protein caveolin-1 (190, 191). Internalization is thought to occur via the clustering of raft components and subsequent sequestering into caveolae. Budding from the plasma membrane is dynamin-dependent and material internalized by this pathway includes extracellular ligands (folic acid and albumin), membrane components (glycosphingolipids), bacterial toxins (cholera toxin), and viruses (SV40) (22, 46, 180).

Following internalization, cargo enters the endosomal system, a network of organelles and vesicular intermediates that differ in both biochemical composition and subcellular localization (160). Carriers and compartments along the endocytic pathway are distinguished on the basis of morphology, specific membrane, lipid, and protein composition, and intralumenal pH. Cargo is first delivered to the early endosomes (EE), vesiculo-tubular organelles that are located in the cell periphery and are identified by the membrane protein early endosomal antigen-1 (EEA1) and the small GTPase Rab5. From the EE, cargo is sorted either to the degradative lysosomal pathway, or back to the plasma membrane. Cargo may be recycled directly or pass through recycling endosomes identified by the GTPases Rab4 and Rab11 (89, 230, 252, 274). Cargo in the degradative pathway is transported to the late endosomal (LE) compartment (also termed multi-vesicular bodies), positive for both Rab7 and Rab9 (11, 233, 274). From LEs, cargo is delivered to lysosomes where degradation in this acidic organelle is carried out by numerous hydrolases and lipases (130). Section 1.2.3.2 highlights

specific interactions between LEs and lysosomes that occur in the delivery of internalized cargo to lysosomes.

1.2.2 The role acidification and Ca^{2+} along the endocytic pathway

Organelles along the endocytic pathway have different lumenal ionic compositions, most notably regarding proton (H^+), chloride (Cl^-), and calcium (Ca^{2+}) concentrations. The ionic environment of endosomal compartments has a major role in both the trafficking and degradation of internalized material. Protons have a role both in the sorting of endocytosed cargo and in maintenance of the acidic environment required for hydrolase activity (67, 81, 249, 264). Calcium ions are necessary for specific fusion events that occur between late endosomes and lysosomes (149, 152).

The following section discusses the role of organelle acidification in endocytic transport and the role of Ca^{2+} in LE-lysosome interaction. Current discrepancies regarding TRP-ML1 function are centered on whether this channel mediates specific Ca^{2+}-dependent fusion events or functions to maintain the ionic environment within the lysosomal lumen required for efficient lipid metabolism.

1.2.2.1 Organelle acidification and endocytic transport

Intracellular organelles have characteristic lumenal pH ranges that are suited to their specific biochemical functions. Organelle acidification has multiple roles along the endocytic pathway as internalized molecules encounter an increasingly lower pH as they transit through EEs, LEs, and lysosomes (264) (Figure 1.3). The slightly acidic pH

of EEs (pH 6.2) facilitates receptor-ligand dissociation, so that receptors may be recycled back to the plasma membrane. Similarly, the harsh acidic pH of lysosomes (pH <5.5) enables the activation hydrolases that have been delivered to this compartment (249, 264). Organelle pH is maintained and regulated by balancing rates of intralumenal H^+ pumping, counterion conductance, and H^+ leak (84, 264, 265). Protons are pumped into the lumen against their concentration gradient by the vacuolar-type ATPase (V-ATPase) (74, 181). As protons are pumped into the lumen, V-ATPase function is limited by the build-up of an increasingly positive membrane potential. The build-up of excess positive charge can be relieved by counterion conductance through anion channels or transporters (Cl^- channels) allowing acidification to continue (85, 110, 217). The intrinsic rate of H^+ leakage from the lumen also contributes to steady state organelle pH. However, it is not known whether the primary mechanism for H^+ leakage occurs via passive leak through the membrane, or by the presence of specific H^+-permeable channels.

Acidification of endosomal compartments has an important role in the regulation of trafficking throughout the endocytic pathway (166). An excellent example is the recycling of cell surface receptors. After internalization, the receptor-ligand complex dissociates in either the early endosomal (pH 6.2-6.3) or recycling endosomal compartments (pH 6.4-6.5) due to their slightly acidic pH. One of the most prominent examples of receptor recycling is the transferrin receptor (TfR) (145). TfR binds iron-loaded transferrin at the cell surface under neutral pH conditions. Upon internalization of the receptor-ligand complex the more acidic EE pH facilitates iron dissociation from transferrin. Subsequently, TfR binds apotransferrin (transferrin lacking iron) and is

recycled to the plasma membrane. Here, neutral pH conditions result in apotransferrin dissociation allowing the cycle to continue (58). Disruption of organelle acidification disturbs the uptake of transferrin and affects TfR recycling (50, 125).

Proper organelle acidification is also important to transport along the degradative portion of the endocytic pathway. Disruption of pH inhibits delivery of markers such as horseradish peroxidase (HRP) from early to late endosomes (20), while other work suggests the LE-lysosome transport step is hindered (253). Recent reports suggest that acidification has a role in specific late endosome-lysosome fusion interactions (30, 153, 200) that occur during the process of lysosome formation. Lastly, the ClC family of Cl^- channels and transporters have important roles in regulation of organelle pH (109-111). ClC channels are localized to various endosomal compartments, and are thought to conduct Cl^- ions directly or work as Cl^-/H^+ exchangers to allow for organelle acidification in combination with the V-ATPase. Mutations in several of the ClC channel family members (ClC-3, ClC-5, ClC-6, and ClC-7) cause diseases resulting in abnormal endocytosis (Dent's disease), osteoclast function (osteopetrosis), and lipid processing (85, 117, 197, 198, 271).

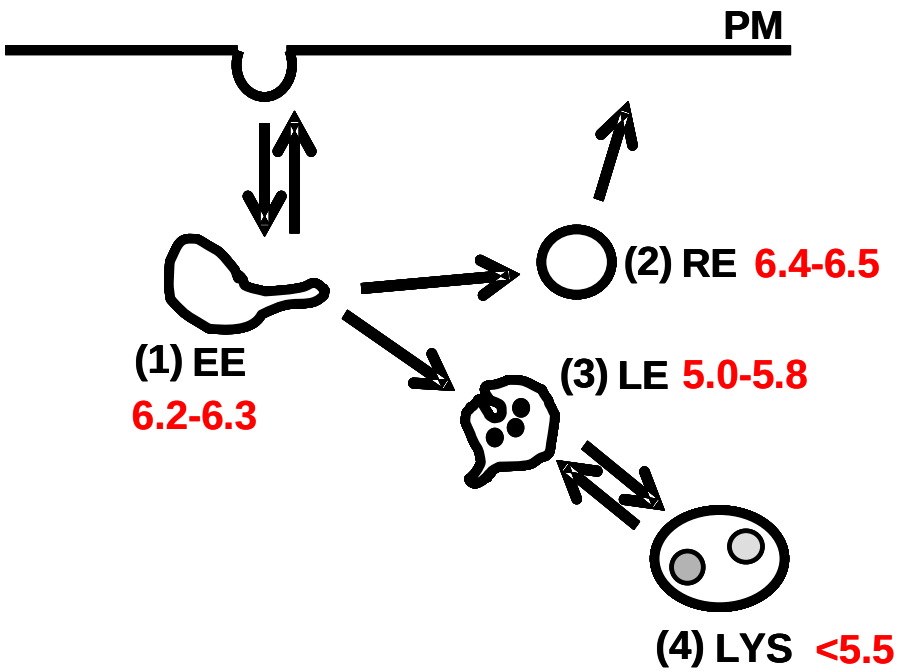

Figure 1.3 Organelle pH along the endocytic pathway.

Organelle pH (values displayed in red) steadily decreases as internalized material is internalized from the plasma membrane, and subsequently transported to lysosomes. Internalized lipids and proteins are consolidated into early endosomes (EE) (1) where the slightly acidic pH facilitates dissociation of receptor-ligand complexes. Material destined to be recycled is sorted to recycling endosomes (RE) (2) where pH is more alkaline. Material destined for degradation proceeds to late endosomes (LE) (3) and lysosomes (LYS) (4), where the distinctly more acidic pH of these compartments facilitates degradation by acidic hydrolases.

1.2.2.2 Late endosome-lysosome interactions and Ca^{2+}

Two hypotheses have emerged to explain the membrane dynamics involved in LE-lysosome interaction. The first is termed ‘kiss and run’, and proposes LEs and lysosomes undergo repeated transient fusion (‘kissing’) and fission (‘running’) events during which internalized material is transferred (152, 153, 177, 236). This is supported by experiments in which small soluble markers were found to move more readily between LEs and lysosomes compared to larger markers (236). The second is termed the ‘hybrid organelle’ or ‘biogenesis’ model in which direct fusion between LEs and lysosomes occurs and requires re-formation of lysosomes (150-152, 154). Fusion results in the formation of a hybrid organelle where internalized material is thought to be either degraded directly or condensed for transfer to terminal lysosomes. The reformation (or ‘biogenesis’) of lysosomes requires condensation of lysosomal material and retrieval of membrane fusion components. Support for this model has come from electron microscopy (EM) studies (31, 178), and cell-free content mixing assays using membrane fractions isolated from rat liver (179). Content mixing resulted in a new population of membrane-bound organelles that had an intermediate density compared with starting LEs and lysosomes. EM analysis revealed that these hybrid structures appeared less electron dense than mature lysosomes and contained markers from LEs and lysosomes (31).

Most likely, lysosomal delivery occurs via a combination of ‘kiss-and-run’ and ‘hybrid organelle’ type interactions (30). Live cell microscopy has shown that content mixing occurs *in vivo*. Immunoelectron microscopy analysis has produced images demonstrating the point of fusion displaying electron-dense lysosomal content diffusing

into the lumen of the hybrid organelle (31). These findings have allowed for the development of characteristic features of LE-lysosome fusions: 1) content mixing is observed only when organelles are in direct contact; 2) organelles can transiently fuse or undergo long term interactions; 3) contents are sometimes exchanged via tubules that emanate from LE or lysosomes (152).

Beginning to emerge are the mechanistic details that facilitate LE-lysosome fusion and the identification of machinery involved in these interactions. A schematic representation of LE-lysosome interactions is shown in Figure 1.4. Fusion of LEs and lysosomes requires many of the factors involved in other vesicular fusion processes including N-ethylmaleimide sensitive factor (NSF), soluble NSF attachment proteins (SNAPs), Rab GTPases, and intralumenal Ca^{2+}. LE-lysosome interactions have discrete steps involving organelle tethering, formation of a *trans*-SNARE (SNAP receptor) complex, membrane fusion, and lysosome re-formation.

Organelle tethering is a prelude to fusion and involves formation of short-distance contacts between the two target organelle membranes (~10-25 nm). Tethering factors specific for heterotypic LE-lysosome fusion have not been fully characterized, but Rab7 has been shown to contribute to this process. Over-expression results in clustering of LEs while expression of dominant-negative Rab7 has the opposite effect, resulting in dispersion of LEs (38). Other candidates include VPS18 and VPS39 which have described roles in endosome-endosome homotypic fusions (41, 199).

Following tethering, a *trans*-SNARE complex assembles between cognate Q (glutamine)- and R (arginine)-SNARE partners that is essential for fusion between endosomal compartments. The use of function-blocking antibodies has identified

specific SNAREs involved in heterotypic LE-lysosome fusions. The same Q-SNARES (syntaxin7, syntaxin8, and VTI1b) are required for both homotypic late endosome and heterotypic LE-lysosome fusions (4, 201). While the R-SNARE VAMP8 mediates homotypic events, VAMP7 is involved in heterotypic LE-lysosome interactions (201).

Membrane fusion is also dependent upon the release of lumenal Ca^{2+} from the fusing organelles (149). LE-lysosome fusion was inhibited by treatment with either the membrane-impermeable Ca^{2+} chelating agent BAPTA [1,2-bis-(*o*-aminophenoxy)ethane-N,N,N',N'-tetra-acetic acid] or the membrane permeable ester EGTA-AM [EGTA (ethylene glycol tetra-acetic acid)-acetoxymethyl ester] (200). The inhibitory effects of both treatments were reversed by $CaCl_2$. The mechanism by which release of lumenal Ca^{2+} results in endosomal membrane fusion after SNARE complex remains unclear, but evidence from homotypic fusion experiments suggests that it may be a calmodulin-mediated event (151, 152, 196).

The result of LE-lysosome fusion is formation of a hybrid organelle that maintains properties of both late endosomes (MPRs) and lysosomes (hydrolases). As described above, hybrid organelles have an intermediate density (178), and maintain specific markers of both LEs and lysosomes. The final aspect of the hybrid organelle cycle is re-formation of the individual lysosome that occurs to ensure recovery of both LEs and lysosomes. The re-formation process requires lysosomal content condensation, the removal of LE constituents, and the retrieval of lysosome-specific SNARE components (152, 153). Re-formation has been observed in both cell-free assays (179) and in live-cell microscopy studies (30). Tubulo-vesicular structures frequently ‘budded’ from hybrid organelles and were found to contain VAMP7, suggesting that retrieval of fusion

machinery requires tubular-based sorting. Finally, lysosomal content condensation and SNARE retrieval requires both acidification and lumenal Ca^{2+} as re-formation is inhibited by treatment with bafilomycin A1 or EGTA-AM (200) .

Both H^{+} and Ca^{2+} have essential roles in various stages of endocytic transport. TRP-ML1 has been implicated to function in both the processes of organelle acidification and endosomal membrane interactions. The remaining sections introduce MLIV as a storage disorder and highlight potential mechanisms of MLIV pathogenesis.

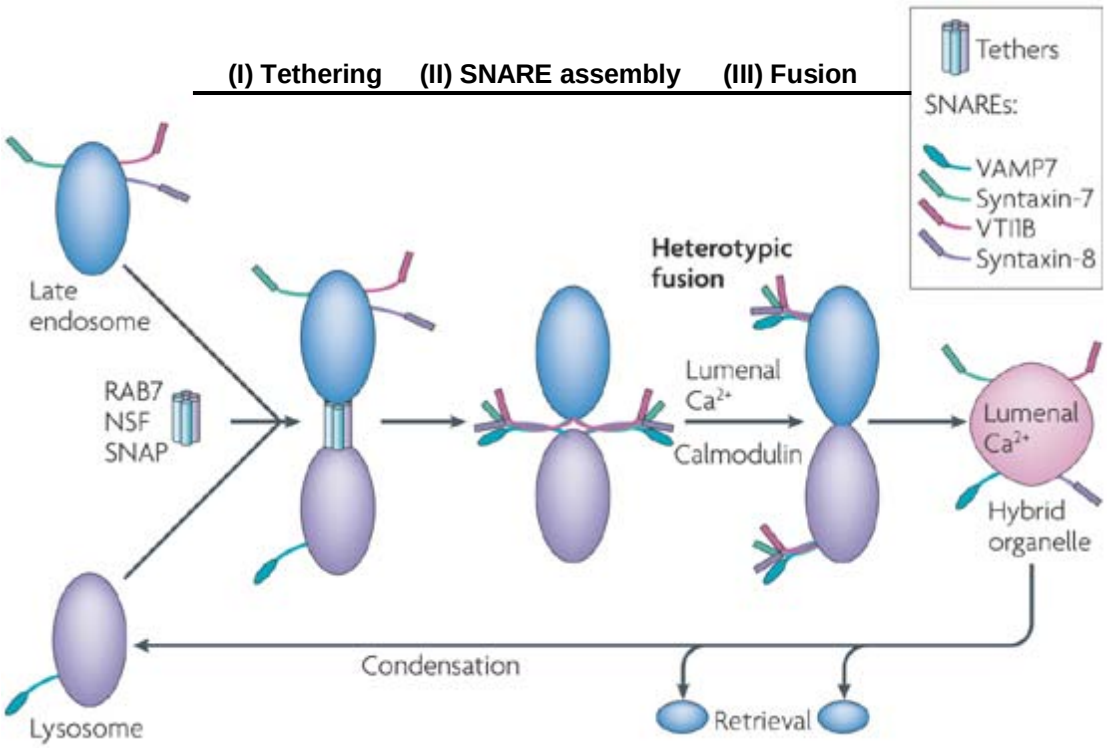

Figure 1.4 The mechanism of late endosome-lysosome fusion.

This diagram shows the mechanistic details of fusion reactions that occur between late endosomes and lysosomes that result in the formation of hybrid organelles. (I) The GTPase Rab7 is thought to mediate the tethering of late endosomes and lysosomes while also requiring N-ethylmaleimide sensitive factor (NSF) and soluble NSF attachment proteins (SNAPs). (II) *trans*-SNARE complex formation between late endosomes and lysosomes requires the R-SNARE VAMP7 and the Q-SNARE complex comprised of syntaxin 7, Vti1b, and syntaxin 8. (III) The release of luminal Ca^{2+} leads to membrane fusion between late endosomes and lysosomes and formation of the hybrid organelle. Reformation of lysosomes from hybrid organelle structures requires both SNARE component retrieval and condensation of lumenal content, and is dependent upon both Ca^{2+} and pH. Figure adapted from Luzio, JP, Pryor, PR, and Bright, NA. (2007) (152).

1.2.2.3 Autophagy and lysosomal dysfunction

In addition to degrading proteins and lipids that transit through the biosynthetic and endocytic pathways, lysosomes also function in the process of autophagy. Autophagy is a lysosome-dependent mechanism of intracellular degradation that is used for the continuous turnover of cytosolic components and maintenance of overall cellular homeostasis (132). Autophagy contributes to the turnover of cytosolic components ranging from individual macromolecules (proteins, lipids, nucleic acids) to entire organelles (mitochondria) (132, 159). Autophagy has important roles in development, immune defense, programmed cell death, and neurodegeneration (143, 222). Critical to this process is the formation of autophagosomes, double-membrane vesicles responsible for the delivery of cytosolic constituents to lysosomes. Core molecular machinery has an important role in facilitating interactions that occur between autophagosomes and lysosomes in the delivery of sequestered material (266). These specific interactions are similar to events that occur between late endosomes and lysosomes in the trafficking of endocytic cargo (152). Specific proteins involved in these interactions are beginning to be described, providing mechanistic insight into these processes. Features of these specific membrane interactions are discussed in more detail below.

Variation in autophagic pathways is created through the mechanism by which substrates are delivered to lysosomes. Several forms of autophagy have been described including macroautophagy, microautophagy, and chaperone-mediated autophagy (CMA) (132, 159). Both macro- and microautophagy require the formation of a limiting membrane that sequesters the cytosolic region to be degraded (266).

Macroautophagy involves the turnover of large cytosolic regions, including damaged organelles (mitochondria). Macroautophagy requires the formation of an autophagosome which mediates transport of sequestered material to lysosomes. In contrast, microautophagy involves direct uptake of cytoplasm at the lysosome surface via invagination of the lysosomal membrane. Thus, macroautophagy requires true autophagosome formation and microautophagy does not (152, 266). In macroautophagy, membrane-bound vesicles (autophagosomes) fuse with lysosomes to form a hybrid-like organelle called an autolysosome. The mechanism of autophagosome-lysosome interactions is thought to involve much of the same machinery described in the process of LE-lysosome fusion. Autolysosome formation is similar to other heterotypic fusions events, requiring the Q-SNARES syntaxin-7 and VTI1B (152). Rab7 has also been implicated in autolysosome formation, specifically at the level of autophagosome-lysosome tethering (104). It is also suggested that autolysosome formation is reduced in cells depleted of the integral membrane protein LAMP2 (83).

In both macro- and microautophagy an entire region of cytosol is internalized and all its components are degraded within the lysosomal lumen simultaneously. In contrast, the process of CMA is much more stringent. Selective cytosolic proteins are targeted and imported into the lysosomal lumen individually (159). This mechanism of transport is the hallmark feature of CMA. The targeting motif of CMA substrates is a series of five consecutive amino acid residues conforming to the general sequence of KFERQ (66). This motif is recognized in the cytosol by a molecular chaperone, hsc70, a member of the hsp70 family of molecular chaperones (47). This association facilitates targeting to

the lysosomal membrane where substrates directly interact with the LAMP-2A cytosolic tail, enabling lysosomal import (54, 118, 119).

Autophagy is dependent upon proper lysosomal function as lysosomes are essential for the autophagosome maturation and degradation of autophagic substrates. Defects in autophagic pathways have been reported in several lysosomal storage disorders (122, 242), including defects in autophagosome accumulation and autophagosome-lysosome interaction (220). Recent evidence also implicates autophagic defects in association with MLIV (108, 257). Given the unique localization and proposed function of TRP-ML1 in membrane trafficking and/or lysosomal ion homeostasis, it is not surprising that this protein may have a potential role in autophagic pathways. In Chapter 4, the role of TRP-ML1 in autophagy will be discussed

1.3 LYSOSOMAL STORAGE DISEASES

Lysosomal storage disorders (LSDs) are caused by the defective function of a lysosomal protein resulting in the intra-lysosomal accumulation of undigested metabolites. In principle, mutations in the genes that encode any of the approximately 60 soluble lysosomal enzymes or various membrane-associated proteins could result in storage disorders. Almost 50 LSDs have been identified, and ~40 of these involve soluble hydrolases (75). Most LSDs are inherited in a recessive manner and are monogenic, but multiple mutations may occur within the same gene. The frequency of LSDs is about 1:8000 live births (164). LSDs are progressive disorders with the central

nervous system being most affected while typical symptoms include blindness, mental retardation, and motor/sensory problems (113).

LSDs are classified based on the characterization of either the defective enzyme or the accumulated material. Primarily, the latter is used for description; however, there is considerable variability among LSD classification (75). Nonetheless, LSDs can be grouped into the following categories: sphingolipidoses, mucopolysaccharidoses (MPS), oligosaccharidoses and glycoproteinoses, lipidoses, LSDs caused by defects in integral membrane proteins, and non-traditional LSDs. Mucolipidosis Type IV (discussed in Section 1.4), belongs to the small group of LSDs caused by defects in lysosomal integral membrane proteins. MLIV is linked to defects in specific membrane transport and/or dysregulation in lysosomal ion homeostasis. The remainder of this section highlights diseases associated with lysosomal membrane proteins (1.3.1) and examines altered lipid trafficking and intracellular cholesterol homeostasis in LSDs (1.3.2).

1.3.1 Diseases associated with lysosomal membrane proteins

An essential function of the lysosomal membrane is to prevent unwanted degradation of both intra-organelle and cellular components by acidic hydrolases. The lysosomal membrane also mediates the entry of small molecules (amino acids and sugars) as well as the exit of digested material. Several known LSDs are attributed to mutations in the major membrane proteins of lysosomes. This section will introduce storage diseases caused by mutations in lysosomal membrane proteins. A brief summary of the basic characteristics of these disorders is summarized in Table 1.

Table 1.1 Diseases associated with lysosomal membrane proteins.

Diseases Associated with Lysosomal Membrane Proteins		
Disease	**Defective Protein**	**Storage Material**
Cystinosis	Cystinosin	Cysteine
Danon Disease	LAMP-2	Glycogen
Sialic acid storage disease (SASD)	Sialin	Sialic acid
Batten disease (JNCL)	CLN3	Subunit c of the mitochondrial ATP synthase
Mucolipidosis type IV (MLIV)	TRP-ML1	Various lipids and acid mucopolysaccharides
Niemann-Pick type C disease (NPC)	NPC1	Cholesterol and sphingolipids
JNCL-like disease	ClC-7	Subunit c of the mitochondrial ATP synthase

1.3.1.1 Cystinosis and sialic acid storage disease

Cystinosis and sialic-acid storage disease (SASD) are caused by defects in the transporters cystinosin and sialin. Sialin transports free sialic acid from lysosomes, and mutations in this protein cause lysosomal accumulation of free sialic acid resulting in neurodegenerative deficits common to LSDs (210). Cystinosin, a 367 amino acid protein with 7 transmembrane segments, is responsible for the transport of cysteine from the lysosome lumen to the cytosol. Mutations in this protein result in the intra-lysosomal accumulation and crystallization of cysteine resulting in severe retinopathy and nephropathy (115, 237).

1.3.1.2 Danon Disease

Dannon disease is a lysosomal glycogen storage disease that is due to LAMP-2 deficiency (57, 260). This is an X-linked disorder, not presenting until after the first decade of life, characterized by severe cardiomyopathy and skeletal muscle weakness (171). The precise function of LAMP-2 is uncertain, however, recent studies suggest that this protein is involved in autophagy (72, 118, 119). Autophagic defects are linked to the cardiomyopathies found in Danon disease (270). It has been shown that LAMP-2 functions as a receptor for the lysosomal import of soluble proteins during chaperone-mediated autophagy (CMA)(119).

1.3.1.3 Neuronal Ceroid Lipofuscinosis

Neuronal ceroid lipofuscinoses (NCLs) are a group of neurodegenerative disorders that are characterized by accumulation of autofluorescent ceroid lipopigment in patient cells (133). Mutations in CLN3 result in the juvenile form of NCL (Batten disease; JNCL)

which is the most common NCL form. CLN3 is a 43 kDa polytopic protein that has been demonstrated to localize to lysosomes (107, 120). CLN3 has been proposed to have many functional roles including lysosomal pH homeostasis, arginine transport, membrane trafficking, and anti-apoptotic functions (133).

1.3.1.4 ClC-7

ClC-7 is a Cl^-/H^+ antiporter that is localized primarily to lysosomes and late endosomes (85, 127). ClC-7, like other ClC channels, is thought to function as the primary Cl^- permeation pathway that allows for efficient organelle acidification. In humans, loss of ClC-7 was originally described to cause osteopetrosis, a condition that results in defective bone reabsorption by osteoclasts (109, 111). It has also been observed that ClC-7 loss causes severe neurodegeneration and lysosomal storage in a mouse model that is characteristic of the phenotype observed in NCLs (117).

1.3.1.5 Niemann-Pick type C disease

Niemann-Pick type C (NPC) is an autosomal recessive disease that displays progressive neurological degeneration and is usually diagnosed during early childhood years. Most NPC cases are caused by mutations in the late endosomal/lysosomal membrane protein NPC1 (95%), while the remaining 5% are attributed to mutations in the soluble lysosomal protein NPC2. NPC is described as a primary defect in cholesterol traffic. The primary defect in association with NPC is in the efflux of unesterified cholesterol from the lysosome. However, the accumulation of other glycosphingolipids (GSLs) is also characteristic of this disorder, suggesting that transport defects in one lipid species may also lead to the accumulation of other lipids.

1.3.2 Lysosomal lipid storage and membrane traffic

NPC pathogenesis exemplifies the complex relationship between lysosome function and endocytic transport. Moreover, a new concept is introduced that is a common theme among LSDs (including MLIV): increased storage of one lipid species can result in the subsequent storage of other lipids (226). Both intracellular cholesterol and GSL transport have important roles in LSD pathogenesis. Thus, it is necessary to examine this relationship more carefully.

1.3.2.1 LDL-derived cholesterol transport

Intracellular trafficking plays a major role in maintaining the correct distribution of internalized cholesterol and in the efficient efflux of cholesterol from endocytic compartments. The primary way by which cells acquire cholesterol from the circulating blood is through clathrin-mediated internalization of the low density lipoprotein (LDL) (103). LDL-derived cholesterol is important for many cellular functions including synthesis of cellular membranes, bile acids, and steroid hormones (103). LDL particles are composed of an inner core of esterified cholesterol that is surrounded by a phospholipid shell containing the protein apoB which mediates binding to the low density lipoprotein receptor (LDLR). LDL bound to the LDLR is incorporated into CCVs and transported to EEs where moderately acidic pH facilitates receptor-ligand dissociation allowing recycling of LDLR. LDL constituents are transported to LEs and lysosomes where cholesterol ester hydrolysis occurs via lysosomal acid lipase (34, 35, 76, 112, 162). Hydrolysis produces free (unesterified) cholesterol that is exported from

LEs-lysosomes to both the plasma membrane and endoplasmic reticulum, possibly via NPC1 and/or NPC2 (161, 176).

1.3.2.2 Endocytic transport of glycosphingolipids

Glycosphingolipids (GSLs) are a diverse class of lipids composed of a ceramide backbone and a sugar headgroup. GSLs are important in a variety of processes including cell signaling, cell growth, and embryonic tissue development (60). GSLs are synthesized in the ER and Golgi and are enriched at the plasma membrane where they interact with cholesterol to form specific membrane microdomains called 'lipid rafts'. GSL distribution is coordinated at several levels including membrane transport steps from the cell surface. GSLs are internalized from the cell surface and transported to lysosomes where they are degraded. Constituents of these lipid molecules exit the lysosome and are subsequently transported for further metabolic processing and re-use (214, 244).

GSL endocytosis occurs through a clathrin-independent process. GSL internalization is inhibited by both over-expression of dominant-negative (DN) dynamin and by treatment of cells with cholesterol-depleting agents. Additionally, internalization is enhanced by overexpression of caveolin-1 and co-localizes exclusively with albumin upon internalization (188, 224, 225), suggesting GSL endocytosis occurs via caveolae. Within the endosomal system, metabolism and Golgi-targeting of GSLs requires passage through both LEs and lysosomes. Transport from these compartments is inhibited by over-expression of DN Rab7 and Rab9 (157, 188).

1.3.2.3 The glycosphingolipid-cholesterol connection

Both cholesterol and GSL transport abnormalities can contribute to LSD pathogenesis and lipid accumulation. However, it is not fully understood how these two pathways work in concert during disease pathogenesis. It was originally suggested that GSL accumulation in LSDs was limited to those cells where deficiencies in GSL-hydrolyzing enzymes existed. Surprisingly, GSL accumulation was also found to occur in several other storage diseases in which the primary deficit was not specifically attributed to defective activity of GSL-hydrolyzing enzymes (including MLIV and NPC) (188, 226). Thus, GSL accumulation is a more general feature of LSDs and suggests that GSL transport is affected by alterations in the intracellular distribution and/or total levels of cellular cholesterol (204). It is documented that cholesterol and sphingolipids physically interact in both reconstituted and native cellular membranes (33, 37). GSL trafficking in both normal and LSD cell lines is sensitive to changes in intracellular cholesterol levels (158, 204, 205). In LSD cells, proper Golgi localization of fluorescent GSLs can be restored upon depletion of cellular cholesterol. Conversely, in normal cells, cholesterol overload induces the accumulation of GSLs in lysosomes (203, 204).

Two potential mechanisms have emerged to explain the relationship between GSLs and cholesterol transport abnormalities in storage disorders. The first suggests that GSL accumulation results in the increased expression and/or re-distribution of proteins that are involved in the regulation of intracellular cholesterol homeostasis (203). As a result of GSL accumulation, cholesterol levels are altered within endocytic compartments due to aberrant interactions with proteins involved in cholesterol efflux. An alternative mechanism suggests that there is an increased preference for physical

interaction between GSLs and cholesterol resulting in the ‘trapping’ of cholesterol within these compartments. Thus, the level of cholesterol accumulation is dependent on its ability to interact with a particular GSL species (188, 189, 224).

It is essential to highlight the dynamic relationship between LDL-derived cholesterol and glycosphingolipids in lysosomal storage diseases, as abnormalities in both of these pathways are associated with MLIV (29, 44, 105, 202). In the final section of this introduction (1.4), MLIV will be specifically introduced. I will highlight specific information regarding clinical and genetic features of MLIV, discuss functional aspects of TRP-ML1, and explore underlying mechanisms of MLIV pathogenesis.

1.4 MUCOLIPIDOSIS TYPE IV

Mucolipidosis type IV (MLIV) is a neurodegenerative, autosomal recessive, LSD characterized by psychomotor retardation and visual impairment due to various ophthalmologic abnormalities. Less than 200 MLIV cases have been diagnosed with the highest frequency of occurrence among the Ashkenazi Jewish population (227, 228). MLIV is caused by mutations in the *MCOLN1* gene, which encodes the mucolipin-1 (TRP-ML1) protein, a TRP (transient receptor potential) channel family member. Variable lysosomal storage is observed in all tissue types of affected individuals. Based on the heterogeneous nature of storage material (both water and lipid soluble storage material), MLIV is classified as a mucolipidosis. Other classes of mucolipidoses include

MLI (sialidosis), MLII (I-cell disease), and MLIII (pseudo-Hurler polydystrophy). Sialidosis (also called cherry-red spot syndrome) is caused by the deficiency of the enzyme sialidase (α-N-acetylneuraminidase) which is responsible for the catabolism of sialoglycoconjugates. This disorder is associated with progressive impaired vision, mental retardation, macular cherry-red spots, and skeletal dysplasia (39, 148). I-cell disease and pseudo-Hurler disease are both disorders affecting the activity of N-acetyl-glucosamine-1-phosphotransferase (GlcNAc-phosphotransferase) (131,128), a critical enzyme that participates in the M6P-dependent targeting of newly synthesized lysosomal hydrolases. Due to this abnormality these classes of mucolipidoses are characterized by the mass mistargeting (secretion) of lysosomal hydrolases into the blood and extracellular matrix. Consequently, storage of both water and lipid soluble material occurs. Similar to other classes of mucolipidoses, the primary features of MLII and MLIII include severe developmental delay, retardation, and ocular defects. I-cell disease is more severe compared to MLIII, as the skeletal muscle system is also severely affected (232).

MLIV lysosomal storage is attributed to mutations in an ion channel and is not the result of the mistargeting or abnormal activity of specific lysosomal hydrolases. As a result, many unique aspects regarding MLIV pathophysiology arise.

1.4.1 Clinical features of MLIV

Most MLIV patients are diagnosed within the first 1-2 years of life with profound psychomotor retardation and ophthalmologic abnormalities including corneal opacity and retinal degeneration (3, 211). Upper developmental limits are reached at 12-15

months for both speech and motor function. Patients often develop spasticity and hypotonia and usually cannot walk independently. Despite early onset of this disease, MLIV progression is protracted when compared to other classes of mucolipidoses. Most patients reach a steady-state without further deterioration for at least 2-3 decades of life (5, 48). The oldest surviving individual affected with MLIV is 45 years old (1). MRI studies reveal brain abnormalities substantiating observed developmental and neurological deficits (1, 223). Iron deficiency is common among MLIV patients, and most exhibit elevated blood gastrin levels caused by the failure of gastric parietal cells to secrete HCl (218). EM studies support this finding as parietal cells were shown to have accumulated numerous lysosomal inclusion bodies (147, 218). Considerable variability in the clinical symptoms and severity of MLIV have been described including both late-onset and milder forms of MLIV (42, 209).

1.4.2 Cellular features of MLIV

Morphological studies (EM) of MLIV patient tissues show the abnormal accumulation of lamellar membranous structures and heterogeneous material present within cytoplasmic organelles. This characteristic storage is observed in every tissue type of MLIV patients and is autofluorescent (80), a feature common among LSDs. Storage material includes gangliosides, phospholipids, cholesterol, and neutral lipids in addition to water soluble materials such as mucopolysaccharides, and glycoproteins (5, 6, 15, 16). Different compositions of storage content are present between somatic cells and neurons. While gangliosides are the predominant storage material in neural tissues, phospholipids accumulate in somatic tissues (73).

Early studies using radiolabeled lipids (phosphatidylcholine and gangliosides) indicated a significant intracellular retention of these compounds in MLIV fibroblasts. Surprisingly, these substances were shown to be degraded and discharged at levels comparable to control cells (14, 273). Similarly, studies using the fluorescent lipid analogue BODIPY-LacCer demonstrated that this lipid was degraded normally in MLIV fibroblasts (44). However, other work suggests that there are deficiencies in the hydrolases involved in the catabolism of other lipid substrates (8).

These initial findings led to the suggestion that lipid degradation does occur normally, indicating storage in MLIV is associated with abnormal lipid transport. This hypothesis was offered as an explanation for the unusual protracted course of MLIV development, as many patients remain in a non-deteriorating state for up to three decades. This is in contrast to a disorder such as I-cell disease in which there is an almost complete lack of lysosomal hydrolase activity. More comprehensive models of MLIV pathology were developed after the discovery that this disorder is the result of mutations in the *MCOLN1* gene.

1.4.3 Molecular genetics of MLIV

Genome scanning and analysis of MLIV families first mapped the disease locus to chromosome 19p1.2-1.3 in 1999 (228), and the *MCOLN1* gene was cloned in 2000 (12, 19, 240). The *MCOLN1* gene of 14 kb contains 14 exons including a transcript of 2 kb encoding the mucolipin-1 (TRP-ML1) protein of 580 amino acids. MLIV is found in the highest frequency among the Ashkenazi Jewish (AJ) population with a carrier frequency of 1:100 (13). Approximately 20 MLIV-causing mutations have been reported in MLIV

patients of both Jewish and non-Jewish descent (227, 272). Two founder mutations have been identified, comprising 95% of the mutated alleles among AJ MLIV patients that date to 40 generations ago (1, 5).

Two other genes, *MCOLN2* and *MCOLN3* have also been identified and cloned, and are localized at chromosome 1p22.3. The *MCOLN* genes code for TRP-ML proteins that show 60% amino acid homology to each other (12, 227, 272). Similar genes have been identified in mice, *C. elegans*, and *Drosophila* (12, 69). Currently, there are no reports associating *MCOLN2* or *MCOLN3* with human disease. However, mutations in *mcoln3* are associated with deafness, vestibular defects, and pigmentation abnormalities in mice (64).

1.5 MUCOLIPIN-1 AND MLIV PATHOGENESIS

This section will highlight TRP-ML1 and examine its functional properties with respect to regulation of membrane traffic. TRP-ML1 will be first introduced as a TRP channel family member. TRP-ML1 localization, modification, and processing, will also be discussed. Lastly, TRP-ML1 function and proposed roles in MLIV pathogenesis will be examined.

1.5.1 General features of TRP channels

Transient receptor potential (TRP) family members are a diverse group of channel proteins that are expressed in almost every tissue type and are conserved in both invertebrates and vertebrates. TRP channels were first described in *Drosophila* where the *trp* gene was identified as critical for maintaining the light response (91, 262). TRPs are classified on the basis of sequence homology rather than by ligand or ion selectivity because their selectivities and modes of activation are so diverse (51). All TRPs share the common characteristics of six transmembrane (TM) spanning segments which are predicted to assemble as homo- or hetero-tetramers, varying degrees of amino acid sequence homology, and permeability to both mono- and di-valent cations (51, 255). TRPs are cation channels, although the permeability for different cations varies greatly, giving rise to their diverse roles in sensing various types of both external and intracellular stimuli. Most notably, TRPs have been implicated in the response to sensation of light, sound, chemical, temperature, mechanosensation, osmosensation, and touch (51, 102, 187, 255). Due to their wide-ranging expression patterns and diversity in permeability characteristics TRP channels are implicated in numerous diseases including abnormalities of the nervous system, kidney, lung, heart, cardiovascular system, and cancer (124, 183).

Based on their relative amino acid homology, mammalian TRPs are divided into two groups containing seven subfamilies. Group 1 TRPs include TRPC, TRPM, TRPV, TRPA, and TRPN, while group 2 TRPs include TRPP and TRPML subfamilies (255). The TRPC (canonical) and TRPM (melastatin) subfamilies consist of 7 and 8 different members, respectively. The TRPV (vanilloid) subfamily comprises 6 members, while the

most recently described subfamily, TRPA (ankryin), has only 1 current member. The final group 1 subfamily, TRPN (no mechanoreceptor potential C or NOMPC) has yet to be identified in a mammalian system, and has only been described in *C. elegans*, *Drosophila*, and zebrafish (51, 192, 255). Group 2 TRPs include the TRPML (mucolipin) and TRPP (polycystin) subfamilies. Both subfamilies contain 3 members and are associated with the human diseases MLIV and autosomal dominant polycystic kidney disease (ADPKD) (82, 206), respectively. TRPP and TRPML groups share a similar topology to group 1 members. However, both TRPML and TRPP are characterized by a large extracellular loop present between TM segments 1 and 2. TRP-ML1 displays 22% overall amino acid similarity with PKD2 with the most homologous region occurring between the fifth and sixth TM segments (~45% similarity), the proposed pore-forming region of the channels (206, 255).

TRP-ML1 is the founding member of the TRP-ML subfamily which includes two other closely related proteins, TRP-ML2 and TRP-ML3 (~ 50% amino acid similarity). Additionally, both the *C. elegans* and *Drosophila* genomes each encode one TRP-ML protein, CUP-5 and CG874, respectively (255). Both of these proteins share approximately 30% amino acid homology to TRP-ML1.

1.5.2 The subcellular localization of TRP-ML1

TRP-ML1 is a 580 amino acid transmembrane protein with a molecular mass of ~65 kDa and is oriented with both the amino- and carboxy-termini in the cytoplasm. Unlike most other TRP-family members, TRP-ML1 has been demonstrated to maintain an

intracellular distribution (121, 156, 170, 202). TRP-ML1 is primarily localized to late endocytic structures that are positive for lysosomal markers (LAMP-1, cathepsin D, dextran). However, little information is available regarding the mechanistic details of TRP-ML1 transport to lysosomes. Examination of the TRP-ML1 amino acid sequence has revealed two di-leucine motifs present within the cytosolic tails (E_{11}TERLL$_{16}$ and E_{573}EHSLL$_{578}$) that may mediate lysosomal trafficking. Both of these motifs conform to the [D/E]xxxL[L/I] type consensus sequence and limited analysis has suggested that the intracellular distribution of TRP-ML1 is not impaired upon deletion of the C-terminal targeting motif (E_{573}EHSLL$_{578}$) (156). In Chapter 2, I examine the role of these two motifs in the lysosomal targeting of TRP-ML1 and assess the role of AP complexes as potential mediators of TRP-ML1 trafficking.

1.5.3 Processing and regulation of TRP-ML1

In addition to the sorting information present within its cytosolic tails, TRP-ML1 also contains a large extracellular loop located between the first and second TM segments of the protein. Among TRP channels, only TRP-ML1 and PKD-2 possess this feature, and it is suggested that it may serve as a site for regulation of channel activity (206). Within this loop there are 4 consensus sites for N-glycosylation (NxS/T) (272). Although the predicted molecular mass of TRP-ML1 is 65 kDa, it has also been shown that there is a lower molecular mass form that migrates at ~37 kDa (121). Importantly this feature has been observed for both the endogenous and over-expressed protein. Thus, this initial observation suggests that TRP-ML1 is subject to proteolytic processing. In Chapter 2, I

describe experiments using site-directed mutagenesis to determine the relative position of proteolytic cleavage within the extracellular loop of TRP-ML1.

Examination of TRP-ML1 proteolysis is important because very little is known regarding how activity of this channel may be regulated. Recent reports indicate that TRP-ML1 proteolysis functions to inactivate channel activity and is mediated by cathepsin B (121). However, it is not known whether multiple proteases participate in the processing of TRP-ML1. Studies presented in Chapter 2 suggest that TRP-ML1 processing may involve proteases other than Cathepsin B, and that proteolysis may occur at a site prior to the lysosome. Nonetheless, this is the first evidence suggesting that TRP-ML1 channel activity is regulated via proteolytic processing.

In addition to proteolysis, recent studies also suggest that TRP-ML1 activity can also be regulated through phosphorylation (258). Two protein kinase A (PKA) phosphorylation sites were identified within the C-terminal tail of TRP-ML1. It was shown that activation of PKA resulted in decreased TRP-ML1 activity, while decreases in PKA activity had the opposite effect. Thus, regulation of TRP-ML1 channel activity is complex and involves both proteolytic processing and phosphorylation.

1.5.4 Localization of other TRP-ML proteins and ML-ML interactions

TRP channels are thought to function as both homo- and hetero-tetramers (255). Little information is available describing the intracellular distribution and function of TRP-ML2 and TRP-ML3. It is not known whether TRP-ML1 proteins interact with one another, or if this potential interaction has any effect on TRP-ML1 function. Using a co-immunoprecipitation approach it has been demonstrated that endogenous TRP-ML1 co-

precipitates with both TRP-ML2 and TRP-ML3 (272). Studies using FRET analysis suggest that all three TRP-ML members interact to form multimeric complexes. Furthermore, the lysosomal localization of TRP-ML3 is dependent upon its association with TRP-ML1 and TRP-ML2 (254). Expressed individually, both ML1 and ML2 maintain a steady-state lysosomal distribution whereas TRP-ML3 is largely retained in the ER. TRP-ML3 was only found localized to lysosomes upon co-expression with either of the other TRP-ML proteins.

Studies examining TRP-ML2 suggest that it is localized to both cytoplasmic vesicles and the plasma membrane, functioning in the Arf-6-dependent trafficking of a subset of GPI (glycosylphosphatidylinositol) -anchored proteins (116). TRP-ML3 function in human cells has not been extensively examined; however in the mouse model system mutations are associated with hearing and pigmentation defects in varitint-waddler (Va) mice (64). TRP-ML3 is localized to cytoplasmic vesicles within the hair cells of the cochlea, suggesting that this protein functions in the transduction of sound (234). Pigmentation defects in these mice implicate a role for TRP-ML3 in melanosome function.

1.5.5 TRP-ML1 channel activity

A limiting factor in understanding TRP-ML1 function is the determination of the ion permeability characteristics of TRP-ML1. Endogenous TRP-ML1 channel activity has not been characterized, due primarily to the intracellular localization of this protein. Ion permeability characteristics have been described using overexpression systems, but no clear consensus has emerged. Overexpression studies in *Xenopus* oocytes and

HEK293 cells described TRP-ML1 as an outwardly rectifying channel permeable to multiple cations including Na^+, K^+, and Ca^{2+} (121, 136). Activity has also been examined using isolated endosomal vesicles from TRP-ML1 over-expressing cells whereTRP-ML1 is described as a non-specific cation channel whose activity is modulated by both Ca^{2+} and pH (40, 208).

Recent work has also described TRP-ML1 as being a H^+-permeable channel that functions in the regulation of lysosomal pH (121, 231). Specifically, it was suggested that TRP-ML1 may function as a H^+-leak pathway preventing lysosomal over-acidification (231). In contrast, studies performed using 'activating' mutations in TRP-ML1 demonstrate that the channel displays inward rectifying current and is H^+-impermeable, suggesting that TRP-ML1 may not function as a H^+-leak channel *in vivo* (86, 267).

1.6 MECHANISMS OF MLIV PATHOGENESIS

Due to ambiguity regarding TRP-ML1 channel properties, there is considerable debate surrounding the physiological function of this protein. Thus, there is no clear mechanism to describe MLIV pathogenesis. It is agreed that TRP-ML1 functions along the endocytic pathway. However, it is uncertain whether TRP-ML1 functions to regulate specific membrane trafficking steps, or helps maintain proper lysosomal ionic conditions required for efficient lipid metabolism.

Intraorganelle Ca^{2+} is required for the specific interactions between endosomal compartments during endocytic transport (149, 200). It has been postulated that TRP-ML1 regulates these Ca^{2+}-dependent trafficking steps due to its intracellular localization and Ca^{2+} permeability. It has been demonstrated that LacCer (GSL) trafficking is perturbed in MLIV fibroblasts (44, 202, 231). Normal Golgi targeting of this lipid is able to be restored upon expression of exogenous TRP-ML1 that is both properly localized and has functional channel activity (202). In addition, transport defects are not the result of abnormal LacCer-hydrolyzing enzyme function, as both GM_1-β-galactosidase and β-galactosylceramidase activities were reported to be normal in MLIV fibroblasts (44).

LacCer trafficking defects in MLIV fibroblasts indicate that there are endocytic abnormalities in TRP-ML1-deficient cells. Evidence provided by the *C. elegans* model system provides specificity to these observations, suggesting that defects occur at the level of LE-lysosome interaction. Genetic knock out of the *cup-5* (TRP-ML1 homologue) gene result in defects in the process of lysosome biogenesis (69, 70, 248). In wild type animals the CUP-5 protein is localized to presumed sites of hybrid organelle fusion where it is suggested that this protein functions in the process of lysosome re-formation. In *cup-5*$^{-/-}$ animals there is an abnormal accumulation of hybrid organelles that retain markers of both LEs and lysosomes. In these mutants the endocytic delivery of dextran was impaired, but exogenous addition of TRP-ML1 (or TRP-ML3) was able to correct this abnormality (248).

Further support for the role of TRP-ML1 in mediating LE-lysosome interaction comes from *in vitro* content mixing assays performed on isolated LE and lysosomal membrane fractions prepared from control and MLIV fibroblasts (138). It was shown that

interaction between LEs and lysosomes is impaired in fractions prepared from MLIV fibroblasts. Similar results were also obtained using an *in vivo* FRET-based approach examining the fluid phase intermixing of internalized dextrans (138). Overall, these observations suggest that TRP-ML1 regulates the endocytic delivery of internalized material to lysosomes. Therefore, this hypothesis predicts that there should be a global defect on endocytosis, affecting the delivery and degradation of internalized lipids and proteins. It must also be determined whether abnormalities in trafficking in MLIV fibroblasts are the result of chronic lipid accumulation. This is an essential question because abnormal endocytic transport may not be directly caused by loss of TRP-ML1 function. In Chapter 3, I will specifically address these issues by examining the endocytic delivery and degradation of various protein and lipid markers in both MLIV fibroblasts as well as in cells where TRP-ML1 expression has been acutely down-regulated by using specific siRNA nucleotide duplexes.

The maintenance of organelle pH is essential for both the efficient trafficking and degradation of internalized cargo during endocytosis (264). Recent studies have described TRP-ML1 to be a H^+-permeable channel that functions in the regulation of lysosomal pH (231). Although data regarding lysosomal pH in MLIV fibroblasts are disparate (7, 126, 202, 231), this model implies that TRP-ML1 is involved in the regulation of the overall ionic environment of the lysosome, where deficiencies in this process affect the activity and/or stability of the enzymes responsible for lipid metabolism.

As stated above, significant discrepancies regarding lysosomal pH in TRP-ML1-deficient cells exist. While it has been demonstrated that lysosomes in MLIV fibroblasts

accumulate more of the pH-sensitive reagent acridine orange (AO) (231) suggesting increased acidity, others have shown that lysosomal pH is either higher (7) or unchanged (126, 202) in these cells. A complicating issue in performing these studies is the autofluorescent nature of the accumulated lipid material within these cells (80). In Chapter 3, I measured the lysosomal pH of cells subjected to acute TRP-ML1 down regulation, where chronic lipid accumulation had not yet occurred.

Despite the controversy regarding lysosomal pH, there is also evidence that lipid hydrolysis is negatively affected in TRP-ML1-deficient cells. Using isolated lysosomal membrane fractions, it was found that the activity of lysosomal lipases is decreased in MLIV fibroblasts resulting in the abnormal processing of specific lipid substrates (231). It was shown that lipase activity could be rescued by expression of wild type TRP-ML1 in these cells. In addition, it was also demonstrated that treatment of MLIV fibroblasts with chloroquine or nigericin reversed the presence of lipid inclusions found within these cells. Taken together, these studies suggest that MLIV may be connected to defects in overall lysosome ionic homeostasis that result in lipid processing deficiencies.

Studies have also probed the LDLR-mediated endocytic pathway using both [^{14}C]-sphingomyelin (SM) in complex with apolipioprotein E (apoE), or [^{14}C]-cholesteryl oleate (CO) to examine whether the transport or processing of these lipids is altered in MLIV fibroblasts (105). Both [^{14}C]-SM and [^{14}C]-CO were found to be metabolized more slowly in MLIV fibroblasts compared to control cells. Although minor delays in lysosomal transport were observed, the primary defect was in the catabolism of these substrates. Although no defect in lysosomal pH was documented, these findings again suggest that

lipid accumulation in MLIV is attributed to abnormal lipid hydrolysis rather than defective endocytic transport.

Current models of MLIV pathogenesis are incomplete, as there is evidence to support a role for TRP-ML1 in both the regulation of membrane trafficking and in lipid metabolism. The 'biogenesis' model of MLIV pathogenesis predicts that there will be global effects on endocytic transport for both lipids and proteins. In Chapter 3, I will specifically examine the role of TRP-ML1 in regulation of membrane traffic. I will also probe the LDLR-mediated pathway to examine the lysosomal delivery and degradation of both the lipid and protein components of LDL in TRP-ML1-deficient cells.

1.7 GOALS OF THIS DISSERTATION

SPECIFIC AIM 1: To characterize TRP-ML1 trafficking to lysosomes and proteolytic processing. TRP-ML1 is described as a lysosomal protein. However, little information was available regarding the mechanism of TRP-ML1 targeting to lysosomes. It is essential to determine how TRP-ML1 traffics to lysosomes, as this will provide a better understanding of where this protein is active and where potential sites of regulation may be. My initial experiments suggested that TRP-ML1 is also subject to proteolytic processing. Therefore, the goal of Aim 1 was to characterize TRP-ML1 delivery to lysosomes and to identify where along the biosynthetic pathway proteolysis

occurs. Furthermore, I also identified the region within the TRP-ML1 amino acid sequence where cleavage occurs. The results of these studies are presented in Chapter 2.

SPECIFIC AIM 2: To determine the molecular events that lead to MLIV pathogenesis. Two primary models exist to explain TRP-ML1 function and subsequent MLIV pathogenesis. The goal of this aim was to determine if TRP-ML1 functions to regulate specific membrane trafficking events along the endocytic pathway, or if any observed abnormalities in trafficking were due to the chronic build-up of undigested lipid material present in MLIV patient fibroblasts. In addition, I sought to examine whether there were selective defects in protein or lipid hydrolysis in TRP-ML1-deficient cells. The results of these studies are presented in Chapter 3.

2.0 POSTTRANSLATIONAL CLEAVAGE AND ADAPTOR PROTEIN COMPLEX-DEPENDENT TRAFFICKING OF MUCOLIPIN-1

Mark T. Miedel, Kelly M. Weixel, Jennifer R. Bruns, Linton M. Traub, and Ora A. Weisz

The Journal of Biological Chemistry. Vol. 281, No. 18: 12751-12759 (2006).

2.1 ABSTRACT

Mucolipin-1 (TRP-ML1) is a member of the transient receptor potential ion channel superfamily that is thought to function in the biogenesis of lysosomes. Mutations in TRP-ML1 result in mucolipidosis type IV, a lysosomal storage disease characterized by the intracellular accumulation of enlarged vacuolar structures containing phospholipids, sphingolipids, and mucopolysaccharides. Little is known about how TRP-ML1 trafficking or activity are regulated. Here we have examined the processing and trafficking of TRP-ML1 in a variety of cell types. We find that a significant fraction of TRP-ML1 undergoes cell-type independent cleavage within the first extracellular loop of the protein during a late step in its biosynthetic delivery. To determine the trafficking route of TRP-ML1, we systematically examined the effect of ablating adaptor protein complexes on the localization of this protein. Whereas TRP-ML1 trafficking was not apparently affected in fibroblasts from *mocha* mice that lack functional AP-3, siRNA-mediated knockdown

revealed a requirement for AP-1 in Golgi export of TRP-ML1. Knockdown of functional AP-2 had no effect on TRP-ML1 localization. Interestingly, cleavage of TRP-ML1 was not compromised in AP-1 deficient cells, suggesting that proteolysis occurs in a prelysosomal compartment, possibly the *trans*-Golgi network. Our results suggest that posttranslational processing of TRP-ML1 is more complex than previously described, and that this protein is delivered to lysosomes primarily via an AP-1 dependent route that does not involve passage via the cell surface.

2.2 INTRODUCTION

Mucolipidosis type IV (MLIV) is an autosomal recessive lysosomal storage disorder characterized clinically by developmental abnormalities of the brain, impaired neurological and gastric functions, and ophthalmologic defects that include corneal opacity and retinal degeneration (6). At the cellular level, lysosomal storage bodies appearing as enlarged vacuolar structures are found in every cell type of affected individuals with the accumulated products, including a broad range of phospholipids, sphingolipids, and mucopolysaccharides (6, 17). Other classes of mucolipidoses include sialidosis (MLI), I-cell disease (MLII), and pseudo-Hurler polydystrophy (MLIII), where accumulation is a result of the impaired targeting and/or activity of the lysosomal hydrolases involved in the catabolism of the stored lipids. However, lysosomal hydrolase activity is not impaired in mucolipidosis type IV as the accumulated lipid products have been previously shown to be catabolized normally (14). Rather, mucolipidosis type IV pathophysiology has been linked to mutations in the transient

receptor potential (TRP) channel family member mucolipin-1 (TRPML subfamily; herein referred to as TRP-ML1), where mutations result in a defect in membrane sorting along the late endocytic pathway (19, 228, 240).

Mammalian TRP channels are a large class of proteins that are characterized by a common structure and permeability to both monovalent cations as well as Ca^{2+} ions (51, 102, 172). At least 20 mammalian TRP channels have been identified that comprise six TRP subfamilies. TRPs have widespread tissue distributions and have been implicated in diverse cellular functions including roles in mechanosensation, osmosensation, sensation of fluid flow in vascular endothelia, sensation of temperature, pain, and touch, and transepithelial transport of Ca^{2+} and Mg^{2+}. Specifically, mucolipin-1 (TRP-ML1) is a 580-amino acid protein that has a molecular mass of 65 kDa and has been localized to late endosomes/lysosomes in several cell types (156). Two other mammalian mucolipin family members have also been identified, TRP-ML2 and TRP-ML3. While little is known regarding TRP-ML2 function, mutations in the mouse *Mcoln3* gene are associated with deafness and pigmentation defects in varitint-waddler (Va) mice (64). TRP-ML1 is suggested to be a multiple sub-conductance and non-specific cation channel where activity is modulated by both Ca^{2+} and pH (40, 208), indicating that this protein may be involved in trafficking or fusion events between late endosomes and lysosomes in the late endocytic pathway (136, 138). TRP-ML1 has six predicted transmembrane-spanning segments and is oriented with both the amino- and carboxy-termini in the cytoplasm (Figure 2.4A), a characteristic trait of all TRP channel family members. The TRP domain of TRP-ML1 spans transmembrane segments 3-6 with the pore region occurring between the fifth and sixth segments. Additionally, TRP-ML1 has

a large extracellular loop, located between the first and second transmembrane segments that have four consensus N-linked glycosylation sites. Among other TRP family members, only polycystin-2 (TRPP subfamily) shares this feature of having a large extracellular loop. It is thought that this large extracellular loop may be involved in channel activation as both TRP-ML1 and polycystin-2 have relatively short amino- and carboxy-terminal cytoplasmic tails that often serve as activation regions for other cation channels. TRP-ML1 also has a carboxy-terminal dileucine targeting motif that has been postulated to serve as the lysosomal targeting signal for TRP-ML1 (19, 240).

Much of what is presently known regarding TRP-ML1 has come from studies in *Caenorhabditis elegans* where the TRP-ML1 functional orthologue, CUP-5, has been identified. Mutations in the *cup-5* gene have been described to cause a defect in lysosome biogenesis since CUP-5 is localized to both late endosome-lysosome fusion sites as well as to mature lysosomes. The observed endocytic abnormalities observed in *cup-5* mutants were rescued upon addition of either human TRP-ML1 or TRP-ML3 (248). Therefore, it is hypothesized that ML1 may be responsible for regulating fusion events during the biogenesis of lysosomes (70, 196, 248). However, little is known about how TRP-ML1 is targeted to late endosomes/lysosomes, or how this ion channel may function to regulate membrane trafficking events along this pathway.

Here, we have investigated the posttranslational processing and trafficking of TRP-ML1. We find that TRP-ML1 is cleaved at a site between the second and third N-glycans of the first extracellular loop. Delivery of TRP-ML1 to lysosomes occurs via a direct pathway dependent on adaptor protein complex-1 (AP-1) and does not involve passage via the cell surface. TRP-ML1 cleavage occurs late in the biosynthetic

pathway, after the glycans have been sialylated, but prior to lysosomal delivery, as inhibition of lysosomal delivery does not prevent cleavage. The apparently exclusive requirement for AP-1 in TRP-ML1 delivery suggests that surface delivery of this channel may have physiologically detrimental effects on cells.

2.3 MATERIALS AND METHODS

DNA constructs. Constructs encoding human TRP-ML1 (corresponding to Accession Number BC005149) double-tagged with HA at the amino terminus and with myc upstream of the carboxy-terminal dileucine motif, or tagged individually with HA or myc epitopes were provided by Kirill Kiselyov (121). A double-tagged TRP-ML1 construct in which a premature stop codon was inserted into the TRP-ML1 open reading frame prior to the lysine residue at amino acid position 577 (TRP-ML1 ΔLLVN) was also a gift of Dr. Kiselyov.

Site-directed mutagenesis. The mutations N179A, N220A, N230A, R200A, and K219A were generated using the QuikChange site-directed mutagenesis kit (Stratagene) according to the manufacturer's protocol. Mutations and overall plasmid integrity were confirmed by direct DNA sequencing. The following forward (F) and reverse (R) primer pairs were used to introduce desired mutations:

N179A (F): 5'-CGTGGACCCGGCC**GCC**GACACATTTGAC-3'

N179A (R): 5'-GTCAAATGTGTC**GGC**GGCCGGGTCCACG-3'

N220A (F): 5’-GGAAAGCAGCTCCAGTTACAAG**GCC**CTCACGCTC-3’

N220A (R): 5’-GAGCGTGAG**GGC**CTTGTAACTGGAGCTGCTTTCC-3’

N230A (F): 5’- CCACAAGCTGGTC**GCT**GTCACCATCCACTTCC-3’

N230A (R): 5’-GGAAGTGGATGGTGAC**AGC**GACCAGCTTGTGG-3’

R200A (F): 5’-GATCCCCCCGAG**GCG**CCCCCTCCGCC-3’

R200A (R): 5’-GGCGGAGGGGG**CGC**CTCGGGGGGATC-3’

K219A (F): 5’-GGAAAGCAGCTCCAGTTAC**GCG**AACCTCACGCTCAAATT-3’

K219A (R): 5’-GAATTTGAGCGTGAGGTT**CGC**GTAACTGGAGCTGCTTTCC-3’

Insertion of an external HA epitope tag. We used a modified version of the QuikChange (Stratagene) site-directed mutagenesis protocol (263) to incorporate an HA epitope tag into the first extracellular loop between amino acids 249 (Glu) and 250 (Ile) of myc-tagged TRP-ML1 [referred to as ML1-HA(ext)]. The following primers were used: (underlined and bolded text indicate nucleotides corresponding to the HA epitope sequence).

(Forward) 5’-

CAGAGCCTCATCAATAATGAG**ATGTACCCATACGATGTTCCAGATTACGCT**ATCCC

GGACTGCTATACCTTC-3’

(Reverse) 5’-

GAAGGTATAGCAGTCCGGGAT**AGCGTAATCTGGAACATCGTATGGGTACAT**CTCA

TTATTGATGAGGCTCTG-3’

Cell culture and transient transfection. HEK293 and HeLa SS6 cells were maintained in Dulbecco's Modified Eagle's Medium (DMEM) supplemented with 10% fetal bovine serum (FBS) and 100µg/ml penicillin/streptomycin. Primary cultures of rabbit cornea epithelial cells were provided by Emily Guerriero and Nirmala SundarRaj (University of Pittsburgh), and were maintained in DMEM-F12 supplemented with: 40µg/ml Gentamicin, 0.5% DMSO, 5µg/ml bovine insulin, 10ng/ml human epidermal growth factor, 0.1 µg/ml Cholera toxin, 50 U/ml penicillin, 50µg/ml streptomycin, and 8% FBS. NIH 3T3 and *mocha* fibroblasts were provided by Gudrun Ihrke (Uniformed Services Univ. of the Health Sciences) and were maintained in DME supplemented with 10% FBS and 100 µg/ml penicillin and streptomycin. For transient transfections, cells were plated in either 6 or 24 well plates at 30% confluence and incubated until cells reached ~75-80% confluence. Transient transfections using Lipofectamine 2000 (Invitrogen) were performed according to the manufacturer's protocol. For HEK 293 cells or fibroblasts cultured in 6 well plates the DNA-to-Lipofectamine 2000 ratio used was 2µg DNA: 5µl Lipofectamine. For HeLa SS6 cells or fibroblasts grown in 24 well plates the ratio used was 0.8µg DNA: 2µl Lipofectamine 2000.

Immunoblotting of TRP-ML1. Transiently transfected cells were solubilized in 1.5 % (v/v) C12E9 (Calbiochem) in buffer containing 150mM NaCl, 1mM EDTA, and 40mM HEPES, pH 7.4. This detergent solution was additionally supplemented with 1µg/ml aprotinin and complete mini EDTA-free protease inhibitor cocktail tablets (Roche). Samples were immunoprecipitated using monoclonal anti-HA (HA.11; Covance) or

monoclonal anti-c-myc (Upstate) antibodies. Antibody-antigen complexes were recovered using Pansorbin cells (Calbiochem). Samples were then washed one time each in HBS (10mM HEPES, 150mM NaCl, pH 7.4) containing either 1% Triton X-100 or 0.01 % SDS, then washed one final time in HBS alone. Samples were solubilized in Laemmli sample buffer and heated to 60°C for 30 min, and loaded onto 4-15% Tris-HCl precast gels (BioRad). Electrophoresis and transfer to Highbond-ECL nitrocellulose membrane (Amersham Biosciences) was performed using the Criterion Western Blotting system (BioRad). Membranes were then incubated for 2 h with anti-HA-HRP or anti-c-myc-HRP (Roche). HRP reactive bands were detected using Super Signal West Pico chemiluminescent substrate (Pierce) and membranes were exposed to Kodak X-Omat Blue film. The relative molecular mass of immunoreactive bands was assessed using Precision Plus Protein Standards (BioRad). Samples treated with N-glycanase (New England Biolabs) were immunoprecipitated with monoclonal anti-HA antibody and immunocomplexes recovered as described above. Samples were washed and eluted for 30 min at 60°C with 10mM Tris-HCl, pH 8.6, 0.2% SDS, and 7.5% glycerol. Following elution, samples were subjected to brief centrifugation, the supernantants were recovered and 0.5 µl N-glycanase (New England Biolabs; 1.5 U active enzyme) was added to each sample. Control samples were treated identically except that N-glycanase was omitted from the incubation. Samples were incubated overnight at 37°C unless otherwise indicated. The following day, 2-fold concentrated Laemmli sample buffer was added to each sample (to a final volume of 30µl) and incubated at 60°C for 30 min. Samples were electrophoresed on 4-15% Tris-HCl gels and immunoblotted as described above.

Metabolic labeling of TRP-ML1. Transiently transfected HEK293 cells on 6 well plates were starved in cysteine- and methionine-free medium for 30 min, then radiolabeled with 1mCi/ml Tran[^{35}S]-Label (MP Biomedicals) for 2 h. Cells were chased in serum-free DMEM for 0 or 2 h, then solubilized and ML1 immunoprecipitated as described above. Samples were then either treated with N-glycanase as described above or directly solubilized in Laemmli sample buffer and incubated for 30 min at 60°C prior to electrophoresis on 4-15% Tris-HCl gels. Dried gels were analyzed using a phosphorimager (BioRad) and relative molecular mass of visualized bands was compared to Rainbow [^{14}C] methylated protein molecular weight markers (Amersham Biosciences). Where indicated, the following drugs were added during both the radiolabeling and chase periods: leupeptin (Sigma; 20µM), CA-074-Me (Calbiochem; 2µM), and Brefeldin A (Calbiochem; 10µg/mL).

Indirect Immunofluorescence. Transiently transfected cells grown on coverslips were fixed with 4% paraformaldehyde, permeabilized with 0.1% Triton X-100 in PBS containing 1% bovine serum albumin, and incubated in blocking solution (PBS containing 1% bovine serum albumin) for 30 min. Samples were incubated for 60 min in primary antibody at the following dilutions: mouse monoclonal anti-HA (1:500); rat monoclonal anti-HA (clone 3F10; Roche; 1:250; polyclonal anti-cathepsin D generated against the human peptide [1:250]; (71) monoclonal AP.6 directed against AP-2 α subunit (American Type Culture Collection 1:10); monoclonal anti-γ adaptin (BD biosciences; 1:250); monoclonal anti-giantin (1:400; gift from Dr. Adam Linstedt at

Carnegie Mellon University, Pittsburgh, PA), and monoclonal anti-lamp-2 directed against either the human epitope [H4B4] or mouse epitope [ABL-93] (Developmental Studies Hybridoma Bank, Iowa City, IA developed by J. Thomas August; 1:10). After washing, samples were incubated for 60 min with species-appropriate secondary antibodies conjugated to either AlexaFluor- 488 or AlexaFluor-647 (Invitrogen-Molecular Probes) diluted in blocking buffer (1:500). Confocal imaging was performed on an Olympus IX-81 (Melville, NY) equipped with an UltraView spinning disc confocal head (Perkin Elmer, Shelton, CT) and an argon-ion, argon-krypton and helium-cadmium laser combiner. Images were acquired with a 60x or 100x plan-apochromat objective (NA 1.4) and the appropriate filter combination. The TIFF images were imported into Adobe Photoshop (Adobe, Mountain View, CA) to adjust contrast and image size.

Antibody uptake assay. NIH 3T3 or *mocha* fibroblasts grown on coverslips were transfected where indicated to express ML1-HA(ext). Cells were incubated for 1 h at 37ºC in the presence of appropriate antibodies [monoclonal HA for ML1-HA(ext)-transfected cells or anti-murine lamp-2 (ABL-93; Developmental Studies Hybridoma Bank) for untransfected cells] diluted to 50µg/mL in DMEM containing 1% BSA and 25mM HEPES, pH 7.4. Leupeptin (20µM) was included during the incubation to minimize degradation of any lysosomally-delivered antibody. Cells were then washed three times with ice-cold PBS, fixed with 4% paraformaldehyde for 10 min, quenched with PBS-glycine, then permeabilized for 3 min with 0.5% Triton X-100, and blocked for 15 min in blocking solution. Following block, cells were incubated with fluorophore-

conjugated secondary antibody and processed for immunofluorescence as described above.

siRNA-mediated knockdown of AP-1 γ and AP-2 α subunits. Double-stranded siRNAs targeting human forms of either the AP-1 γ or AP-2 α subunit were purchased from Dharmacon (Lafayette, CO). For the AP-1γ subunit, the target sequence used was 5'-AAGTTCCTGAACTTATGGAGA-3' corresponding to nucleotides 528-548 of the human AP-1 complex γ1 subunit mRNA (Accession Number Y12226). For the AP-2 α subunit, the target sequence used was 5'-GCATGTGCACGCTGGCCA-3' corresponding to nucleotides 1233-1250 of the human AP-2 α2 subunit mRNA (Accession Number NM_012305) Three potential target sequences were tested in each case. HeLa SS6 cells were plated in 24 well dishes and allowed to grow to ~50% confluence. Cells were transfected with a non-silencing negative control siRNA duplex (Qiagen) or siRNA oligonucleotides targeted against the γ-subunit of AP-1 and/or the α-subunit of AP-2 using the *Trans*IT-TKO oligonucleotide transfection reagent (Mirus). For single knockdowns, 3μl siRNA oligonucleotide (20μM) and 4.5μl transfection reagent were added per well; for samples transfected with both α- and γ-siRNAs, 3μl of each oligonucleotide and 4.5μl transfection reagent were added. After 24 h, cells were transfected with cDNA encoding double-tagged ML1 [0.8μg; provided by Kirill Kiselyov; generated by Abigail Soyombo and Shmuel Muallem; University of Texas Southwestern] and Lipofectamine 2000 (2μl) and allowed to grow for an additional 18-24 h. Cells were either processed for immunofluorescence as described above or for immunoblotting. For Western blotting, cells were trypsinized and quenched with an

equal volume of DMEM, 10% FBS. After centrifugation, cell pellets were washed once with PBS and then solubilized in 95˚C 2-fold concentrated Laemmli sample buffer. After determination of relative protein concentrations by Coomassie stain, equal amounts of protein were loaded on a second 4-15% Tris-HCl gel and processed for Western blot using monoclonal anti-AP-2 α (Santa Cruz; 1:5000), polyclonal anti-AP-1 γ [AE/1; (247); 1:2000], and E7 anti-β-tubulin monoclonal antibody (1:5000; Developmental Studies Hybridoma Bank, Iowa City, IA developed by M. Klymkosky). TRP-ML1 was detected in siRNA-treated samples after solubilization, immunoprecipitation, and immunoblotting as described above.

[^{3}H]-palmitate labeleing. [^{3}H]-palmitic acid for metabolic labeling of cells was obtained from Perkin-Elmer Corp. HeLa or HEK293 were transfected with the appropriate TRP-ML1 cDNA constructs as described above. For optimal palmitate labeling, cells were grown on 6 well (35 mm) culture dishes. If necessary, multiple wells are able to be combined to enhance signal detection. Cells were briefly washed with PBS to remove culture medium. The final volume of labeling medium for each well is 2 mL and is comprised of DMEM supplemented with 1% FBS and [^{3}H]-palmitate. For each dish to be labeled, ~175 µCi [^{3}H] palmitate/dish was used. [^{3}H] palmitate is supplied at a concentration of 5 mCi/mL (in ethanol) and should be stroed at -20ºC. Once in labeling media, cells are incubated overnight (at least 12h) at 37ºC in a humidified incubator containing CO_2. After labeling is complete, cells are washed gently 3X with PBS, solubilized with 1.5% C12E9 as described above, immunoprecipitated with anti-HA antibody, and subjected to SDS-PAGE. Following electrophoresis, samples are

transferred to a nitrocellulose membrane. Following transfer, the membrane is dried and exposed to a ^{3}H screen (for at least 4-5 days) and subjected to densitometry analysis to determine amount of palmitate labeling

2.4 RESULTS

2.4.1 TRP-ML1 is cleaved late in the biosynthetic pathway

Western blot analysis of transiently-expressed TRP-ML1 demonstrated multiple immunoreactive species that could represent proteolytic processing. To examine this further, we expressed a construct encoding TRP-ML1 containing an amino-terminal HA and an internal carboxy-terminal myc epitope tag in HEK293 cells. Cell lysates were immunoprecipitated with anti-HA antibody, immunoblotted using HRP-conjugated anti-HA, and then stripped and reprobed using HRP-conjugated anti-myc antibody. As shown in Fig. 2.1A, full length TRP-ML1 was detected using either antibody as a doublet at ~60-70 kD that likely represents the immature and mature glycosylated forms of the protein. In addition, a ladder of more slowly migrating bands was also observed (see also Fig. 2.1C), consistent with multimerization of this highly hydrophobic protein. Numerous approaches to dissociate these multimers were unsuccessful. In the anti-HA blot, an additional band at ~37 kDa was detected, whereas when the same blot was re-probed with anti-myc, a distinct band at ~40 kDa was seen. These data suggest that TRP-ML1 is cleaved into two roughly equal-sized fragments that can be co-isolated

upon immunoprecipitation with an antibody against the N-terminal tag. The same results were obtained when TRP-ML1 was immunoprecipitated using anti-myc antibody (Fig. 2.1C). Consistent with its hydrophobic character, the carboxy-terminal myc-reactive product also appeared to be sensitive to aggregation, as bands corresponding to dimers and higher order multimers of this cleavage product were routinely visualized by antibodies against the myc epitope.

To determine whether the proteolytic cleavage event occurs early or late in the biosynthetic processing of TRP-ML1, we radiolabeled HEK293 cells transiently expressing TRP-ML1 for 2 h, and solubilized the cells after a 0 or 2 h chase period. Lysates were immunoprecipitated using either anti-HA or anti-myc antibody and examined by SDS-PAGE. As shown in Fig. 2.1B (top panel), TRP-ML1 was initially precipitated as a ~65-75 kDa doublet representing immature and fully glycosylated (sialylated) full length protein. After the 2 h chase period, the immature glycosylated form of TRP-ML1 was no longer detected, consistent with N-glycan processing. At this time point, a broad band migrating at ~40 kDa was also detected, presumably representing the amino- and carboxy-terminal TRP-ML1 cleavage fragments, which migrate with similar mobility on SDS-PAGE. The appearance of these cleavage products concomitant with maturation of the glycans on TRP-ML1 strongly suggests that proteolysis occurs after sialylation rather than early in the biosynthetic pathway. To further examine TRP-ML1 processing, HEK293 cells were treated with Brefeldin A (BFA) to prevent transit of newly synthesized TRP-ML1 along the biosynthetic pathway. In cells treated with BFA, both cleavage and N-glycan processing are abolished, as is indicated by the absence of the ~40 kDa cleavage product and the loss of the ~65-75

kDa doublet after the 2 h chase period (Fig. 2.1B; bottom panel). These results strongly suggest that cleavage of TRP-ML1 occurs at a post-ER site. Importantly, the cleavage site within TRP-ML1 appears to be cell type-independent, as similar products were observed when TRP-ML1 was expressed in several other cell types, including HeLa, Madin-Darby canine kidney (MDCK), and rabbit cornea epithelial cells (Fig. 2.2).

Based on the sizes of the cleavage product, we hypothesized that cleavage occurs within the first, relatively large extracellular loop of TRP-ML1. This loop contains the only four potential N-glycosylation sites on TRP-ML1. Both cleavage products ($_{HA}$ML1 and ML1$_{myc}$) were sensitive to N-glycanase treatment, confirming that cleavage occurs within this loop (Fig. 2.1C). Interestingly, we reproducibly found that N-glycanase treatment of the carboxy-terminal half of the protein produced two distinct bands roughly 3 and 6 kDa smaller than the original fragment (indicated by arrows). These bands likely represent cleavage of either one or two N-glycans from this fragment, respectively. Longer treatments with N-glycanase demonstrated a precursor product relationship between the two, suggesting that cleavage of one of the N-glycans in this fragment is considerably more efficient than the other (Fig. 2.1D). We never observed complete conversion to the more rapidly migrating form, even when the N-glycanase treatment was carried out overnight and spiked with fresh enzyme.

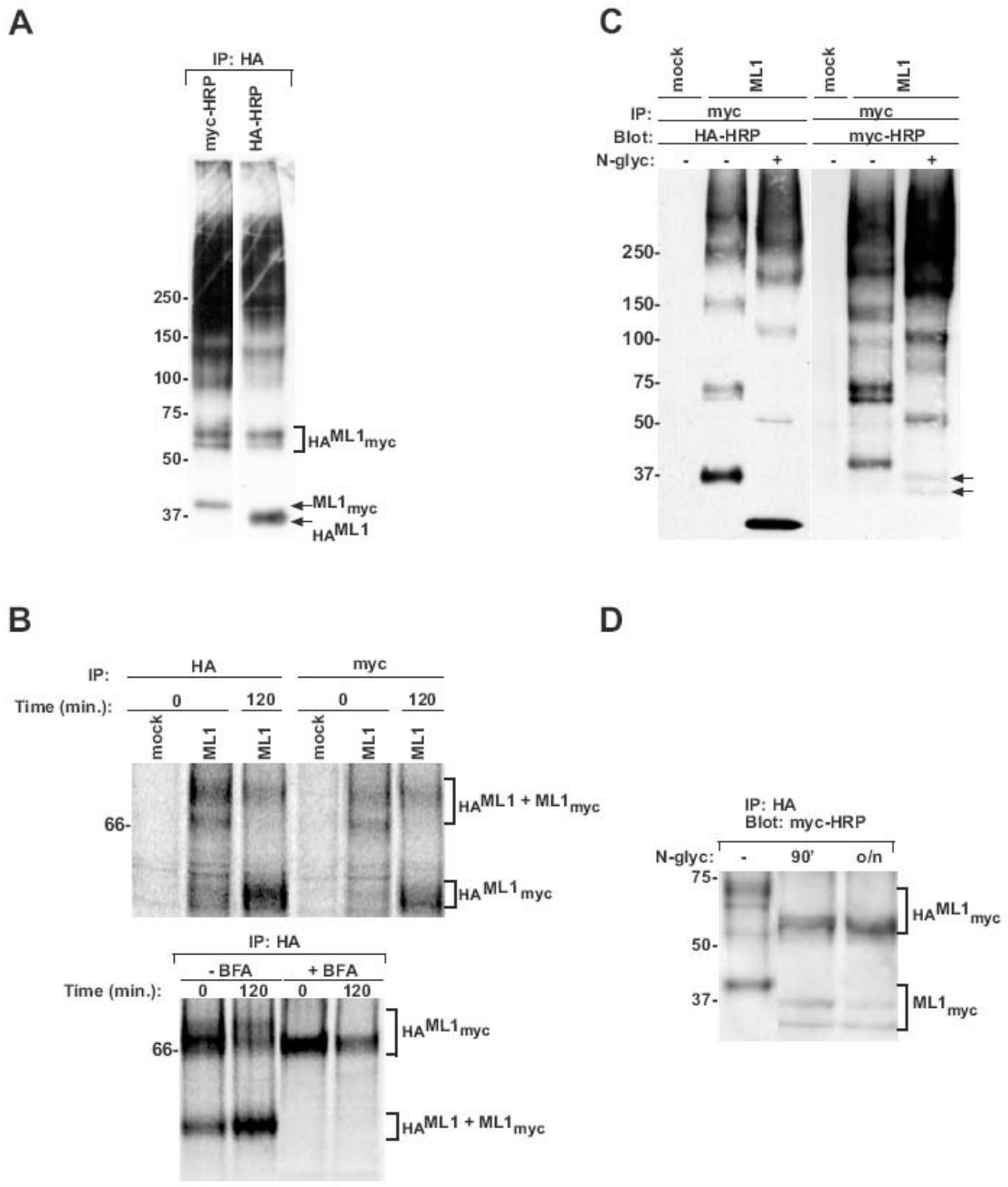

Figure 2.1 TRP-ML1 is cleaved late in the biosynthetic pathway.

(A) TRP-ML1 cleavage products co-precipitate. Cells expressing double-epitope-tagged TRP-ML1 were solubilized and immunoprecipitated using anti-HA antibody. After SDS-PAGE and transfer, the membrane was probed with HRP-myc (left), then stripped and re-probed with HA-HRP (right). (B) TRP-ML1 cleavage occurs late in the biosynthetic pathway. Mock or transfected cells were radiolabeled then chased +/- Brefeldin A (lower panel). Cells were solubilized, and samples immunoprecipitated with either anti-myc, or anti-HA, and subjected to SDS-PAGE. (C) Both N- and C-terminal TRP-ML1 cleavage products are glycosylated. Mock or transfected cells were prepared as described above, and then either mock-treated or treated with N-glycanase prior to SDS-PAGE and blotting with either anti-HA or anti-myc antibodies. (D) Lysates from TRP-ML1 expressing cells were immunoprecipitated with anti-myc antibody, and subjected to N-glycanase treatment for 90 min. or overnight prior to SDS-PAGE and Immunoblotting with myc-HRP antibody.

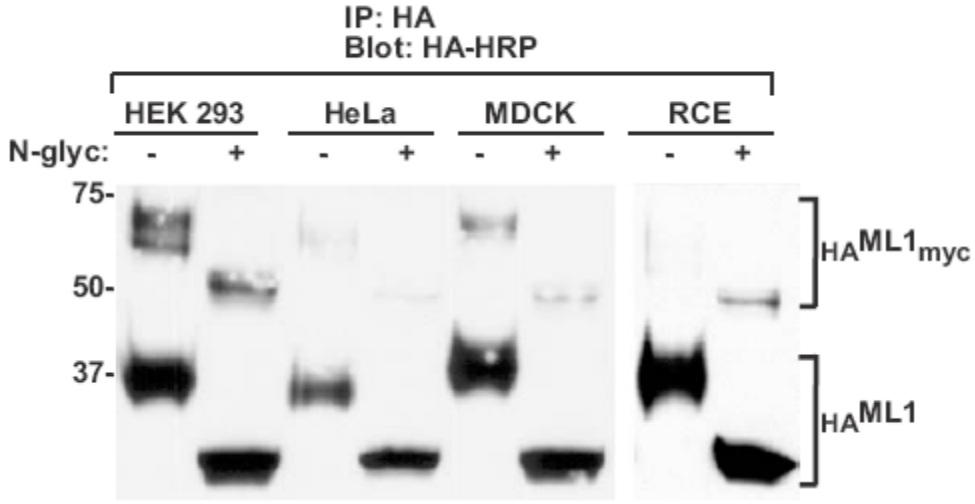

Figure 2.2 Cleavage of TRP-ML1 is not cell type-specific.

The indicated immortalized cell lines or primary cultures of rabbit cornea epithelial cells (RCE) were transiently transfected to express $_{HA}ML1_{myc}$. After solubilization, samples were immunoprecipitated using anti-HA antibody, mock-treated or treated with N-glycanase, and detected by immunoblotting using HRP-conjugated anti-HA antibody.

2.4.2 Cleavage of TRP-ML1 occurs between the second and third N-glycans of the first extracellular loop

Our initial N-glycanase experiments suggest that the carboxy-terminal fragment of TRP-ML1 contains at least two N-glycans. To test this more directly, we used site-directed mutagenesis to disrupt the N-glycosylation consensus sequences of the second, third, or fourth N-glycan, and examined the effect of these mutations on the electrophoretic mobility of the HA- and myc-tagged fragments immunoprecipitated from transiently transfected cells. As shown in Fig. 2.3, abolishment of the 2nd N-glycosylation consensus sequence (N179) affected the mobility of the N-terminal fragment (HA fragment) without disrupting the carboxy-terminal half (myc fragment) of the protein. In contrast, removal of the 3rd or 4th N-glycan had no effect on amino-terminal mobility but resulted in a shift in MW of the carboxy-terminal half of the protein. Interestingly, the resulting mobilities of the N220A and N230A carboxy-terminal fragments were different, suggesting that the 3rd and 4th glycans are normally processed somewhat differently. Such differential processing of N-glycans at distinct positions has previously been observed (155). These data are consistent with cleavage of TRP-ML1 at a site between the 2nd and 3rd N-glycans (amino acids 179-220).

The amino acid sequence of the interval between the 2nd and 3rd N-glycans of TRP-ML1 is shown in Fig. 2.4A. Because this sequence contains two basic residues that are potential cathepsin cleavage sites, we tested the effect on TRP-ML1 cleavage by mutating these residues to alanine. In neither mutant (R200A or K219A) was cleavage demonstrably affected (Fig. 2.4B). Moreover, overnight incubation of TRP-ML1 transfected cells with the cathepsin inhibitor CA-074-Me (2 μM, Fig. 2.4C), a

selective inhibitor of cathepsins B and L, did not reproducibly inhibit TRP-ML1 cleavage as detected either on immunoblots (Fig. 2.4C, left panel) of cell lysates or in metabolically-labeled cells treated with inhibitor during the pulse and chase periods of the experiment (Fig. 2.4C, right panel). However, treatment of ML1-transfected cells with 20 μM leupeptin, which inhibits a broad spectrum of lysosomal serine, plasmin, and cysteine proteases, significantly reduced the amount of TRP-ML1 cleavage products detected in immunoblots and in metabolically-labeled cells (Fig. 2.4C). Thus, it appears that cathepsins are not solely responsible for TRP-ML1 cleavage, although it is possible that multiple proteases may be able to cleave within this region.

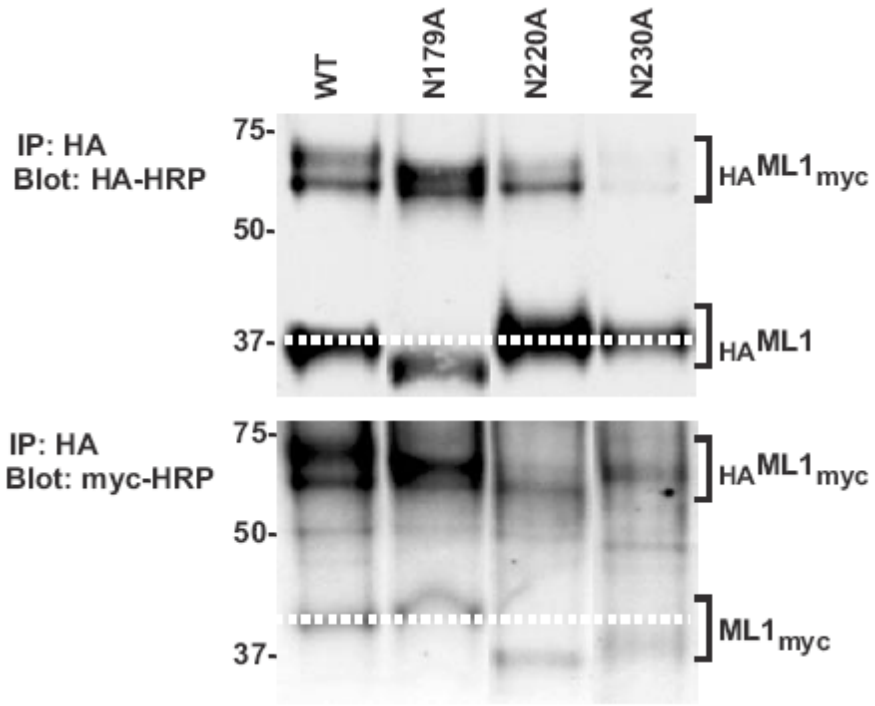

Figure 2.3 Cleavage of TRP-ML1 occurs between the 2nd and 3rd *N*-glycans of the first extracellular loop.

Double-tagged wild-type TRP-ML1 or TRP-ML1 glycosylation mutants (N179A, N220A, and N230A) were transiently expressed in HEK293 cells. After solubilization, cell lysates were immunoprecipitated with anti-HA antibody and samples were immunoblotted using HRP-conjugated anti-HA (top panel) or anti-myc (bottom panel). The dashed lines indicate the mobilities of the $_{HA}$ML1 and ML1$_{myc}$ fragments generated from wild-type ML1 relative to those of the mutant constructs. The migration of MW markers is noted on the left of each gel.

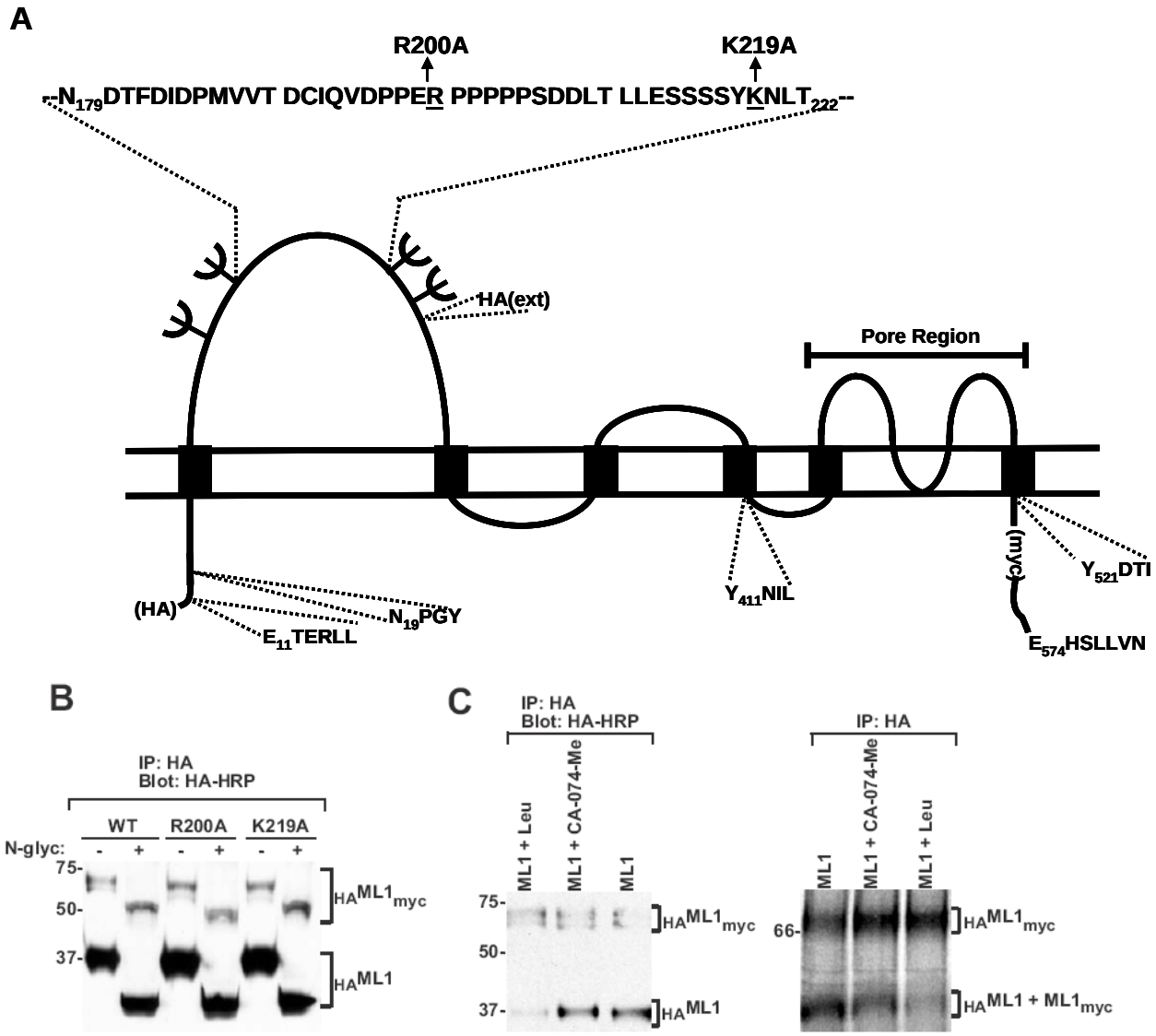

Figure 2.4 TRP-ML1 cleavage is inhibited by leupeptin.

Schematic representation of TRP-ML1 topology that highlights the placement of cytoplasmically-disposed and external epitope tags, important potential targeting motifs, the location of N-glycosylation sites (forked structures), and the sequence of TRP-ML1 between amino acids 179 and 220. Mutations R200A and K219A that disrupt potential cathepsin cleavage sites within this region are highlighted. (Panel B) $ML1_{R200A}$ and $ML1_{K219A}$ are cleaved normally. Cells were transfected with wild type or mutant TRP-ML1 constructs. Samples were immunoprecipitated with anti-HA antibody, mock-treated or treated with N-glycanase, and analyzed by immunoblotting with HRP-conjugated anti-HA. (C) Leupeptin prevents cleavage of ML1. (Left) Leupeptin or the cathepsin-specific inhibitor CA-074-Me was added to cells immediately after transfection, and 2-3 times subsequently over the next 24 h. Lysates were immunoprecipitated with anti-HA antibody and immunoblotted with anti-HA antibodies. (Right) Cells were radiolabeled then chased for 2 h either in the presence or absence of inhibitor. Cells were subsequently solubilized, immunoprecipitated with anti-HA antibodies, and subjected to SDS-PAGE.

2.4.3 Adaptor protein-dependent trafficking of TRP-ML1

ML1 contain several motifs that fit the consensus for AP complex binding, including tyrosine tetrapeptide YXXØ and dileucine motifs (Fig 2.4A). To date, three of the four AP complexes in cells (AP-1, AP-2, and AP-3), as well as the Golgi-localized, γ-ear-containing, ARF-binding (GGA) proteins, have been implicated in the biosynthetic delivery of membrane proteins to late endosomes/lysosomes (27). In previous studies it has been speculated that the C-terminal dileucine motif E_{574}HSLLVN functions as the lysosomal targeting signal of TRP-ML1 (156, 240). This sequence is reminiscent of the consensus motif for protein binding to the VHS domain of the GGAs [DxxLL, typically located 1-2 residues from the carboxy terminus] (27). The aspartic acid residue within this binding motif cannot be substituted even with another negatively charged residue (45); however, the murine TRP-ML1 sequence fits this consensus exactly. A glutathione S-transferase-fusion of the cytoplasmic tail was unable to bind the VHS domain of GGA-1, GGA-2, or GGA-3, suggesting that GGA-mediated sorting is not involved in biosynthetic delivery of TRP-ML1. To test the role of this sequence in lysosomal targeting of TRP-ML1 directly, we examined the localization of a mutant version of TRP-ML1 (ΔLLVN), which lacks the carboxy-terminal four amino acids, in transiently transfected HeLa SS6 cells. Interestingly, this mutant, like wild-type TRP-ML1, exhibited significant co-localization with the lysosomal marker lamp-2 (Fig. 2.5), suggesting that the carboxy-terminal dileucine motif is not directly responsible for TRP-ML1 targeting. Consistent with a previously published report, we also observed TRP-ML1 staining in vesicular compartments that did not co-localize with lysosomal markers (156). However, in contrast with the same study, in which it was also reported that lysosomes in TRP-

ML1-expressing cells were more dispersed throughout the cytoplasm than in control cells, we did not observe any reproducible effect of TRP-ML1 overexpression on the distribution of lysosomal markers. The extent and rate of proteolytic cleavage of ΔLLVN were similar to wild type TRP-ML1 as determined by immunoblotting and metabolic labeling experiments.

We next systematically examined the effect of ablating AP complexes on the steady state distribution of TRP-ML1 in transiently transfected cells. To dissect the role of AP-3 in TRP-ML1 targeting, we compared the distribution of TRP-ML1 expressed in control mouse fibroblasts vs. fibroblasts derived from the *mocha* mouse that lacks functional AP-3 due to absence of the AP-3 δ subunit. The route taken by some lysosomal proteins, including lamp-2, is slightly altered in AP-3 deficient cells such that a greater fraction traffics via the plasma membrane, but the protein ultimately accumulates in lysosomal compartments (61, 106, 269). Antibody uptake experiments were performed to confirm that more lamp-2 traffics through the plasma membrane in *mocha* cells compared with control fibroblasts. After incubation of live cells with anti-lamp-2 antibody for 1 h at 37ºC, cells were fixed, permeabilized, and incubated with secondary antibodies to detect internalized antibody. As shown in Figure 2.6C, internalized anti-lamp-2 antibody was observed in *mocha* cells but not in control fibroblasts. No staining was observed in either cell type when primary antibody was omitted from the assay.

To dissect the role of AP-3 in TRP-ML1 targeting, we used two approaches. First, we compared the steady-state distribution of TRP-ML1 by double-label indirect immunofluorescence in control and *mocha* fibroblasts to that of the lysosomal marker

lamp-2 (Fig. 2.6A; top two rows). Although TRP-ML1 in these cells was distributed in a punctate pattern reminiscent of lysosomes, there was significantly less co-localization between TRP-ML1 and lamp-2 in fibroblasts compared with HeLa cells (Fig. 2.5). Second, to examine whether a greater fraction of TRP-ML1 traffics via the cell surface in *mocha* cells, we used a TRP-ML1 construct [ML1-HA(ext)] in which an HA epitope tag was inserted into the first extracellular loop of the TRP-ML1 coding sequence. Both metabolic labeling and immunoblotting experiments demosntrated that ML1-HA(ext) is biochemically processed to mature and cleaved forms, suggesting that the protein is not grossly misfolded. Moreover, as shown in figure 2.6A (bottom row), the distribution of ML1-HA(ext) is qualitatively indistinguishable from that of the cytoplasmically-tagged TRP-ML1 construct used in the above panels of figure 2.6. However, antibody uptake experiments in 3T3 and *mocha* fibroblasts transiently expressing ML1-HA(ext) failed to reveal intracellular ML1 staining in either cell type (Fig. 2.6B). These results indicate that in the absence of functional AP-3, TRP-ML1 trafficking does not transit through the plasma membrane, and suggest that TRP-ML1 trafficking is not AP-3 dependent.

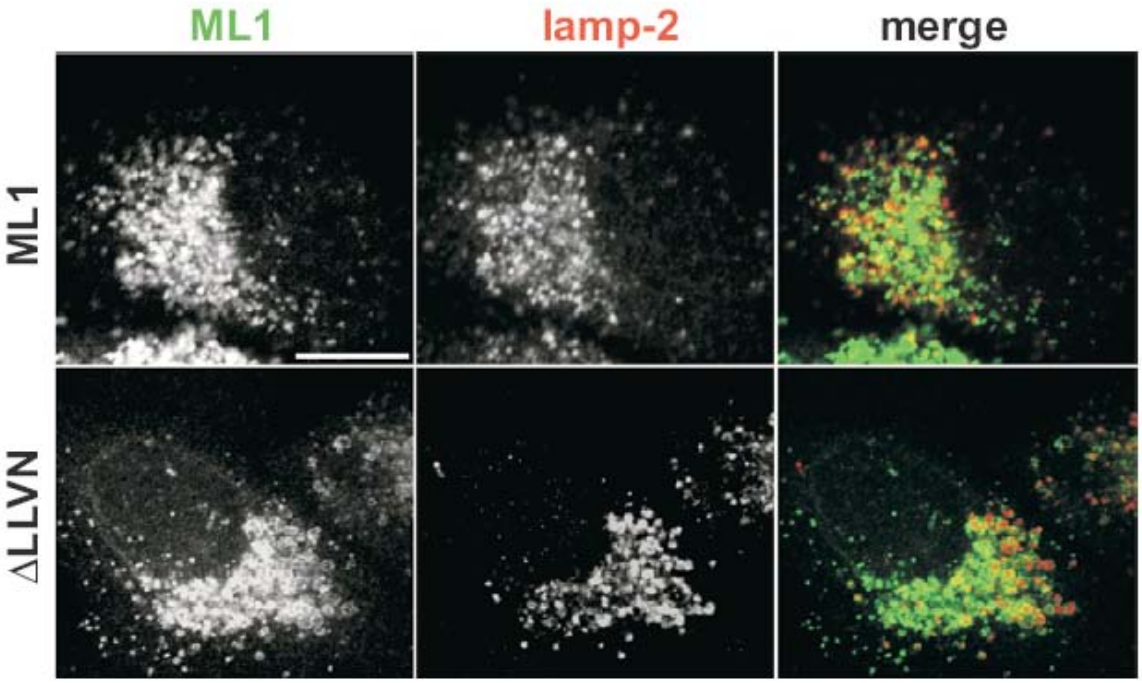

Figure 2.5 The steady state distribution of TRP-ML1 is independent of the carboxy-terminal LLVN sequence.

Transiently-transfected HeLa SS6 cells expressing double-tagged wild-type TRP-ML1 (upper panels) or $ML1_{\Delta LLVN}$ (lower panels) were fixed and processed for double-label indirect immunofluorescence to detect the N-terminal HA tag on each protein (left panels) and the lysosomal marker lamp-2 (middle panels). Merged images are shown in the right hand panels. Scale bar: 10 µm.

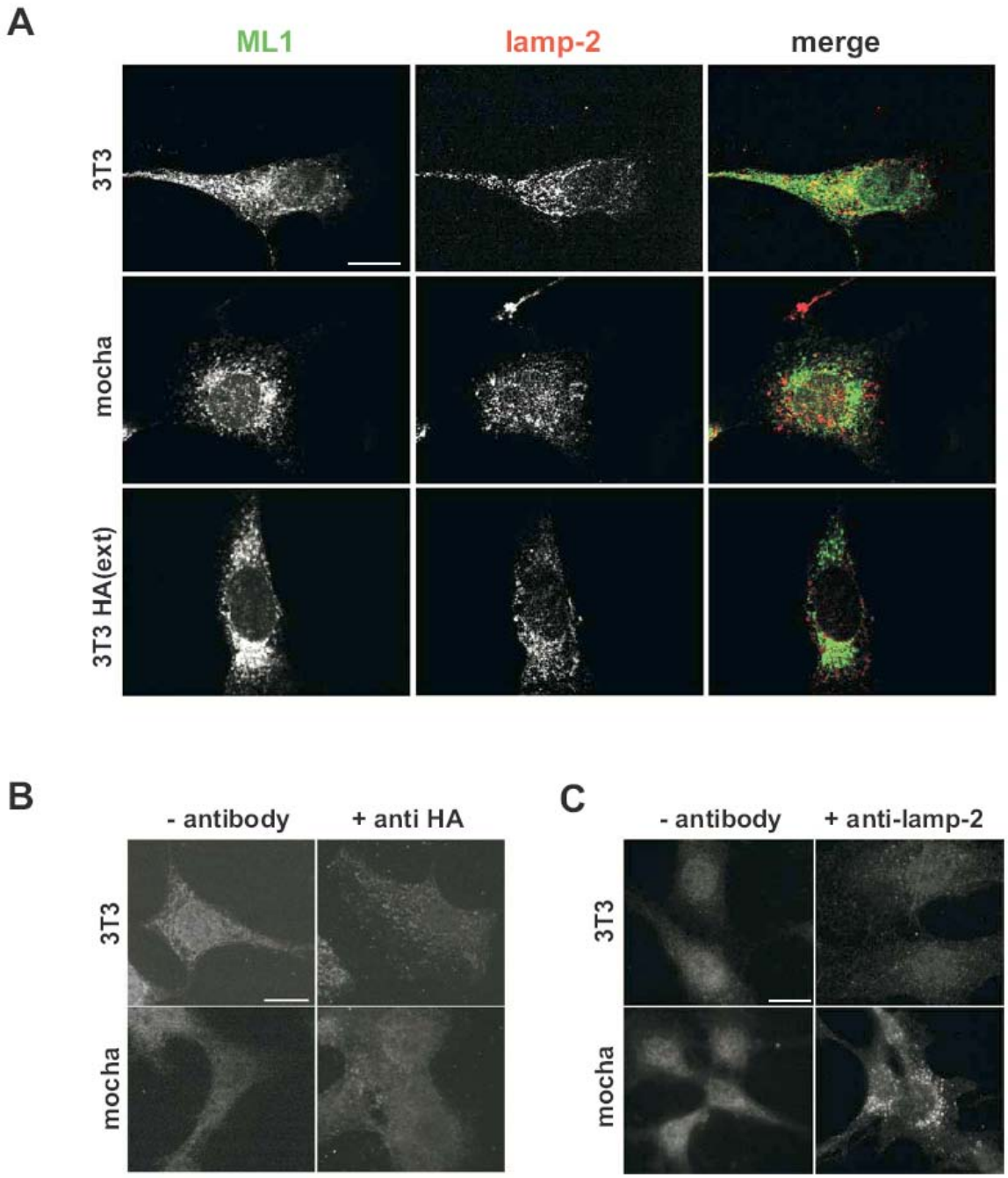

Figure 2.6 TRP-ML1 is not mislocalized in AP-3-deficient cells.

(A) Mouse 3T3 or *mocha* fibroblasts transiently expressing cytoplasmically (top two rows) or 3T3 cells expressing externally-tagged TRP-ML1 [ML1-HA(ext); bottom row] were fixed and processed for double-label indirect immunofluorescence to detect the HA tag and the lysosomal marker lamp-2. Merged panels are shown on the right. Scale bar: 10 µm. (B and C) ML1 trafficking is not AP-3 dependent. 3T3 or *mocha* fibroblasts transiently expressing ML1-HA(ext) were incubated for 1 h at 37ºC with either anti-HA (B) or anti-lamp-2 (C) antibody. Control cells in each panel were incubated under identical conditions in the absence of antibody. Cells were then washed repeatedly with ice cold PBS, fixed, and incubated with secondary antibody. Samples were viewed by confocal microscopy and the images in each panel were acquired under identical conditions. Scale bars: 10 µm.

To test the role of AP-1 and AP-2 in TRP-ML1 targeting, we used a siRNA knockdown approach. HeLa cells were transfected with siRNA oligonucleotides targeted against the γ-subunit of AP-1 and/or the α-subunit of AP-2, and the following day transfected with cDNA encoding epitope-tagged TRP-ML1. Immunoblotting and indirect immunofluorescence confirmed that both γ- and α-adaptin were efficiently and reproducibly knocked down by their respective siRNAs (Fig. 2.7). HeLa cells treated with both siRNAs and transfected with TRP-ML1 remained viable over the course of the experiment, even though knockdown of both adaptins was also very efficient (Fig. 2.7, A and D). Knockdown of α-adaptin had no effect on the distribution of TRP-ML1 (Fig. 2.7B); however, knockdown of γ-adaptin alone or in combination with α-adaptin resulted in a dramatic redistribution of TRP-ML1 (Fig. 2.7, C, and D). In particular, whereas a significant fraction of TRP-ML1 in control cells localized to clusters of enlarged, spherical vesicles in the cytoplasm, TRP-ML1-positive vesicles were rarely observed in cells lacking γ-adaptin. To examine the distribution of TRP-ML1 in these cells further, we performed double label indirect immunofluorescence using antibodies against the HA tag on ML1 and either the *cis-/medial*-Golgi marker giantin or the soluble lysosomal hydrolase cathepsin D (Fig. 2.8). The half-life of cathepsin D is extremely long [>50 h; (71)], and any mis-sorted protein is secreted into the medium; thus this protein serves as an ideal marker for lysosomes in siRNA treated cells. In control cells, we observed significant colocalization with cathepsin D, and in particular, cathepsin D staining was frequently visualized within the lumen of TRP-ML1-positive vesicular profiles (Fig. 2.8A; arrowheads in inset). A small portion of TRP-ML1 in these cells was also observed in a ribbonlike pattern that abutted the giantin staining profile, consistent with transit of newly

synthesized protein through the Golgi and *trans*-Golgi network (TGN; Fig. 2.8B). In contrast, very little colocalization of TRP-ML1 with cathepsin D could be detected in cells treated with siRNA to knock down γ-adaptin. In these cells cathepsin D staining was largely segregated from TRP-ML1-positive compartments (Fig. 2.8A), and the majority of TRP-ML1 staining colocalized with or adjacent to giantin (Fig. 2.8B). Similar results were obtained in cells lacking both α- and γ-adaptin. In addition, biochemical analysis by cell surface biotinylation revealed a slight increase in the amount of TRP-ML1 present at the plasma membrane in cells lacking γ-adaptin compared with control (~1% of total in control cells vs. 2.5% of total upon γ-adaptin knockdown). Together, these data suggest that AP-1 plays a critical role in the export of TRP-ML1 from the Golgi complex, and that TRP-ML1 normally traffics to lysosomes primarily via a direct route that bypasses the plasma membrane. When γ-adaptin is knocked down, TRP-ML1 accumulates in the Golgi complex, although a small amount may traffic via the cell surface to lysosomes. Moreover, AP-3 does not appear to be able to compensate for the lack of AP-1 to target TRP-ML1 to lysosomes in cells lacking γ-adaptin.

Because depletion of γ-adaptin inhibits lysosomal delivery of TRP-ML1, we examined whether cleavage of TRP-ML1 is impaired when individual AP complexes are disrupted. Interestingly, we found no effect on TRP-ML1 cleavage relative to control in cells lacking functional AP-1, AP-2, or AP-3 (Fig. 2.9). Thus, cleavage of TRP-ML1 can occur in the absence of efficient delivery to late endosomes/lysosomes.

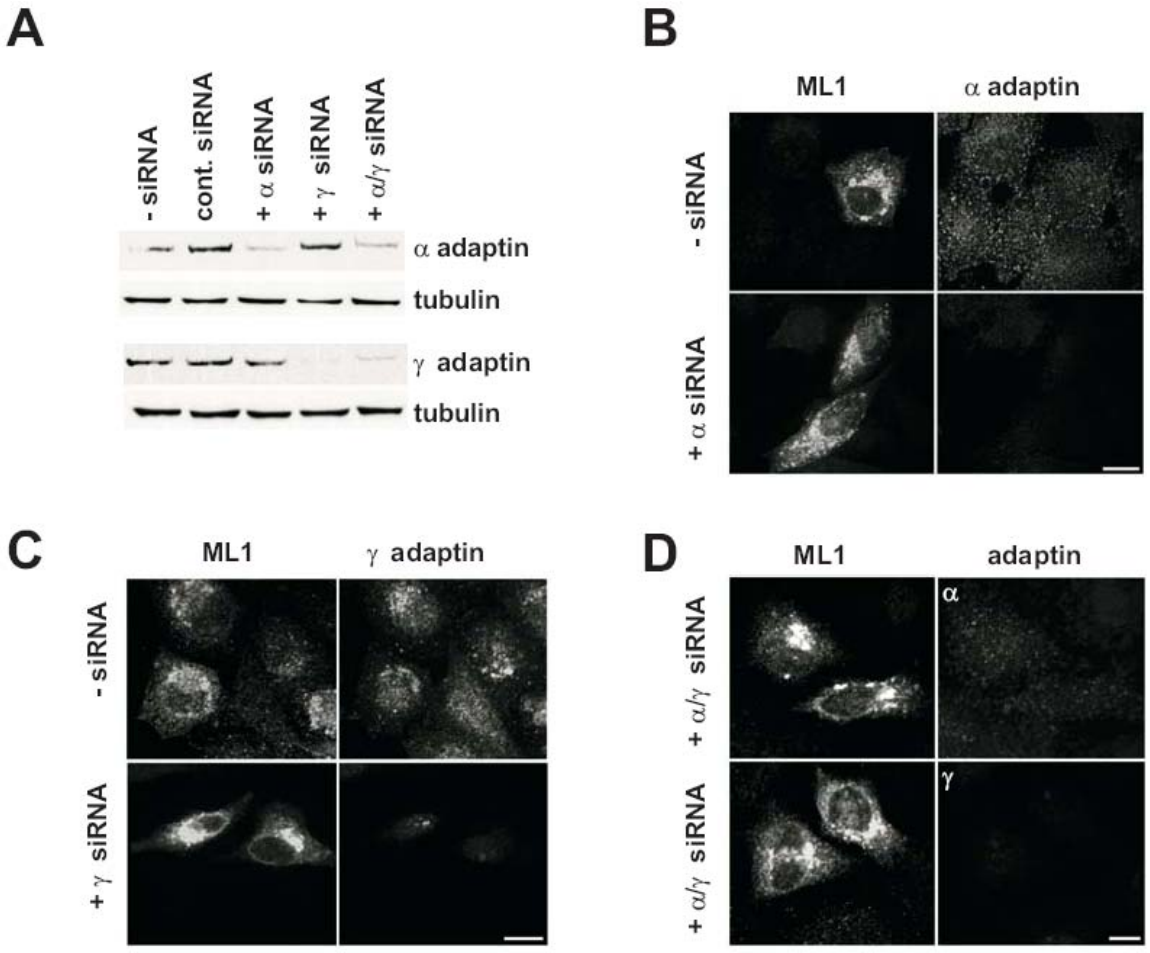

Figure 2.7 TRP-ML1 localization is AP-1-dependent.

(A) siRNA-mediated knockdown of α and/or γ adaptin. HeLa SS6 cells were mock-transfected, transfected with a control siRNA oligonucleotide, or with oligonucleotides targeting α and/or γ adaptin. Approximately equal amounts of cell lysates (normalized by Coomassie staining) were immunoblotted to detect α and γ adaptin as indicated. The bottom portion of each gel was blotted separately to detect tubulin as an additional loading control. (B) ML1-expressing cells that were either mock-transfected or transfected with oligonucleotides targeting α and/or γ adaptin were fixed and processed for double-label indirect immunofluorescence to detect ML1 and either α adaptin (B), γ adaptin (C), or both (panel D) as indicated. Scale bars: 10 μm.

Figure 2.8A

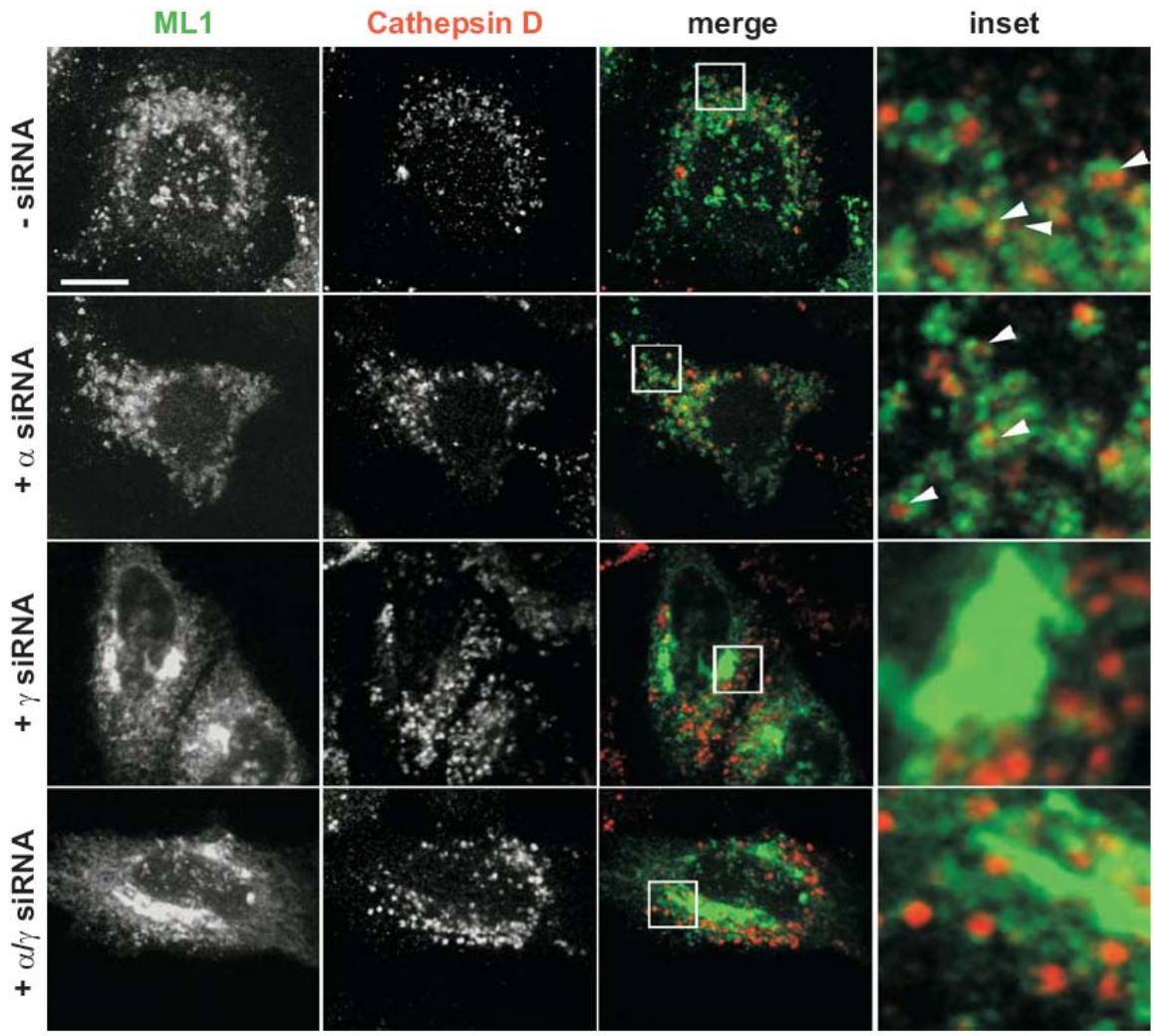

Figure 2.8B

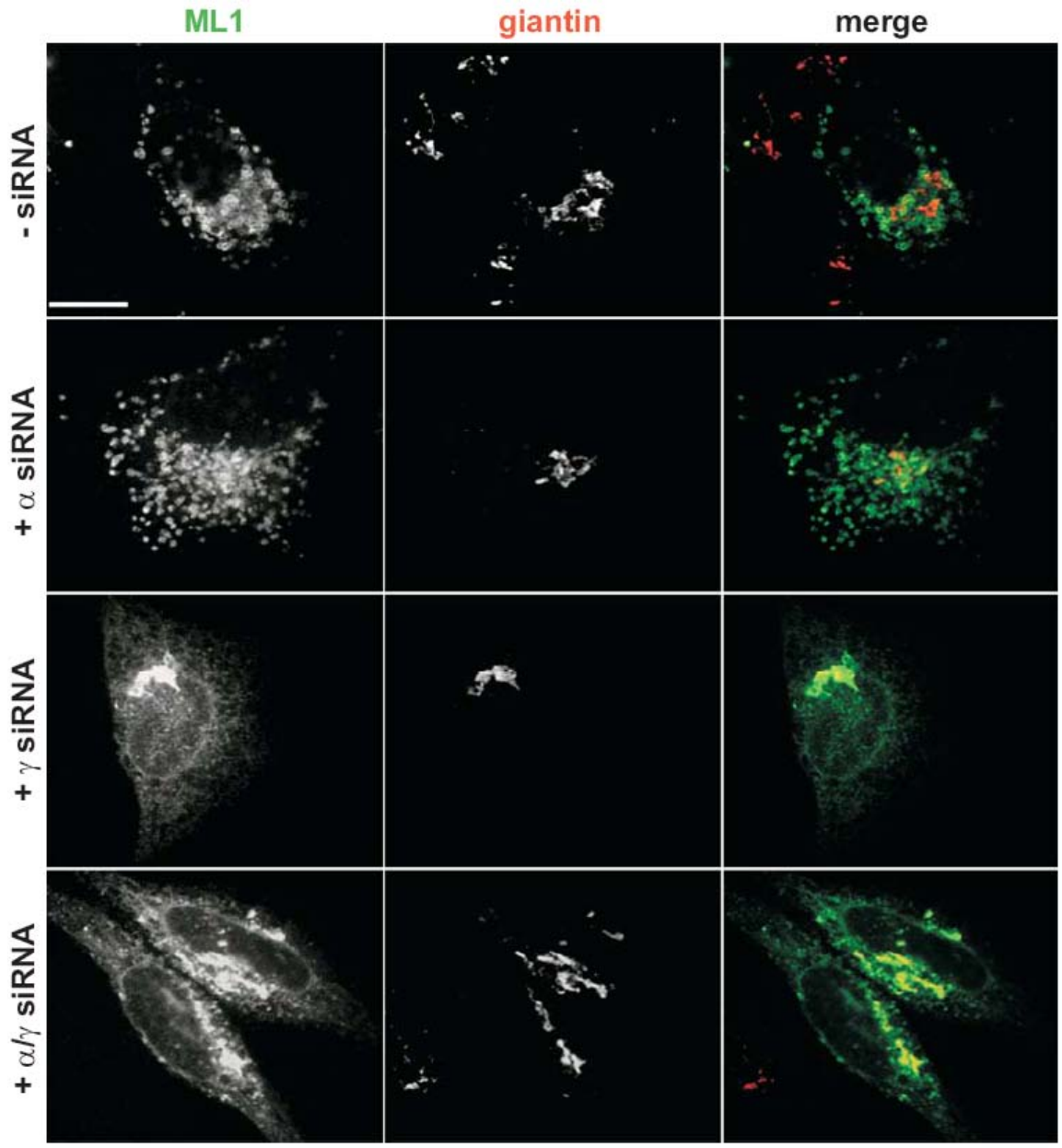

Figure 2.8 TRP-ML1 in γ-adaptin knockdown cells is retained in the Golgi complex.

TRP-ML1-expressing HeLa SS6 cells that were transfected with control siRNA or with oligonucleotides targeting α and/or γ adaptin were fixed and processed for double-label indirect immunofluorescence to detect ML1 and either the lysosomal marker cathepsin D (A) or the Golgi marker giantin (B). Insets in panel A show enlargements of the boxed regions in the merged panels. Arrowheads highlight cathepsin D staining within ML1-positive vesicles in control and α-adaptin knockdown cells. In contrast, the ML1 and cathepsin D staining profiles did not overlap significantly in cells lacking γ-adaptin or in double-knockdown cells. In these cells, ML1 was observed largely concentrated in juxtanuclear regions that are coincident with giantin staining. Scale bar: 10μm.

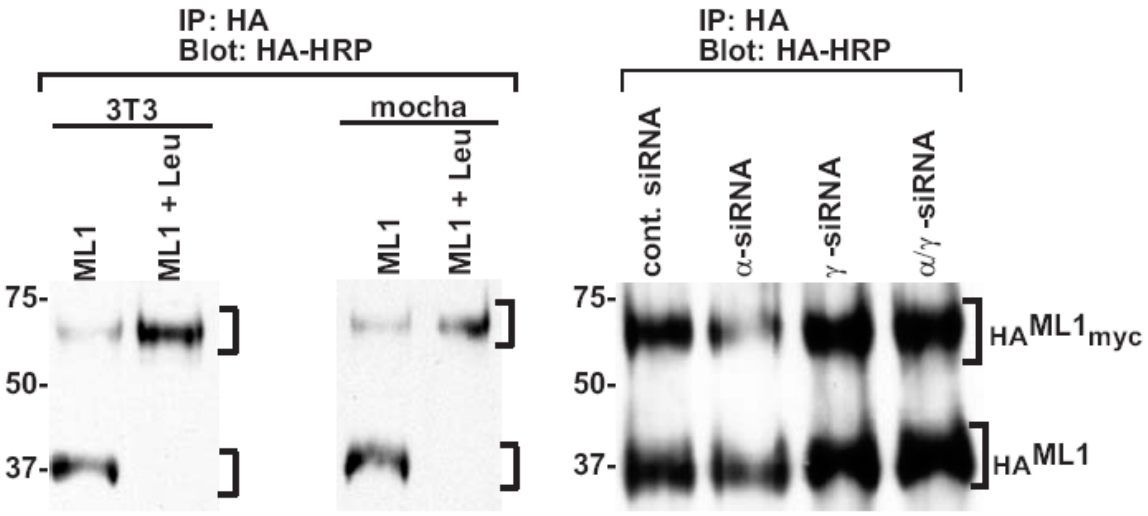

Figure 2.9 Cleavage of TRP-ML1 is unimpaired in cells lacking functional adaptor complexes.

Epitope-tagged ML1 was transiently expressed in 3T3 or *mocha* fibroblasts (left panel), or in HeLa cells transfected with the indicated siRNA oligonucleotides (right panel). Leupeptin was added to the indicated samples after transfection to inhibit cleavage of ML1. After solubilization, samples were immunoprecipitated using anti-HA antibody and detected by immunoblotting using HRP-conjugated anti-HA antibody. Full length ML1 and the amino-terminal cleavage product are indicated.

2.5 DISCUSSION

In summary, our data demonstrate that TRP-ML1 is cleaved by a leupeptin-inhibitable enzyme at a site between the second and third N-glycan of the first extracellular loop. Cleavage is likely to occur at a late step in the biosynthetic traffic of TRP-ML1, after maturation of the N-glycans. These observations are largely consistent with the recently reported findings of Kiselyov et al (121). TRP-ML1 is normally delivered to lysosomes via a direct route that does not require passage through the cell surface, as knockdown of α-adaptin had no effect on the steady state distribution of TRP-ML1. Trafficking of ML1 in AP-3 deficient *mocha* cells appeared to be normal, whereas delivery of lamp-2 in these cells was disrupted. However, in these cells we detect less overall colocalization of TRP-ML1 with various lysosomal markers. Interestingly, cleavage of TRP-ML1 was not prevented when access to lysosomes was prevented by siRNA-mediated knockdown of AP-1. Under these conditions, the majority of TRP-ML1 accumulated in the Golgi complex, suggesting that cleavage of TRP-ML1 normally occurs prior to lysosomal delivery, and possibly in the TGN.

Since TRP-ML1 targeting to lysosomes involves AP-1 but does not require the carboxy-terminal DxxLL-type dileucine motif, what constitutes the AP-1 recognition sequence? There are two tyrosine-containing sequences within cytoplasmically-disposed regions of TRP-ML1 that fit the YXXΦ motif; however one of these (Y_{521}DTI) is predicted to reside partly within the final transmembrane domain and the other (Y_{411}NIL) begins two amino acids after the fourth transmembrane domain. Neither of these sequences is optimally placed for access by AP complexes (185); moreover, both are predicted to have relatively poor affinity for AP-1 (184). Another AP-1 binding candidate

is an adaptor binding [DE]xxxL[LI]-type dileucine motif present at the amino terminus (E_{11}TERLL). We have detected palmitoylation of the amino terminus of TRP-ML1 *in vivo* (Fig. 2.10), and this modification might also contribute to the targeting of the protein. In addition, a potential adaptor-binding NPXY motif (N_{19}PGY) is also present nearby; however, NPXY motifs do not bind to AP-1. Consistent with our results, Vergarajauregui and Puertollano (259) reported while this manuscript was under review that the amino-terminal dileucine sequence plays a key role in lysosomal targeting of TRP-ML1, and moreover, that lysosomal delivery of TRP-ML1 occurs largely via the direct pathway. Surprisingly, however, whereas they report palmitoylation of the carboxy terminal region of TRP-ML1, they did not detect amino-terminal palmitoylation. Future studies will be required to resolve this discrepancy.

What is the significance of TRP-ML1 trafficking to lysosomes via the direct pathway? Recent studies suggest that TRP-ML1 is an outwardly-rectifying monovalent cation channel that may function as a proton leak channel to regulate lysosomal pH (121, 231). Based on these characteristics, significant levels of surface TRP-ML1 are predicted to result in depolarization of the cells and could disrupt normal cell function. Thus, trafficking to lysosomes via the direct route may be an obligatory pathway for TRP-ML1 that serves to limit its site(s) of activity.

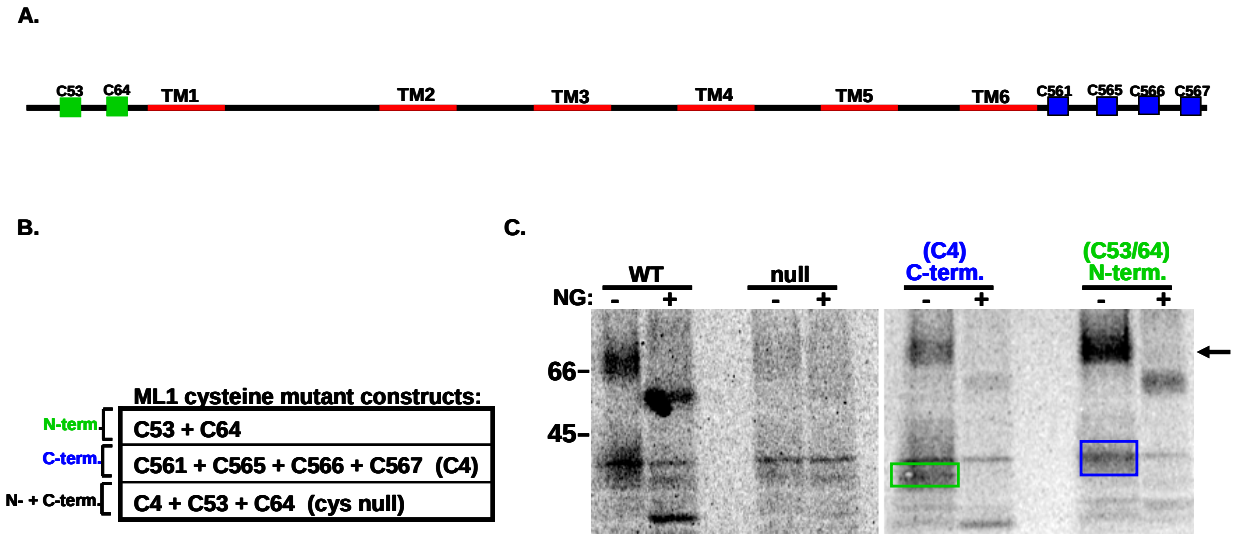

Figure 2.10 TRP-ML1 is palmitoylated on both its N- and C-terminal cytosolic tails.

(A) Schematic representation of cysteine residues within the TRP-ML1 cytosolic tails that may serve as palmitoylation sites. N-terminal cysteine residues are labeled green while C-terminal cysteines are labeled blue (B) Table representing constructs used to determine TRP-ML1 palmitoylation status. The first construct (C53/64) has both N-terminal (green) cysteine residues mutated to alanine. The second construct (C4) has all 4 C-terminal (blue) cysteine residues mutated, while the final construct (cys null) has both N- and C-terminal cysteine residues mutated. (C) HeLa SS6 cells were transfected with either HA-tagged wild type (WT), C53/64, C4, or cys null cDNAs were labeled with [^{3}H]-palmitate, solubilized, and immunoprecipitated with ant-HA antibodies. Samples were either left untreated (-) or treated with N-glycanase (NG) (+) before being subjected to SDS-PAGE and densitometry analysis. As indicated above, cells expressing the C4 (lanes 5 and 6) construct still demonstrate full length TRP-ML1 labeling (arrow) as well as labeling of the N-terminal TRP-ML1 fragment (green box). Cells expressing the C53/64 (lanes 7 and 8) construct are also positive for full length TRP-ML1 labeling (arrow) as well as labeling of the C-terminal TRP-ML1 fragment (blue box). These results demonstrate that both cytosolic tails of TRP-ML1 are palmitoylated. Expression of the cys null (lanes 3 and 4) construct abolishes TRP-ML1 palmitate labeling entirely while expression of WT (lanes 1 and 2) TRP-ML1 is positive for palmitate labeling.

2.6 ACKNOWLEDGEMENTS

Epitope-tagged TRP-ML1 constructs were generated by Abigail Soyombo and Shmuel Muallem and provided by Kirill Kiselyov. We thank Gudrun Ihrke, Adam Linstedt, Balraj Doray, Stuart Kornfeld, Emily Guerriero, and Nirmala SundarRaj for cell lines and reagents, and Kirill Kiselyov, Matthew Hawryluk, Peter Keyel, and Rebecca Hughey for numerous helpful discussions. This work was supported by NIH R01-DK54407 to O.A.W. K.M.W. was supported by NIH T32-DK61296.

The abbreviations used are: AP, adaptor protein; DMEM, Dulbecco's Modified Eagle's Medium; FBS, fetal bovine serum; GGA, Golgi-localized, γ-ear-containing, ARF-binding; HRP, horseradish peroxidase; MDCK, Madin-Darby canine kidney; TRP-ML1, mucolipin-1; TGN, *trans*-Golgi network; TRP, transient receptor potential.

3.0 MEMBRANE TRAFFIC AND TURNOVER IN TRP-ML1-DEFICIENT CELLS: A REVISED MODEL FOR MUCOLIPIDOSIS TYPE IV PATHOGENESIS

Mark T. Miedel, Youssef Rbaibi, Christopher J. Guerriero, Grace Colletti, Kelly M. Weixel, Ora A. Weisz, and Kirill Kiselyov

The Journal of Experimental Medicine. Vol. 205 No. 6: 1477-1490 (2008).

3.1 ABSTRACT

The lysosomal storage disorder mucolipidosis type IV (MLIV) is caused by mutations in the TRP-ML1 ion channel. The “biogenesis” model for MLIV pathogenesis suggests that TRP-ML1 modulates postendocytic delivery to lysosomes by regulating interactions between late endosomes and lysosomes. This model is based on observed lipid trafficking delays in MLIV patient fibroblasts. Since membrane traffic aberrations may be secondary to lipid build-up in chronically TRP-ML1 deficient cells, we depleted TRP-ML1 in HeLa cells using siRNA and examined the effects on cell morphology and postendocytic traffic. TRP-ML1 knockdown induced gradual accumulation of membranous inclusions and thus represents a good model in which to examine the direct effect(s) of acute TRP-ML1 deficiency on membrane traffic. Ratiometric imaging

revealed decreased lysosomal pH in TRP-ML1 deficient cells, suggesting a disruption in lysosomal function. Nevertheless, we found no effect of TRP-ML1 knockdown on the kinetics of protein or lipid delivery to lysosomes. In contrast, by comparing degradation kinetics of LDL constituents, we confirmed a selective defect in cholesterol but not apoB hydrolysis in MLIV fibroblasts. We hypothesize that the effects of TRP-ML1 loss on hydrolytic activity have a cumulative effect on lysosome function resulting in a lag between TRP-ML1 loss and full manifestation of MLIV.

3.2 INTRODUCTION

The gene MCOLN1, coding for TRP-ML1, is mutated in the rare lysosomal storage disorder mucolipidosis type IV (MLIV) (12, 19, 228, 240), which is clinically characterized by severe developmental delays and psychomotor retardation, constitutive achlorohydria, and retinal degeneration and corneal opacities (5, 218, 227, 272). As in all lysosomal storage disorders, MLIV is characterized at the cellular level by the buildup of membranous and electron-dense organelles containing undigested lipid products. However, the stored lipid products (17, 147) are more heterogeneous than in most storage disorders and include gangliosides, sphingolipids, phospholipids, acidic mucopolysaccharides, and cholesterol (14, 15, 207, 231). Lipid accumulations in other lysosomal storage disorders are a result of the abnormal targeting and/or activity of individual hydrolases involved in lipid processing. Although it has been identified which lipid products accumulate in MLIV, there is no clear consensus as to which enzyme activities are compromised. Previous reports suggest that there is deficient ganglioside

sialidase activity associated with MLIV (8), while other studies argue against this enzyme deficiency (14, 144) . While some reports demonstrate that both phospholipase (16) and acid lipase (105) activities are normal in MLIV patient cells, other data suggest deficits in activities of these enzymes in MLIV cells (231). It is possible that such differences reflect variations between the primary fibroblasts used in these studies or compensatory changes in enzyme activity at the gene expression level.

Both immunofluorescence and subcellular fractionation studies demonstrate that TRP-ML1 is localized to lysosomes (121, 170, 202, 259), and it is thought that lipid accumulations associated with MLIV are a result of imbalanced ion homeostasis along the endocytic pathway resulting from TRP-ML1 dysfunction (14, 44, 272). A consensus on TRP-ML1 permeability characteristics is only beginning to emerge, while native TRP-ML1 activity has not been studied. Recombinant TRP-ML1 was characterized in the plasma membrane where it is targeted under over-expression conditions (121, 136) and in artificial lipid bilayers using TRP-ML1 purified from over-expressing cells or synthesized in a cell free system (40, 208). These experimental systems yielded outwardly rectifying monovalent cation permeable channels. On the other hand, “activating” mutations in TRP-ML1 resulted in an inwardly rectifying current (267). Such mutants were permeable to Ca^{2+}, which is similar to some previously published data on wild type TRP-ML1 (136, 138), whereas other studies have demonstrated a Ca^{2+} block of TRP-ML1 (40, 231).

The “biogenesis” model for MLIV progression suggests that TRP-ML1 regulates lipid trafficking by mediating specific fission and/or fusion events between late endosomes and lysosomes that occur during the process of lysosome biogenesis, a

Ca^{2+}-dependent process (151, 152, 196, 200, 216, 248). In the absence of functional TRP-ML1, endocytosed material destined for degradation accumulates due to impaired access to the hydrolases necessary for catabolism. Moreover, this model predicts that there will be a global defect in the postendocytic delivery of both lipids and proteins to lysosomes. The notion that TRP-ML1 directly regulates membrane traffic is based on the observations that TRP-ML1-deficient cells display aberrant mixing of lysosomal and endosomal content (138, 248) and that trafficking of a fluorescent conjugate of BODIPY-C5-lactosylceramide (LacCer) along the endocytic pathway is delayed in these cells (44, 202, 231). This model is also supported by studies performed in *Caenorhabditis elegans* where the functional TRP-ML1 orthologue, CUP-5, has been identified (69, 70). Knockout of the *cup-5* gene has been associated with defects in lysosome biogenesis. There is increased colocalization of late endosomal and lysosomal markers in *cup-5* mutants, and loss of this gene results in the abnormal accumulation of vacuolar structures that are interpreted to represent hybrid late endosomal-lysosomal structures (248). Again, the observed endocytic abnormalities observed in *cup-5 mutants* were alleviated by exogenous expression of functional human TRP-ML1.

The “metabolic” model suggests that similar to the ClC channels, TRP-ML1 regulates lysosomal ion homeostasis and thus directly affects the activity of lysosomal digestive enzymes (111). It was hypothesized that TRP-ML1 functions as a H^+ leak pathway to prevent the over-acidification of the lysosomal lumen, and that the activity of lysosomal lipases are disrupted as a consequence of the ionic imbalance in TRP-ML1-deficient lysosomes (231).

An additional complexity that must be clarified to properly describe MLIV pathogenesis and TRP-ML1 function is whether any defects in membrane traffic or lipid metabolism are the primary cause of MLIV, or are instead secondary effects due to the chronic accumulation of undigested lipids in these cells. The membrane trafficking studies discussed above were performed in chronically TRP-ML1-deficient fibroblasts. It is possible that the buildup of lipids and other undigested materials in these cells eventually impedes the entry of trafficking markers into lysosomes and manifests as delays in membrane traffic. Indeed, exactly the same lipid traffic delays were reported in a number of lysosomal storage disorders whose main causes are entirely metabolic and are not directly related to membrane traffic [GM1 and GM2 gangliosidoses, Fabry's disease and Niemann-Pick A or B; (188, 272)]. To circumvent this issue, we used an siRNA approach to examine the consequences of acute downregulation of TRP-ML1 function on postendocytic delivery to lysosomes.

Understanding whether TRP-ML1 regulates membrane traffic or lipolysis is a key step in determining whether enzyme replacement therapies will be effective as treatment for MLIV. A finding that TRP-ML1 directly regulates membrane traffic will make it unlikely that enzyme replacement therapies for MLIV will succeed. If, however, TRP-ML1 regulates lysosomal ion homeostasis, then replacement therapies, perhaps based on enzymes modified to work in an MLIV-specific lysosomal environment, are likely to be useful.

3.3 MATERIALS AND METHODS

Cell lines and reagents. HeLa SS6 cells were maintained in Dulbecco's modified Eagle's medium (DMEM; Sigma) supplemented with 10% fetal bovine serum (FBS; Atlanta Biologicals, Atlanta, GA) and 100 µg/ml penicillin/streptomycin (Invitrogen, Carlsbad, CA). Skin fibroblasts (SF) from patients with MLIV (WG0909), a heterozygous relative (WG0987), and MLII (WG0229) were from the Repository for Mutant Human Cell Strains. All SF cell lines were maintained in DMEM supplemented with 10% fetal bovine serum (FBS) and 100 µg/ml penicillin/streptomycin. All reagents were from Sigma Aldrich (St Louis, MO) unless indicated otherwise.

siRNA-mediated knockdown of TRP-ML1. Two double stranded siRNAs targeting the human form of mucolipin-1 (TRP-ML1; accession number BC005149) were designed and synthesized using Invitrogen's (Carlsbad, CA) proprietary BLOCK-iT^{TM} RNAi protocol. The first TRP-ML1 specific target sequence (ML1 siRNA #1) used was 5'-CCCACATCCAGGAGTGTAA-3', corresponding to nucleotides 959-977 of the human TRP-ML1 mRNA. The second target sequence (ML1 siRNA #2) was 5'-CCGCTACCTGACCTTCTT-3', corresponding to nucleotides 1328-1345 of the human TRP-ML1 mRNA. All studies, unless otherwise noted were performed using TRP-ML1 siRNA #1. To generate the siRNA resistant construct HA-ML1$_R$, the codons encoding amino acids IQEC starting at position 281 of TRP-ML1 (targeted by siRNA #1) was mutated from CAT CCA GGA GTG to TAT TCA AGA ATG to create siRNA resistance without affecting the corresponding amino acid sequence. For knockdown of endogenous TRP-ML1, HeLa SS6 cells were plated in 24-well dishes and allowed to

grow to ~50-60% confluence. Cells were transfected with a nonspecific control siRNA duplex (Dharmacon; Lafayette, CO) or TRP-ML1 specific siRNA duplexes. For each individual well, 3 µl of 20 µM siRNA oligonucleotide and 4.5 µl of *Trans*IT-TKO oligonucleotide transfection reagent (Mirus; Madison, WI) were used. Cells were harvested for protein concentration or Western analysis after 1, 3, or 5 days post-transfection. For cells transfected with siRNA twice over the 5 day knockdown period, 2 days post-initial transfection, cells were re-plated onto 24 well plates, re-transfected as described above the same day, and harvested for analysis either 24 or 72 h later. For knockdown of exogenously expressed HA-epitope tagged ML1 (HA-ML1) (121, 170), cells were plated and transfected with siRNA as described above. 24 h after siRNA transfection, cells were transiently transfected with cDNA encoding HA-ML1 using Lipofectamine 2000 (Invitrogen; Carlsbad, CA) according to the manufacturer's protocol and harvested for Western analysis 24 h later. Samples were immunoprecipitated and immunoblotted as has been previously described (121, 170).

Electron microscopy. Cells grown on plastic dishes were fixed by 30 min incubation with a solution containing 2.5% glutaraldehyde in 0.1M Na-cacodylate, washed with 0.1M Na-cacodylate, post-fixed with a solution containing 1% OsO4, washed with PBS and stained *en block* for 30 min with 2% uranyl acetate. Following dehydration by immersion in 30% to 100% ethanol, the samples were embedded in resin by immersion in 30% to 100% resin:propylene oxide mixtures. Fixed samples were mounted on grids and analyzed with a JEOL 100CX transmission electron microscope. For immunostaining with lamp1 antibodies, following fixation and freeze-thaw permeabilization of the

membranes at –80ºC in a cryoprotectant solution containing glycerol and sucrose, cells were blocked in BSA with goat serum, incubated overnight with monoclonal anti-lamp1 antibodies (Santa Cruz Biotechnology, Santa Cruz, CA), rinsed and biotinylated secondary antibodies were added. After an extensive wash, the samples were incubated with avidin-peroxidase complexes for 30 min followed with another wash. Next, 3,3'-diaminobenzidine and H_2O_2 was added for 4-10 min and, after another wash, the samples underwent secondary fixation with 1% OsO_4 for 1 h. This procedure yields dark stain associated with lamp1 immunoreactivity.

For colloidal gold uptake experiments, 10 nm gold particles were incubated with gelatin and BSA at pH 5 to coat the particles. Next, the particles were washed and added to the cells for 1 hour to load the endocytic pathway. Following 6 to 16 h chase, cells were fixed and processed for electron microscopy as described above.

Measurement of lysosomal pH. Determination of lysosomal pH was performed as has been previously described (62, 100). HeLa cells treated with siRNA for 5 d were plated onto 0.17 mm ΔT live-cell cover glass dishes (Biotechs, Butler, PA). Twelve h prior to the start of imaging, cells were loaded with 3 mg/ml each of fluorescein (FITC)- and tetramethylrhodamine (TMR)-conjugated 10,000 MW dextrans (Invitrogen; Carlsbad, CA) to allow accumulation in lysosomes. To measure pH differences between cells, a standard curve was determined for each experiment. Prior to imaging for the standard curve, cells were rinsed once with MES buffer containing 115 mM KCl, 5 mM NaCl, 1.2 mM $MgSO_4$, 25 mM MES that had been calibrated using an Accumet (Fisher Scientific) pH meter to 3, 4, 5, 6, 7 or 8. After rinsing, the cells were imaged in the same buffer

supplemented with 10 µM nigericin and 10 µM monesin in order to equilibrate intracellular and extracellular pH. Experimental dishes were imaged in DMEM without sodium bicarbonate. Images were taken using an Olympus IX81 with a 60X, 1.40 NA PlanApo oil-immersion objective. Pairs of images were captured from random fields of cells using a spinning disc confocal system (Perkin Elmer, Waltham, MA). Images were acquired and analyzed with Metamorph Software (Molecular Devices Corporation, Downington, PA). For analysis, equivalent FITC and TMR images were subjected to a morphological filter (Tophat) to remove background fluorescence. A binary mask was then applied so that only matched spots from each image were compared. After applying a threshold, the total gray value for each imaged was recorded for both channels and the TMR:FITC ratio was determined. TMR:FITC ratios were plotted against pH values and curves were fitted using linear regression analysis. At least 20 images were analyzed for each condition in 4 independent experiments. Student's t-test was used to determine statistical significance.

Lactosylceramide traffic. To examine LacCer trafficking at long chase times, HeLa cells were labeled with 5 µM LacCer complexed to BSA in serum-free DMEM for 60 min. at 37ºC. Cells were then gently washed 3 times with PBS and incubated with DMEM + 10% FCS for 5 h at 37ºC. Following chase, cell surface LacCer was back-extracted by washing cells for 30 min. in DMEM without bicarbonate supplemented with 2% (w/v) fatty acid-free BSA at 4ºC. Cells were then washed briefly with PBS and images were acquired in DMEM without bicarbonate at 20ºC. Images were acquired using an Olympus IX81 equipped with an Ultraview spinning disc confocal microscope system

(Perkin Elmer). Cells were imaged using a 60X objective and the LacCer was excited using the 488nm laser, while the dextran was excited using the 647nm laser. These two excitation filters were uses to account for the aggregation-dependent shift in red fluorescence that is characteristic of the BODIPY fluorophore. Under these experimental conditions, little red LacCer fluorescence was observed, so LacCer images in Figures 5 and 6 were acquired using only the 488nm laser.

For shorter experiments examining lysosomal delivery kinetics, HeLa cells were loaded with BODIPY-C5-LacCer (Invitrogen; Carlsbad, CA) and analyzed as before (231). Following loading and chase, cells were incubated with the lysosomal marker Lysotracker Red (Invitrogen; Carlsbad, CA) and confocal images taken. The images were analyzed using RGB colocalization add-in to ImageJ as described in (108, 231). In each image, the percentage of LacCer in lysosomes ($\%laccer_{Lys}$) was estimated by dividing the number of pixels contained within the area of overlap between LacCer and Lysotracker stains (N_{over}) by the number of pixels covered by the LacCer staining pattern (N_{laccer}): $\%laccer_{Lys} = 100 \times N_{over}/N_{laccer}$. To estimate N_{laccer}, the threshold settings of LacCer image was adjusted to remove signal from the cytoplasm and binarized by assigning 1 to each LacCer-positive pixel and 0 to LacCer-negative pixels. N_{laccer}, the number of nonzero pixels was calculated using the analysis function of ImageJ. Next, to calculate N_{over}, red (Lysotracker), green (BODIPY- LacCer) and blue (null) images of the same field of view were merged and the resulting RGB image was subjected to the RGB colocalization algorithm yielding a single binary image in which each pixel positive for both green (LacCer) and red (Lysotracker) signals has a value of 1 and each pixel

negative for either green or red signals has a 0 value. N_{over} is the number of pixels with non-zero values.

DiI-LDL labeling. Forty eight hours prior to imaging, cells were plated onto coverslips and pre-incubated in DMEM supplemented with 10% LPDS to up-regulate LDL receptor surface expression. AlexaFluor 647-conjugated dextran (Invitrogen; Carlsbad, CA) was pre-accumulated in lysosomes during a 12 h incubation prior to the start of the experiment. The next day, cells were incubated with DiI-LDL (20 µg/ml; Invitrogen Carlsbad, CA) on ice for 60 min to allow LDL binding. Cells were subsequently washed in PBS and chased in fresh DMEM for either 30 or 120 min at 37ºC. At the end of the timecourse, cells were fixed in 3.7% paraformaldehyde (Sigma Aldrich; St. Louis, MO) solution diluted in PBS for 10 min. and mounted for image analysis. Confocal imaging was performed on an Olympus IX-81 (Melville, NY) equipped with an UltraView spinning disc confocal head (Perkin Elmer, Shelton, CT) and an argon-ion, argon-krypton and helium-cadmium laser combiner. Images were acquired with a 100x plan-apochromat objective (NA 1.4) and the appropriate filter combination. The extent of co-localization between 647-dextran and DiI-LDL positive compartments was determined using Metamorph (Molecular Devices, Downington, PA) image analysis software. The TIFF images were imported into Adobe Photoshop (Adobe, Mountain View, CA) to adjust contrast and image size.

Preparation of [^{14}C] cholesteryl oleate-LDL complexes. In vitro preparation of cholesteryl ester radiolabeled lipoproteins was performed according to a modified version of the

methods previously described by Terpstra et al. (243) and Brown et al. (34). 600 µg of LDL (Biomedical Technologies Inc (BTI)., Stoughton, MA) and 120 mg of lipoprotein-deficient serum (LPDS; Biomedical Technologies, Inc. Stoughton, MA,) were mixed in 0.15 M NaCl containing thiomersol (0.3 mM), aprotinin (1 µg/ml), and glutathione (0.65 mM) at a final volume of ~1.6 ml. Five µCi of Cholesteryl[1-^{14}C]oleate ([^{14}C]-CO; GE Healthcare; Piscataway, NJ) in denatured toluene solution was transferred to a 2.0 ml conical tube and evaporated to dryness under a steady stream of nitrogen for ~15 min, then resuspended in 50 µl absolute ethanol. The resuspended [^{14}C]-CO was incubated for ~30 min in a 37ºC water bath with frequent vortexing to ensure complete resuspension. The LDL-LPDS was then added to the resuspended [^{14}C]-CO and this mixture was incubated overnight at 37ºC under nitrogen. The following day, the sample was transferred to a 0.5-3.0 ml Slide-A-Lyzer (10,000 molecular weight) dialysis cassette (Pierce; Rockford, IL) and dialyzed for 8-12h at 4ºC against 4L of buffer containing 0.15 M NaCl and 0.3 mM EDTA, pH 7.0. After dialysis, the solution was centrifuged in a benchtop microcentrifuge at 12,000 rpm for 5 min. The supernatant solution was collected, supplemented with 0.5% human serum albumin (HSA), and stored for up to 3 weeks at 4ºC.

Degradation of [^{14}C] cholesteryl oleate-LDL. [^{14}C]-cholesteryl oleate (CO)-LDL degradation was performed essentially as has been previously described by Groener et al. (87) with slight modification. HeLa SS6 cells or human skin fibroblasts were cultured in Dulbecco's modified Eagle's medium (DMEM) supplemented with 10% fetal bovine serum (FBS) and 100 µg/ml penicillin/streptomycin. Cells were plated in 12-well plates

at ~50% confluence. 48h prior to the start of an experiment, cells were pre-incubated with DMEM supplemented with 10% LPDS to up-regulate cell surface expression of the LDL receptor. Cells were then incubated with 0.4 ml DMEM containing 10% LPDS and [^{14}C]-CO-LDL (50 µg/ml LDL protein) for 4h at 37ºC. The labeling medium was removed, cells were washed with PBS, and incubated for 30 min at 18ºC in DMEM supplemented with 10% FBS. The experiment was initiated by the addition of fresh DMEM supplemented with 10% LPDS at 37ºC to scavenge the released free fatty acids (87). Where indicated, bafilomycin A_1 (0.5 µM; Sigma Aldrich), was added to culture medium 30 min prior to labeling and maintained throughout the time course. At various times (0.5 to 4h) the medium was collected and replaced. At the end of the time course cells were harvested in buffer containing 50 mM Tris-HCl (pH 7.4) and 1% Tx-100. Radioactivity was measured in both the medium and the cell pellet by liquid scintillation counting. The percent [^{14}C]-CO-LDL degraded was calculated as the amount of radioactivity present in the medium divided by the total radioactivity present in the medium and cell pellet.

Degradation of ^{125}I-apoB-LDL. HeLa SS6 cells or human skin fibroblasts were cultured in DMEM supplemented with 10% FBS and 100 µg/ml penicillin/streptomycin. Cells were plated in 6-well plates at ~50% confluence. 48h prior to the start of an experiment, cells were pre-incubated with DMEM supplemented with 10% LPDS to up-regulate cell surface expression of the LDL receptor. Cells were incubated in DMEM supplemented with ^{125}I- apoB-LDL [25 µg/ml LDL protein; 50 µCi/ml] (Biomedical Technologies, Inc., Stoughton, MA) on ice for 2h (0.6 ml). Cells were then extensively washed in MEM

containing BSA for 3 periods of 10 min. For control samples, bafilomycin A_1 (0.5 µM) was added 30 min. prior to LDL labeling and maintained throughout the time course. At the start of the experiment, cells were incubated with pre-warmed DMEM (0.6ml per well) at 37ºC. At various times (10 to 180 min.) the medium was collected from cells and replaced. After the time course was completed, the cells were solubilized with buffer containing 50 mM Tris-HCl (pH 7.4) and 1% Tx-100 for 15 min. Following solubilization, TCA was added to the medium collected over the time course and to the solubilized cells [final concentration 10% (v/v)]. The samples were incubated on ice for 20 min and then centrifuged at maximum speed in a microcentrifuge at 4ºC for 15 min. Radioactivity in the corresponding supernatants and pellets was counted using a γ counter (Packard Instrument Co.; Downers Grove, IL). The rate of ^{125}I-apoB-LDL degradation was determined by calculating the cumulative release of TCA-soluble counts into the medium over the experimental time course.

Degradation of ^{125}I-EGF and recycling of ^{125}I-tfn. To examine the lysosomal delivery and degradation of EGF fibroblasts or siRNA-treated HeLa SS6 cells were washed briefly with PBS then incubated with ^{125}I-EGF (100 µCi/mL) (Perkin Elmer) on ice for 2h to bind EGF at the cell surface. Cells were extensively washed with MEM (+BSA) on ice to remove unbound ligand. Following the final wash, cells were incubated with 0.6 mL pre-warmed MEM to begin the experimental timecourse. Medium was collected and replaced over a 3 h timecourse at 10, 30, 60, 120, and 180 min. At the final timepoint cells were solubilized from the dish (35 mm) in detergent solution containing 1% TX-100. Samples were then incubated for 15 min. on ice with 10% (w/v) trichloroacetic acid

(TCA). Samples were then centrifuged at 4ºC at 13,000 rpm, and the radioactivity in the corresponding supernatants and pellets was assessed using a γ-counter. The rate of EGF degradation was determined by calculating the cumulative release of TCA-soluble counts into the culture medium over the experimental timecourse. For each experiment performed, timepoints were performed in triplicate culture wells and plotted as mean ± S.E. To examine transferrin (tfn) recycling in control or MLIV fibroblasts, cells were first depleted of tfn by incubation for 60 min. at 37ºC in MEM/BSA. ^{125}I-tfn (iron loaded; Perkin Elmer) was internalized for 45 min. at 37º. Cells were extensively washed, then incubated for 2.5 min. to allow for receptor internalization. The medium was replaced with prewarmed MEM and cells were incubated at 37ºC. At the designated time (5, 15, 30 and 60 min.) the medium was collected and replaced. At the final time point, cells were solubilized, and kinetics of transferrin release was calculated by determining the cumulative percentage pre-internalized tfn released into the medium at each timepoint (using a γ-counter). For each experiment, timepoints were performed in triplicate and plotted as mean ± S.E.

3.4 RESULTS

3.4.1 siRNA-mediated TRP-ML1 knockdown

We identified two siRNA oligonucleotides specific for TRP-ML1 and tested their ability to knock down endogenous as well as heterologously expressed HA epitope-tagged TRP-

ML1 in HeLa cells. Cells were transfected with control (non-silencing) or with one of two TRP-ML1-specific siRNA oligonucleotides. Cells were harvested 24 h after transfection and subjected to Western analysis. We previously demonstrated that the 65 kDa full length TRP-ML1 is cleaved intracellularly into two fragments of roughly equal molecular mass [40 and 37 kDa (121, 170)]. Because it contains only a single transmembrane domain, the amino terminal fragment is less prone to aggregation than the full length or C-terminal half, and thus easier to detect upon SDS-PAGE. The arrowhead in Figure 3.1A marks the migration of the amino terminal fragment of TRP-ML1. Transfection with either of the TRP-ML1-specific siRNA duplexes resulted in virtually complete knockout of native TRP-ML1. Similarly, knockdown of exogenously expressed TRP-ML1 was observed when cells transfected with siRNA were later re-transfected with an HA-tagged version of TRP-ML1 (right panel). Under these overexpression conditions, we could detect both full length and the HA-tagged cleaved fragment on Western blots of cells transfected with control but not with TRP-ML1-specific siRNA duplexes (Figure 3.1A, right).

We next optimized conditions to knock down TRP-ML1 over longer time periods. To determine the duration of TRP-ML1 knockdown, cells were harvested for Western analysis at 1, 3, or 5 days after transfection with either a non-silencing control siRNA duplex or with TRP-ML1-specific oligonucleotides. As before, knockdown was virtually complete within 1 day of transfection; however, native TRP-ML1 reappeared within 3 days after the initial siRNA duplex transfection (Figure 3.1C; top panel). To overcome this, we performed a similar experiment except that the 3 and 5 day samples were re-transfected with TRP-ML1-specific or control siRNA duplexes 48 h following the initial

transfection, and were subsequently harvested for Western analysis at 3 or 5 days. As shown in Figure 3.1C (bottom panel), using these conditions, we were able to knockdown TRP-ML1 almost completely during this time course.

With specific TRP-ML1 knockdown conditions in place, we next sought to determine the onset of MLIV-like lipid inclusion formation over a 5 day knockdown period in HeLa cells. Electron microscopic analysis of cells transfected with either control or TRP-ML1-specific siRNA revealed the progressive accumulation of pleomorphic inclusions scattered throughout the cytoplasm of cells transfected with TRP-ML1 siRNA, while very few such inclusions were observed in control cells (Figure 3.2A). These inclusions are reminiscent of those observed in patient-derived MLIV fibroblasts, some of which contain multilamellar membranes, while others are filled with electron-dense, grey material (Figure 3.2B). Quantitation of the accumulation of storage bodies in both control and TRP-ML1 siRNA transfected cells is shown in Figure 3.2C. In TRP-ML1 siRNA treated cells, inclusions begin to accumulate as early as 1 day after siRNA transfection and gradually increased over the 5 day period. It should be noted that even after 12 days of siRNA treatment, the average number of inclusions observed in HeLa cells (69 inclusions/cell slice; Figure 3.2C) was much lower than that previously determined for MLIV fibroblasts using the same method (~720/cell slice; Figure 3.2C).

In order to confirm that the accumulation of storage bodies in TRP-ML1 siRNA treated cells is a direct consequence of TRP-ML1 loss, we performed knock in experiments in which the TRP-ML1 siRNA treated cells were transfected with an HA-tagged siRNA resistant TRP-ML1 construct (HA-ML1$_R$). Because transfection with cDNA was only ~30% efficient in these cells, we cotransfected them with GFP-

expressing plasmid and the following day, enriched for GFP-expressing cells using FACS. The cells were then transfected with TRP-ML1-specific siRNA oligonucleotides and processed for electron microscopic analysis 48 h later. Knockdown of endogenous TRP-ML1 and expression of the siRNA resistant HA-$ML1_R$ construct were confirmed by Western blotting of duplicate samples (Fig. 3.2D). As shown in Figure 3.2E, siRNA treated cells expressing HA-$ML1_R$ displayed a marked decrease in the number of inclusions compared with TRP-ML1 knockdown cells that were not transfected with cDNA, suggesting that HA-$ML1_R$ expression rescues or prevents inclusion formation in TRP-ML1-deficient cells. These studies confirm that inclusion formation is TRP-ML1 specific. Thus, this experimental system represents an appropriate model in which to study the early stages of MLIV progression. As a result, this approach will enable us to assess the function of TRP-ML1 under conditions that are unbiased by the chronic accumulation of undigested lipid material that may itself have adverse effects on specific lipid and protein trafficking events.

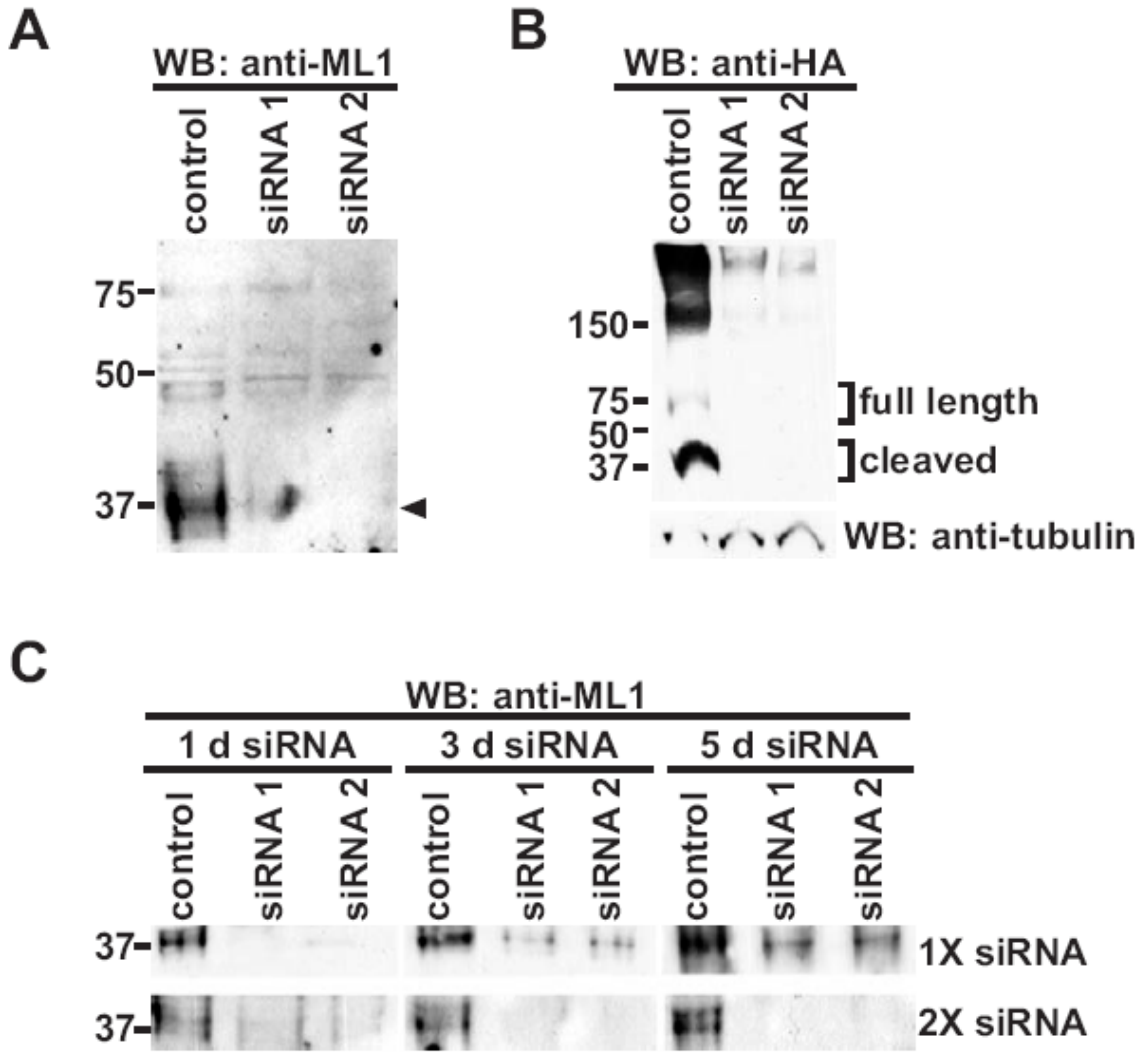

Figure 3.1 siRNA-mediated knockdown of TRP-ML1.

(A) HeLa cells were transfected with either non-silencing control or TRP-ML1 specific siRNA oligonucleotides. Cells were harvested for Western analysis after 24 h. Equal amounts of total protein were loaded for SDS-PAGE as determined by protein assay. Samples were transferred to nitrocellulose and immunoblotted to detect endogenous levels of TRP-ML1 using an antibody directed against the first extracellular loop of the protein. The arrowhead denotes the migration of the cleaved form of TRP-ML1. (B) HeLa cells were transiently transfected with cDNA encoding HA-epitope tagged TRP-ML1 24 h after initial transfection with either control or TRP-ML1 specific siRNA duplexes. After an additional 24 h incubation, cells were solubilized and equal amounts of total protein were immunoprecipitated using anti-HA antibodies. After SDS-PAGE, proteins were transferred to nitrocellulose and probed using HRP-conjugated anti-HA antibody. 10% of the cell lysate was saved prior to immunoprecipitation and immunoblotted using anti-tubulin antibody as an additional loading control (bottom panel). (C) HeLa cells were transfected with either non-silencing control or TRP-ML1 specific siRNA oligonucleotides and were harvested for Western analysis 1, 3, or 5 d post-transfection (top panel), or were re-transfected with siRNA duplexes after 2 d and were harvested for Western analysis at 3 or 5 d (bottom panel). Samples were subjected to SDS-PAGE, transferred to nitrocellulose, and immunoblotted to detect endogenous TRP-ML1.

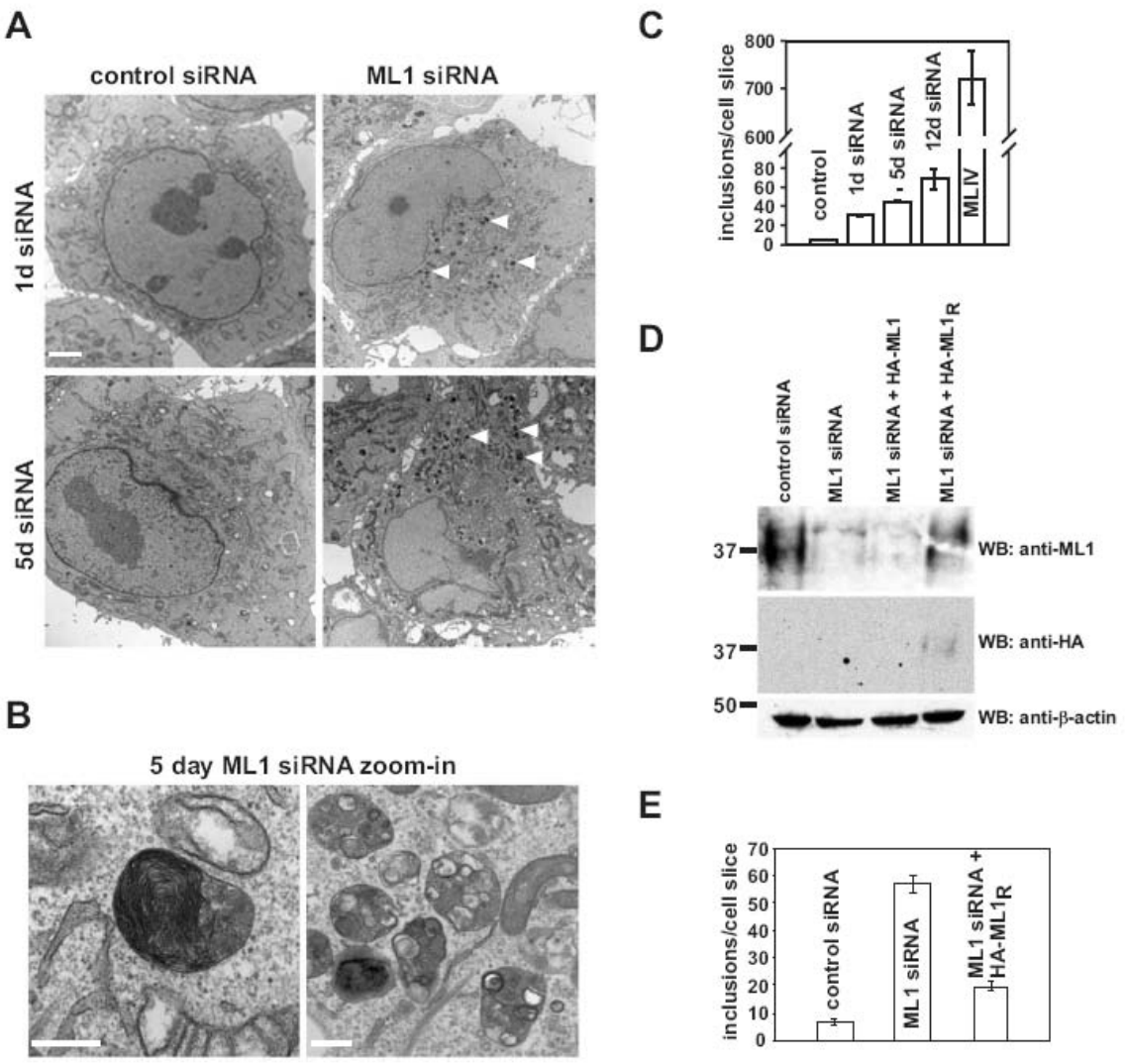

Figure 3.2 Time course of lipid inclusion formation in TRP-ML1-deficient cells.

(A and B) Electron micrographs of HeLa cells after either 1 or 5 d of TRP-ML1 specific or control siRNA oligonucleotide transfection. Scale bars, 2 µm (A); 200 nm (B; left); 500 nm (B; right). (C) Quantitation of the effect of TRP-ML1 knockdown on formation of storage inclusions. The number of inclusions was calculated using the automated particle counting function of ImageJ. Data are expressed as number of inclusions per cell slice ± SEM. (D) Western blot analysis of siRNA treated cells expressing siRNA resistant HA-ML1$_R$. HeLa cells were transfected with either control- or TRP-ML1 specific siRNA as indicated. Twenty four hours after siRNA treatment, cells were co-transfected with plasmids encoding GFP and either HA-ML1 (non-siRNA resistant) or HA-ML1$_R$ (siRNA resistant). The following day cells were sorted by FACS analysis to identify GFP-positive (transfected) cells and were subsequently re-transfected with the appropriate siRNA and returned to culture for 48 h. Cells were harvested and thirty µg of total protein was loaded for SDS-PAGE. Samples were transferred to nitrocellulose and immunoblotted to detect endogenous levels of TRP-ML1 (top panel), HA-ML1 or HA-ML1$_R$ (middle panel), or β-actin (bottom panel) as a loading control. (E) Quantitation of the effect of HA-ML1$_R$ expression on formation of storage inclusions in TRP-ML1 siRNA-treated cells. The number of inclusions was calculated as described above.

3.4.2 Lipid inclusions in TRP-ML1-deficient cells are lamp-1 positive and receive endocytosed cargo

To examine whether the inclusions that accumulate in TRP-ML1 deficient cells represent active components of the endocytic pathway, control and 5 day TRP-ML1 siRNA treated cells were *en-bloc* labeled with antibodies directed against the lysosomal membrane protein lamp-1, and were then subsequently labeled with biotinylated secondary antibodies. Immunoreactivity was detected using avidin-biotin peroxidase complex and 3, 3'-diaminobenzidine. Figure 3.3A shows that inclusions from TRP-ML1 deficient cells are positive for lamp-1 (right panel; dark stain identified by arrows). In contrast, lamp-1 positive compartments in cells transfected with a control siRNA duplex were smaller and more uniformly stained (middle and left panels). This staining pattern is consistent with the idea that the lipid inclusions in TRP-ML1 deficient cells are of late endosomal or lysosomal origin.

We next asked whether the lipid inclusions present in TRP-ML1 deficient cells are accessible to internalized cargo. For these studies, cells transfected with TRP-ML1 specific siRNA for 5 days were loaded for 6 h with albumin-conjugated 10 nm colloidal gold particles, chased for an additional 12 h to allow accumulation in lysosomes and then processed for electron microscopy. Figure 4B (left and middle panels) shows extensive delivery of gold particles to lipid inclusions in TRP-ML1 deficient cells. Similar results were also obtained using MLIV fibroblasts (Figure 3.3B; right panel). These results demonstrate that the observed lipid inclusions are not "dead end" structures, but are able to receive material internalized along the endocytic pathway.

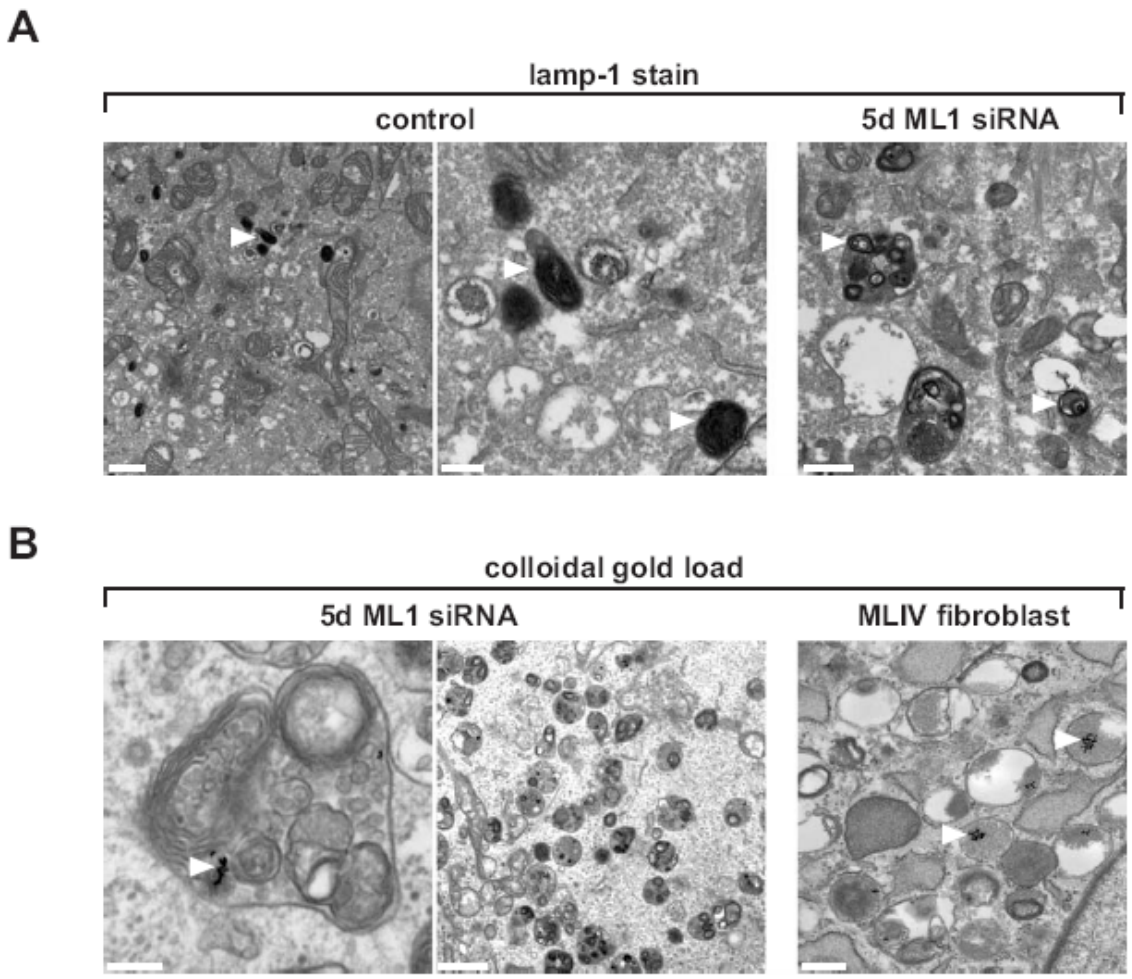

Figure 3.3 Inclusion bodies are LAMP-1 positive and remain accessible to internalized cargo in TRP-ML1-deficient cells.

(A) LAMP-1 immunoreactivity in control and TRP-ML1 deficient cells is indicated by arrows. Control- or TRP-ML1 siRNA-treated HeLa cells (5d) were labeled with antibodies directed against the lysosomal membrane protein LAMP-1 as described in Materials and Methods. Lysosomes from both control- and TRP-ML1 siRNA-treated are positive for LAMP-1 immunoreactivity. Arrowheads indicate lamp-1 positive labeled compartments. Scale bars (left to right), 2 µm, 500 nm, 500 nm. (B) Colloidal gold inside storage inclusions in TRP-ML1 deficient cells. Control- or TRP-ML1 siRNA-treated HeLa cells (5d) were loaded with 10 nm colloidal gold particles and processed for electron microscopy as described in Methods. A large fraction of the inclusions were gold-positive in 5-day siRNA cells indicating that the inclusions were recently formed. In these panels, gold was chased for 16 h. Arrowheads indicate colloidal gold-labeled compartments. Scale bars (from left to right), 200 nm, 2 µm, 500 nm.

3.4.3 Lysosomal pH is reduced upon siRNA-mediated knockdown of TRP-ML1

Prior studies examining the measurement of lysosomal pH in TRP-ML1-deficient cells have produced conflicting results. Early studies performed using ratiometric imaging approaches determined that the lysosomal pH in MLIV cells was elevated almost one full pH unit higher when compared to control cells or to cells isolated from patients with other lysosomal storage diseases (7). In other studies, lysosomal pH in MLIV cells has been reported to be either more acidic (231) or unchanged (126, 202) compared to control cells. One unifying feature in all these studies is that they were performed using isolated patient fibroblasts. These cells are not necessarily appropriate for such experiments due to the long term accumulation of undigested lipids that induce autofluorescence, may interfere with dye loading and/or retention, and may induce compensatory changes in these cells at the level of protein expression. Therefore, we examined lysosomal pH in cells treated with TRP-ML1-specific siRNA for 5 days, allowing us to measure pH in TRP-ML1-deficient cells without any potential effects caused by long-term lipid accumulation. To quantitatively determine lysosomal pH in cells treated with control or TRP-ML1-specific siRNA, cells were loaded for 12 h simultaneously with fluorescein (FITC)- and tetramethylrhodamine (TMR)-conjugated 10 kDa dextrans (3 mg/ml) to allow for accumulation in lysosomes. The FITC-conjugated dextran was used as a pH indicator, while the TMR-conjugated dextran provided a pH-insensitive readout for the ratiometric pH measurements. Following dextran loading, measurements of lysosomal pH were obtained by calculating the ratio of TMR:FITC fluorescence, and fitting these to a standard curve constructed as described in Materials and Methods. As shown in a representative experiment in Figure 3.4, TRP-ML1

knockdown was associated with lysosomal acidification. In this experiment, the average lysosomal pH in cells treated with control siRNA was 5.44 ± 0.06, while in cells treated with TRP-ML1-specific siRNA, the average pH was estimated was 4.04 ± 0.09. Over the course of 4 experiments using identical imaging conditions, the average difference in pH between control and TRP-ML1 siRNA treated cells was 1.12 ± 0.16 pH units. These results indicated that loss of functional TRP-ML1 in cells results in a reduction of lysosomal pH even after a short period of TRP-ML1 knockdown, and that even lysosomes that have not yet accumulated significant amounts of undigested material are functionally affected by loss of TRP-ML1.

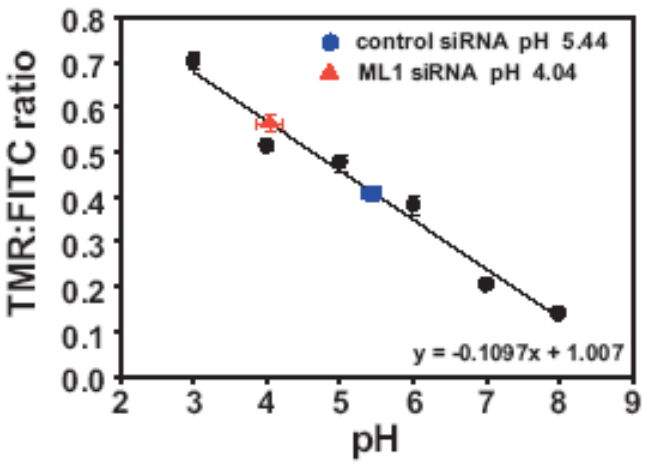

Figure 3.4 Lysosomal pH is lower in TRP-ML1 siRNA-treated cells.

Control or TRP-ML1 siRNA treated (5d) HeLa cells were loaded with FITC- and TMR-conjugated dextrans (3 mg/ml) for 12h. Lysosomal pH was determined by calculating the ratio of TMR:FITC fluorescence. Images were acquired as described in Methods. Ratiometric data was converted to absolute values of pH using TMR:FITC ratios determined from permeabilized cells equilibrated with calibration solutions. Data from 20 random fields of cells were quantified and the pH determined is presented as average pH ± SEM. Similar results were obtained in four independent experiments.

3.4.4 Lysosomal delivery of LacCer is unimpaired in TRP-ML1-deficient cells

Numerous studies have reported that trafficking of the fluorescent lipid analogue LacCer is impaired in MLIV fibroblasts as well as in primary fibroblasts from several other lysosomal storage diseases (44, 188, 202, 231). We thus examined whether TRP-ML1 knockdown cells also display this phenotype. HeLa cells preloaded with fluorescent dextran were treated with control or TRP-ML1 siRNA and were subsequently incubated with BODIPY-C5-LacCer for 60 min and then chased for 5 h at 37^{o}C. As shown in Figure 3.5A, LacCer staining in cells transfected with a control siRNA oligonucleotide was tightly clustered around the nucleus, consistent with efficient delivery to the Golgi complex (top panel). In contrast, the LacCer staining pattern in cells treated with TRP-ML1-specific siRNA was dispersed throughout the cytoplasm and colocalized partly with pre-internalized dextran. These results are consistent with observations in MLIV fibroblasts (44, 202, 231) and with another recent study examining TRP-ML1 knockdown in murine macrophages (245).

We then examined whether expression of the siRNA-resistant construct HA-$ML1_R$ in knockdown cells could rescue the LacCer sorting defect. Cells were co-transfected with a vector encoding the fluorescent protein mCherry (to identify transfected cells) and HA-ML_R. The following day these cells were then transfected with TRP-ML1 siRNA and cultured for 48 h before labeling with LacCer as above. Figure 3.5B shows juxtanuclear localization of LacCer in mCherry-positive (presumably HA-ML_R expressing) cells, consistent with the staining pattern of control cells. Therefore, siRNA–mediated TRP-ML1 knockdown effectively recapitulates the cellular phenotype of MLIV cells.

A crucial question in MLIV pathogenesis is whether the delay in LacCer trafficking occurs at the step of endosome-lysosome interaction as predicted by the biogenesis model. While our previously published data did not support this idea (231), a detailed analysis of the membrane traffic in MLIV fibroblasts performed by Pryor et al. (202) suggested a delay in transfer of the endocytosed material from late endosomes to lysosomes. However, since these studies were performed in MLIV fibroblasts, this effect could be a secondary result of undigested lipid buildup. Therefore, we performed a series of experiments to quantitate the rate of protein and lipid delivery to lysosomes in control and TRP-ML1 knockdown HeLa cells. The premise of these experiments was that if TRP-ML1 directly regulates the delivery of endocytosed material to lysosomes, then acute TRP-ML1 downregulation would result in pre-lysosomal buildup of endocytosed material, whose entry into lysosomes will be significantly delayed.

Figure 3.6 shows the results of our experiments. Control and siRNA transfected cells were loaded with 2 µg/ml LacCer for 15 min at 37ºC to incorporate LacCer into the plasma membrane. Next, the cells were washed and chased for brief periods (up to 60 min) in the presence of 5 mg/ml BSA. After the chase, cells were loaded with Lysotracker Red to identify lysosomes and confocal images of cells were analyzed for overlap between LacCer and Lysotracker Red to quantify lysosomal delivery of LacCer. As shown in Figure 3.6, we found no difference in kinetics of lysosomal delivery of LacCer in control vs. TRP-ML1 deficient cells. As a positive control, we pharmacologically suppressed membrane fusion and confirmed that this induces an observable delay in lipid traffic. To do this, we loaded untransfected HeLa cells with the cell permeable Ca^{2+} chelator BAPTA-AM (1 µM). Since vesicular fusion in the endocytic

pathway requires Ca^{2+}, chelation with BAPTA should suppress membrane fusion and thus replicate the conditions predicted by the “biogenesis” model associated with the loss of TRP-ML1 Ca^{2+} conductance. Figure 3.6 shows that, unlike TRP-ML1 downregulation, BAPTA-AM .inhibited delivery of LacCer to lysosomal compartments. Therefore, the delivery of LacCer to lysosomes is unimpaired in TRP-ML1 deficient cells.

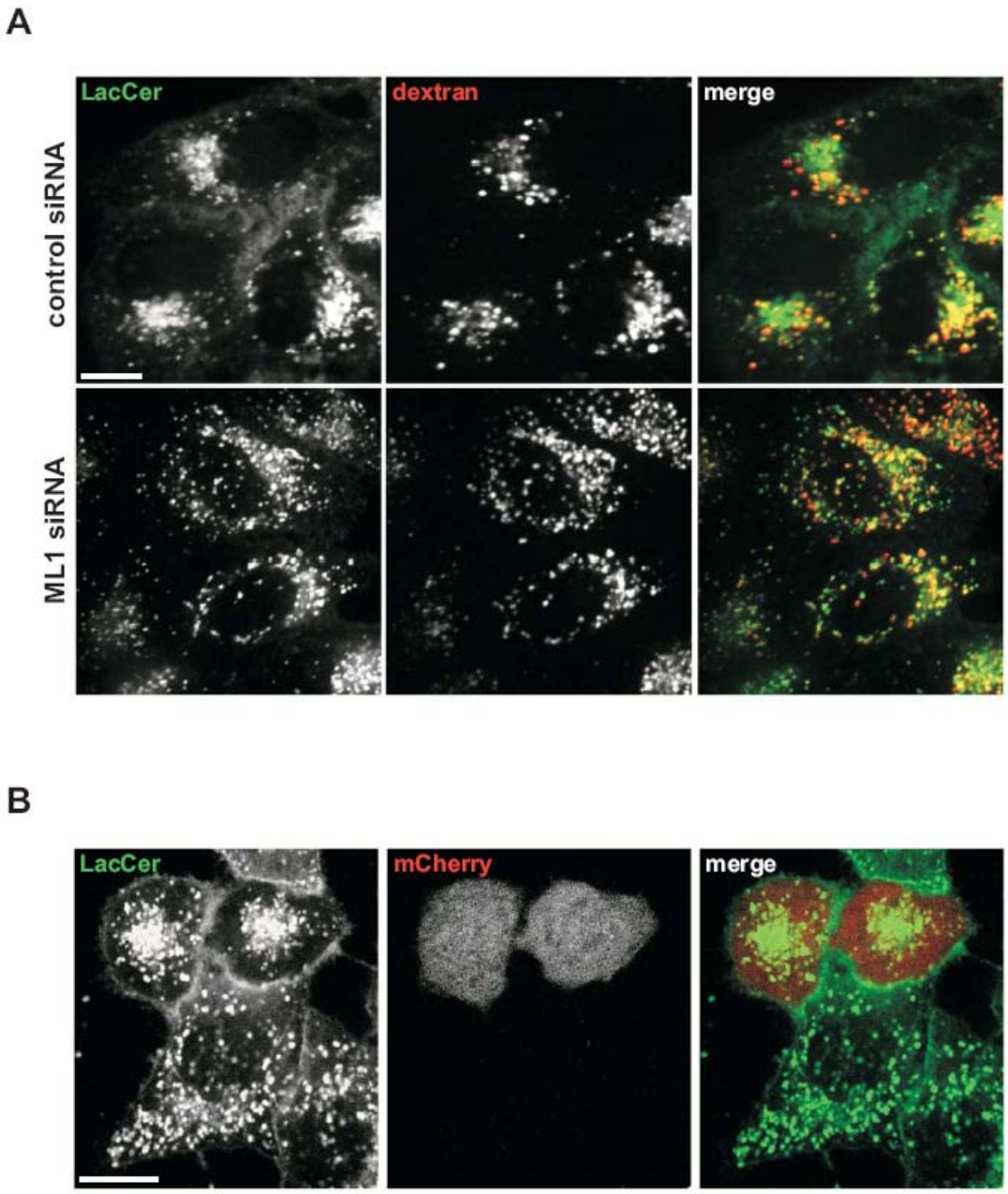

Figure 3.5 Postlysosomal lipid traffic is impaired in TRP-ML1-deficient cells.

(A) Control or TRP-ML1 siRNA treated (5 d) HeLa cells were pre-loaded for 12 h with 647-conjugated dextran. The following day cells were labeled with BOCIPY-C5-LacCer as described in Methods and chased for 5 h. Fluorescence images of both LacCer (green) and 647-dextran (red) were obtained for both control (top panel)- and TRP-ML1 (bottom panel) siRNA-treated cells. Scale bar, 10 µm. (B) LacCer Golgi localization can be restored by expression of HA-$ML1_R$ in TRP-ML1 siRNA treated cells. TRP-ML1 siRNA-treated cells (2 d) were co-transfected with plasmids encoding the siRNA resistant construct HA-ML_R cDNA and the fluorescent protein mCherry (to identify DNA-transfected cells) 24 h prior to siRNA treatment. Cells were loaded and chased with BODIPY-C5-LacCer as in 5A. The juxtanuclear LacCer staining pattern reminiscent of normal cells is observed in mCherry-positive cells but not in neighboring cells that presumably do not express HA-$ML1_R$. Scale bar, 10 µM.

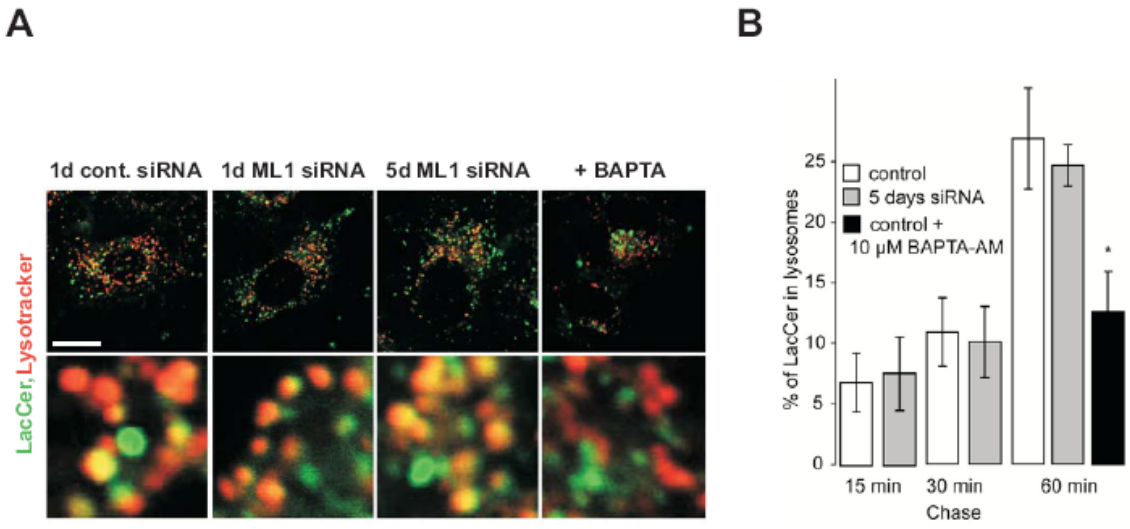

Figure 3.6 Lysosomal delivery of LacCer is normal in TRP-ML1 siRNA-treated cells.

(A) Control and TRP-ML1 siRNA-treated cells were loaded with 2 µg/ml LacCer for 15 min at 37º and Lysotracker to label lysosomes as described in Materials and Methods. Where indicated, cells were incubated with 10 µM BAPTA-AM for 1 h. Delivery of LacCer to lysosomes was measured by quantifying the percent overlap between LacCer and Lysotracker. Scale bar, 10 µm. *: p=0.013 (obtained in 6 separate measurements).

3.4.5 LDL trafficking and degradation in TRP-ML1-deficient cells

To more quantitatively assess lysosomal delivery and function in TRP-ML1 knockdown cells, we examined the kinetics of lysosomal delivery, apoB proteolysis, and cholesterol de-esterification of low density lipoprotein (LDL). Previous studies in MLIV fibroblasts have specifically probed lipid metabolism along the LDL receptor mediated pathway of lysosomal degradation using radiolabeled forms of both sphingomyelin and cholesteryl oleate (105). These studies found that MLIV fibroblasts metabolize both lipids more slowly compared to control cells. Therefore, our first approach was to examine whether delivery of LDL to lysosomes in TRP-ML1-deficient cells was impaired. To determine this, we used fluorescence microscopy to examine and quantitate the delivery of DiI-labeled LDL to lysosomes of HeLa cells transfected with TRP-ML1-specific siRNA. In these studies, cells were treated with either control or TRP-ML1 siRNA duplexes for 5 days. AlexaFluor 647-conjugated dextran was pre-accumulated in lysosomes during a 12 h pre-incubation prior to the start of the experiment. The following day, cells were incubated with DiI-LDL (20 µg/ml) on ice for 1 h and were then subsequently chased in fresh medium for 30 or 120 min at 37ºC. At either time point, cells were fixed and coverslips mounted for analysis. Delivery of DiI-LDL to lysosomes was measured by quantifying the percent of overlap between DiI-LDL and the pre-loaded 647-dextran expressed as the amount of Di-LDL present in dextran-positive compartments. As shown in Figure 3.7A, ~60% of the internalized DiI-LDL colocalized with the pre-loaded 647-dextran by 120 min of chase in both control and TRP-ML1 siRNA-treated cells, suggesting that delivery of LDL in TRP-ML1-deficient cells is unimpaired. We also did not observe a delay in parallel studies quantifying DiI-LDL delivery in MLIV and MLII

fibroblasts relative to control cells, suggesting that chronic lipid build-up in these cells does not affect LDL delivery to lysosomes (Fig. 3.7B). Taken together, these results suggest that delivery of LDL to lysosomes is unaffected by both acute and chronic loss of TRP-ML1 function.

Our second approach was to examine the delivery and lysosomal degradation of both the lipid and protein components of LDL in both control and MLIV fibroblasts as well as in control and in TRP-ML1 siRNA-treated cells. If TRP-ML1 is involved in the interactions between late endosomes and lysosomes, then there should be a defect in the degradation of both the protein and lipid components of LDL along this pathway. To monitor the degradation of the protein component of LDL, cells were incubated with ^{125}I-apoB-LDL for 2 h on ice. Following ligand binding, cells were extensively washed, then incubated with pre-warmed medium for various times. At the indicated times, the medium was removed and replaced, and degradation kinetics were determined by trichloroacetic acid (TCA) precipitation of the medium and of cell lysates solubilized at the end of the time course. The rate of apoB degradation was determined by calculating the cumulative release of TCA-soluble counts into the medium. As shown in Figure 3.8A, the kinetics of degradation of apoB were identical in both control and TRP-ML1 deficient cells as well as in control and MLIV fibroblasts. Similarly, we found no difference in the kinetics of ^{125}I-transferrin recycling in MLIV and control fibroblasts, or in the degradation of ^{125}I-EGF (epidermal growth factor) in both siRNA treated cells and MLIV fibroblasts (Fig. 3.9). These results suggest that there is no defect in postendocytic recycling or lysosomal delivery in TRP-ML1-deficient cells. These results are consistent with the observations of Chen et al. (44), who (using a similar ^{125}I-

transferrin recycling assay) also found no defects in the endocytosis or recycling of transferrin in MLIV fibroblasts.

To examine the degradation of the lipid component of LDL, we used an experimental approach previously used by Groener et al. (87) to monitor the metabolism of radiolabeled cholesteryl oleate. Cells were incubated with [^{14}C]-cholesteryl oleate (CO) in complex with LDL for 4.5 h at 37ºC. Following labeling, cells were incubated for various times with pre-warmed medium supplemented with LPDS. At each time point, the medium was removed and replaced and degradation kinetics were determined by quantitating the cumulative release of free fatty acids into the cell culture medium compared to the amount that remained cell-associated. As shown in Figure 3.8B, the kinetics of [^{14}C]-CO degradation were not different in cells treated with either control or TRP-ML1 specific siRNA for 5 d. Additionally, treatment with TRP-ML1 specific siRNA over a 12 day period also had no effect on cholesterol hydrolysis. However, the rate of [^{14}C]-CO degradation in MLIV fibroblasts was significantly slower when compared to the rates of degradation in either control or MLII fibroblasts.

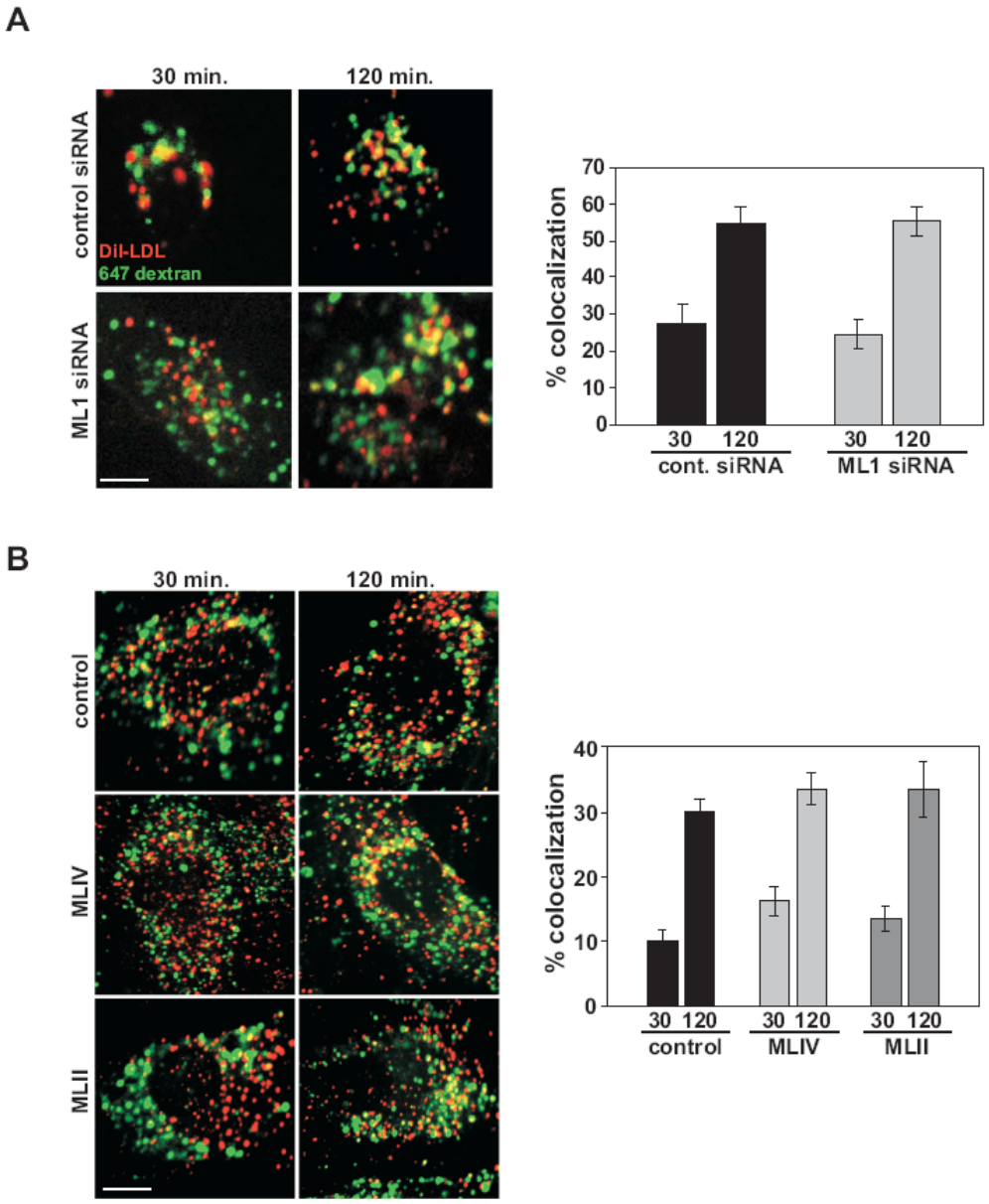

Figure 3.7 LDL delivery to lysosomes is normal in TRP-ML1-deficient cells.

Control or TRP-ML1 siRNA treated (5 d) HeLa cells (panel A) or fibroblasts (panel B) were pre-loaded for 12 h with 647-conjugated dextran. Cells were incubated bind DiI-LDL on ice for 60 min and were then subsequently chased in pre-warmed media at 37ºC for and additional 30 or 120 min. At the indicated time points, cells were fixed and processed for immunofluorescence. Delivery of DiI-LDL to lysosomes in cells was measured by quantifying the percent overlap between DiI-LDL and the pre-loaded 647-dextran. Graphical representations of the quantifications are shown plotted to the right in panels A and B and are expressed as the % overlap ± S.E.M. for n = 20 cells under each condition. Scale bar, 10 µm.

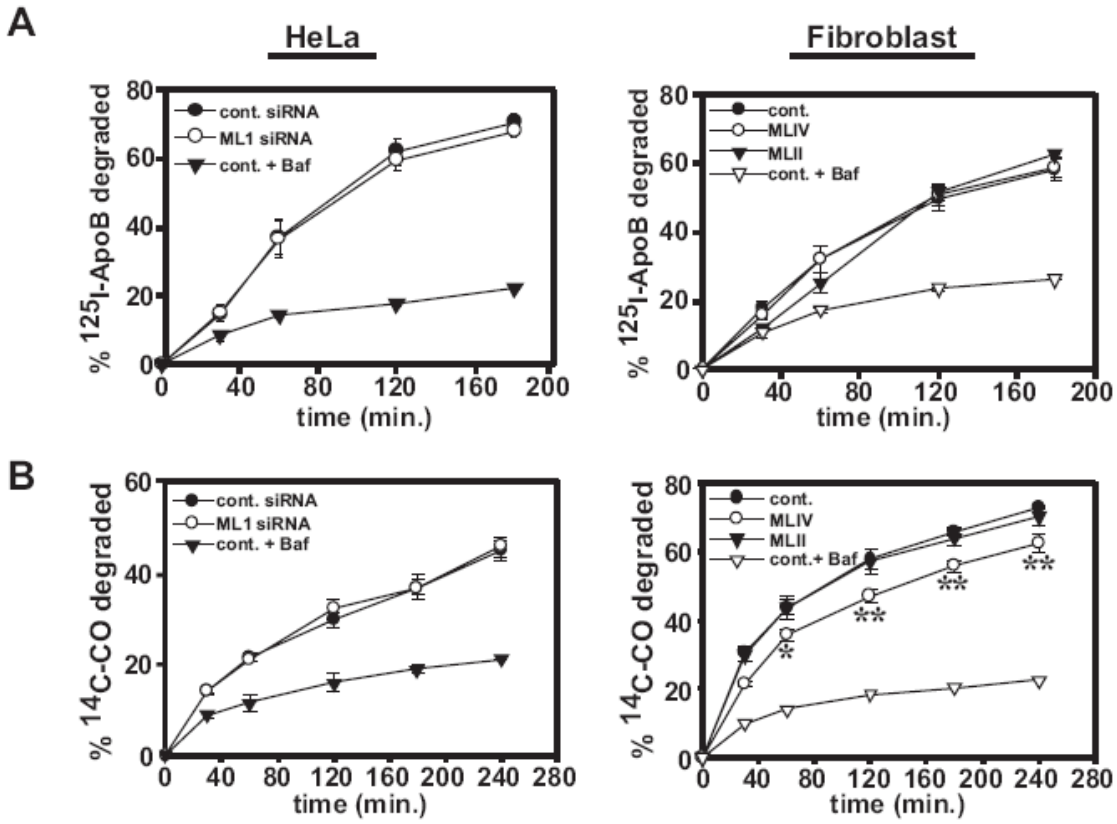

Figure 3.8 Degradation of LDL cholesterol is impaired in MLIV fibroblasts.

(A) siRNA transfected HeLa (5d) or patient fibroblasts were incubated on ice for 2 h with ^{125}I-ApoB-LDL complexes. For control cells, bafilomycin (0.5 µM) was added 30 min. prior to LDL labeling and maintained in the culture medium throughout the experiment. Following ligand binding, cells were washed and incubated in pre-warmed medium. At the indicated time points, the medium was collected and replaced, and cells were solubilized after the final time point. The rate of ApoB degradation was determined by calculating the cumulative release of TCA-soluble counts into the medium as described in Methods. (B) siRNA transfected HeLa (5 d) or patient fibroblasts were labeled with medium containing 10% LPDS and [^{14}C]-CO-LDL complexes (50 µg/ml LDL protein) for 4 h at 37ºC, washed, and incubated for 30 min at 18ºC in medium supplemented with 10% FBS. The time course was initiated by addition of fresh culture medium supplemented with 10% LPDS at 37ºC. At the indicated times the medium was collected and replaced. After the final time point, cells were harvested and radioactivity was measured in both the medium and cell pellet. The cumulative percentage of preinternalized [^{14}C]-CO released into the medium at each timepoint was calculated as described in Methods. The mean ± S.E.M. of three experiments (two for bafilomycin A_1-treated samples) performed in triplicate is plotted in each panel. *: $p = 0.032$; **; $p < 0.008$ by Student's t test.

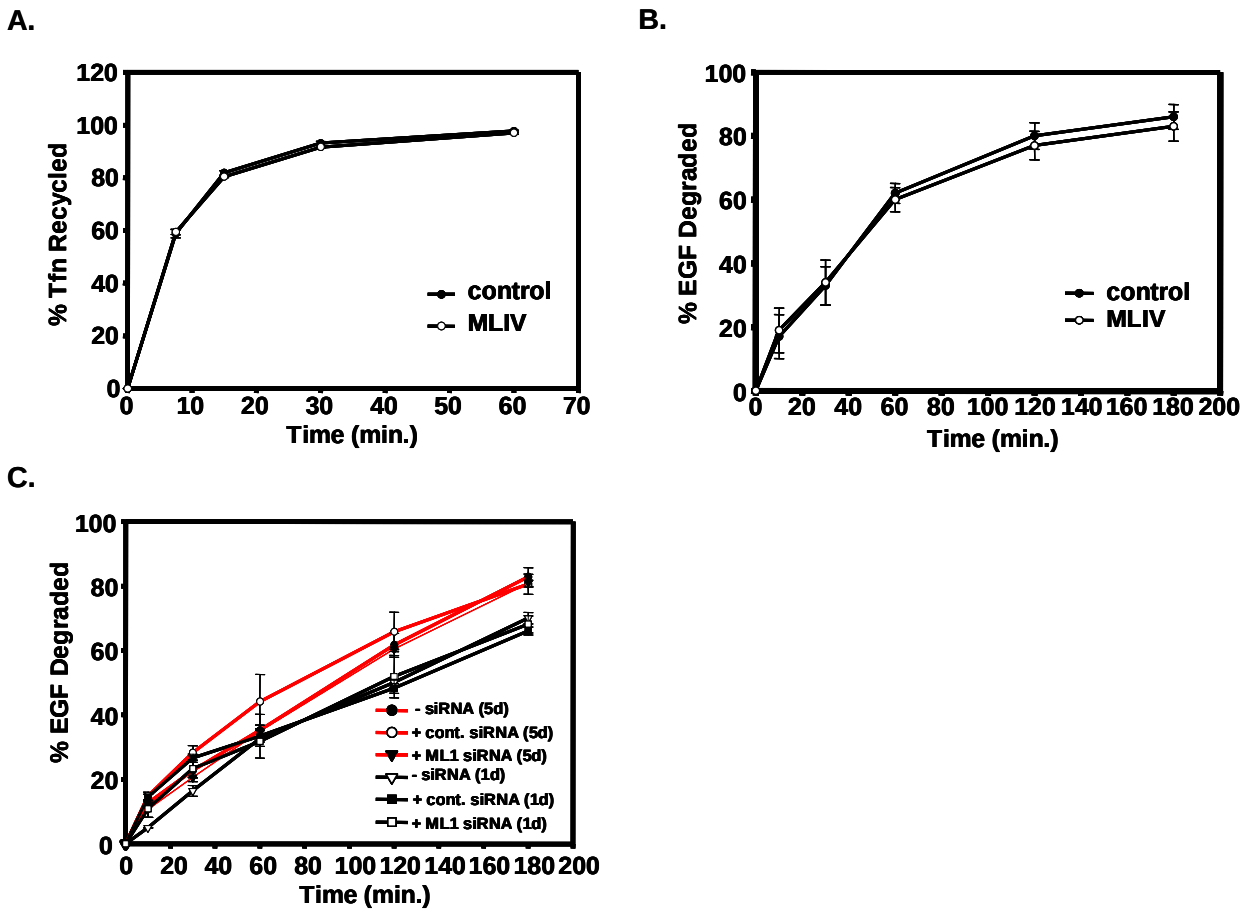

Figure 3.9 Transferrin recycling and EGF degradation is not altered in TRP-ML1-deficient cells.

(A) MLIV or control fibroblasts were depleted of transferrin (Tfn) by incubation for 60 min. at 37ºC in MEM/BSA. ^{125}I-labeled iron-loaded human transferrin was internalized for 45 min. at 37ºC. The cells were extensively washed, then incubated at 37ºC for 2.5 min. to allow for receptor internalization. The medium was replaced with prewarmed MEM/BSA and the cells were incubated at 37ºC. At the designated time, the medium was collected and replaced. After the final timepoint, cells were lysed in detergent solution and the amount of ^{125}I-labeled Tf was determined using a γ counter. Kinetics of release were calculated by determining the cumulative percentage of preinternalized transferrin released into the medium at each time point. The number (n) of experiments represented is 3 and is plotted as the mean ± S.E. (B and C) Fibroblasts (B) or HeLa cells (C) were incubated with ^{125}I-labeled EGF on ice for 2h. The cells were washed extensively and then incubated with prewarmed medium. At various times the medium was collected and replaced. After the timecourse, the cells were solubilized with 1% TX-100 and trichloroacetic acid (10% final concentration) was added and cells were incubated on ice for 10 min. Samples were then centrifuged at maximum speed in a microcentrifuge for 15 min. at 4ºC, and the radioactivity in the corresponding supernatants and pellets counted using a γ counter. The rate of EGF degradation was determined by calculating the cumulative release of trichloroacetic acid-soluble counts into the medium over the timecourse. The number (n) of experiments represented is 6 and is plotted as the mean ± S.E.

3.5 DISCUSSION

The internalization and processing of cargo via the endocytic pathway is a complex process involving numerous steps that include cargo binding and entry, receptor-ligand dissociation, membrane fusion, degradation of internalized lipids, proteins, and carbohydrates, and excretion of digested products through the lysosomal membrane (160, 175). The efficiency of these processes depends on the maintenance of specific ionic environments that are established by the combination actions of ion channels and pumps residing in endocytic compartments (200, 264). New information about these ion transporters regularly emerges from studies on the genetic determinants of lysosomal storage diseases. MLIV is one of several examples of lysosomal storage diseases caused by a dysfunction in the ionic balance of the endocytic machinery. The severity of this disease is compounded by the fact that no unified model exists for MLIV pathogenesis, thus hindering the development of pharmacological interventions.

Since the identification that mutations in the MCOLN1 gene are responsible for the MLIV disease phenotype (12), it has become apparent that this lysosomal cation channel plays a key role in the maintenance and regulation of postendocytic events (5, 14, 44, 105). As described in the Introduction, two models exist to explain the primary defect in MLIV. The “biogenesis” model suggests that MLIV is caused by delayed membrane traffic to lysosomes as a result of impaired endosome-lysosome fusion or fission (196, 202, 216, 248). The “metabolic” model postulates that MLIV results from an ionic imbalance in lysosomes that precludes efficient processing of internalized lipids and other molecules (231).

In principle, a comprehensive model for the regulation of TRP-ML1 channel activity would enable the discrimination between these models. Fusion between various membrane-bound vesicular endocytic compartments is regulated by Ca^{2+} concentration in the vicinity of these compartments, whereas the trafficking and activity of various proteases and lipases depends on the acidic environment maintained within both endosomal and lysosomal compartments (200, 264). TRP-ML1 has been reported to be permeable to both Ca^{2+} and to H^{+}; however, electrophysiological characterization of TRP-ML1 activity under physiological conditions has yet to be performed (40, 136, 138, 208, 231).

In the present studies we sought to determine whether MLIV results from aberrant membrane traffic to lysosomes. An additional issue is whether any observed defects in membrane trafficking or lipid metabolism are a primary result of MLIV pathophysiology, or are instead secondary effects that result from the chronic accumulation of undigested lipids in TRP-ML1-deficient cells. Our goal was to design an experimental system in which we could examine these membrane trafficking steps in cells that lacked TRP-ML1, but had not yet chronically accumulated undigested lipids. Since MLIV has been unequivocally identified as a “single gene disorder”, acute TRP-ML1 knockdown using siRNA is a valid model for the early stages of MLIV pathogenesis. Using this approach, we were able to downregulate TRP-ML1 expression in cells over a period of several days. During this time, lysosomes from these cells gradually accumulated lipid inclusions, but at a level significantly less than previously described in MLIV fibroblasts (231). Formation of inclusions was efficiently rescued by transfection of an siRNA-resistant version of TRP-ML1. Lipids accumulated in lamp-1-

positive organelles, suggesting that the inclusions are of lysosomal origin. Furthermore, colloidal gold internalized by fluid phase endocytosis could access inclusions in both isolated patient fibroblasts and in siRNA-treated cells, demonstrating that these organelles remain active components of the endocytic pathway.

Several studies have reported that the trafficking of fluorescent conjugates of LacCer is hindered in MLIV fibroblasts as well as in other lysosomal storage diseases (44, 188, 202, 231). Consistent with these observations, we observe a similar defect in LacCer handling in cells treated with TRP-ML1-specific siRNA. However, we observed no difference in the delivery of this lipid to lysosomes in control and TRP-ML1 knockdown cells. Therefore, the altered trafficking of LacCer may represent an effect on post-lysosomal membrane traffic and/or lipid metabolism in cells after prolonged accumulation of undigested materials. These results are consistent with a recent report by Thompson et al. (245), suggesting that the primary defect in MLIV lipid handling may be the exit of internalized lipids from lysosomes. We found no effect of acute TRP-ML1 knockdown on the rate of LDL delivery to lysosomes or on the degradation of both the lipid and protein components of this complex. Together, these data argue strongly against the “biogenesis” model for MLIV progression, which predicts that acute loss of TRP-ML1 function will result in a global defect in the delivery of both internalized lipids and proteins to lysosomes.

The role of TRP-ML1 in lysosomal ion homeostasis is currently disputed. Increased accumulation of acridine orange in MLIV fibroblasts has previously been observed (231), consistent with increased acidity of these organelles; however quantitation of lysosomal pH in MLIV fibroblasts by other groups has yielded discrepant

results (7, 126, 202). Similar to Pryor et al., we were unable to document any difference in lysosomal pH between control and MLIV fibroblasts by fluorescence ratio imaging; however, our studies were compromised by the intense autofluorescence in MLIV lipid inclusions that has previously been reported (80). However, we reproducibly observed that lysosomal pH in HeLa cells lacking functional TRP-ML1 was more acidic than control (an approximate decrease by 1.12 pH units). In principle, this finding is consistent with the "metabolic" model for MLIV pathogenesis, which postulates that the increased acidity of lysosomes disrupts lipid hydrolysis.

Previous groups have demonstrated defects in lipase handling in MLIV fibroblasts, including delayed de-esterification of cholesterol esters and decreased lysosomal acid lipase activity (105, 231). Consistent with this, we found that the release of free fatty acids from [^{14}C]-cholesteryl oleate-labeled LDL was slowed in MLIV fibroblasts. Surprisingly, however, we did not detect a deficit in cholesterol metabolism in siRNA-treated cells (after 1, 5 or 12 days).

The apparently normal hydrolysis of LDL cholesterol upon acute loss of TRP-ML1 function demonstrates that the increased lysosomal acidity observed in these cells does not critically impair acid lipase activity. Rather, there appears to be a gradual effect on lysosomal hydrolysis that manifests as a lag period between loss of TRP-ML1 function and the full elaboration of the MLIV disease phenotype. It is possible that a minor deficit in lipid hydrolysis that is undetectable early after TRP-ML1 loss has a cumulative effect whose consequences slowly develop as the disease progresses. Indeed, other lysosomal storage disease models such as Niemann-Pick Type C [NPC] (103, 161) teach us that a defect in a single component of lysosomal machinery may

sabotage processing of unrelated classes of lipids. NPC disease is caused by the mutation in either the late endosomal membrane protein NPC1 or the soluble lysosomal protein NPC2, and results in abnormal cholesterol transport along the late endocytic pathway. Similar to MLIV, NPC is caused by defective cholesterol trafficking rather than by a specific enzymatic abnormality. Although the primary defect is in cholesterol transport, the accumulation of other lipids, including sphingolipids has also been demonstrated in NPC (103).

In summary, our results suggest that TRP-ML1 does not directly regulate membrane traffic; thus enzyme replacement therapies remain a potentially viable treatment option for MLIV. Future studies are needed to determine whether TRP-ML1 plays an essential role in maintaining lysosomal ion homeostasis directly, so that replacement enzymes may be designed to operate in the unique environment of the TRP-ML1-deficient lysosome.

3.6 ACKNOWLEDGEMENTS

This work was supported by an ML4 foundation grant (to KK), by seed money award from Pittsburgh Life Science Greenhouse (to KK), NIH grant DK54407 (to OAW), and by the CTSI Multi-disciplinary Pre-doctoral Fellowship program awarded through the Clinical and Translational Science Institute and the Institute for Clinical Research Education at the University of Pittsburgh, grant 5TL1RR024155-02 (to MTM). The authors have no conflicting financial interests.

Abbreviations used are: CO, cholesteryl oleate; DMEM, Dulbecco's Modified Eagle's Medium; EGF, epidermal growth factor; FBS, fetal bovine serum; FITC, fluorescein; HSA, human serum albumin; LacCer, BODIPY-C5-lactosylceramide; LDL, low density lipoprotein; LPDS, lipoprotein deficient serum; MLII, mucolipidosis type II; MLIV, mucolipidosis type IV; NPC, Niemann-Pick Type C disease; PBS, phosphate buffered saline; TCA, trichloroacetic acid; TMR, tetramethylrhodamine; TRP, transient receptor potential; TRP-ML1, mucolipin-1.

4.0 DISCUSSION AND FUTURE DIRECTIONS

Since the first described case of MLIV in 1974 and the subsequent cloning of the *MCOLN1* gene in 2000, numerous groups have made valuable contributions to our current understanding of MLIV progression and TRP-ML1 function. When this dissertation work began five years ago, fewer than ten published reports examining the functional biology of TRP-ML1 were available. Since then, the list of TRP-ML1-specific papers has more than doubled. This work has led to a better model of TRP-ML1 function and the molecular mechanisms that drive MLIV pathogenesis. Several unresolved issues must be answered to unequivocally describe the molecular mechanisms responsible for the progression of MLIV. It is still not evident how TRP-ML1 functions with respect to lipid transport and/or metabolism. The primary goal of this dissertation was to determine the role of TRP-ML1 in the regulation of membrane trafficking. I addressed this question in two ways. First, I examined the mechanism of TRP-ML1 delivery to lysosomes. Secondly, I tested the role of TRP-ML1 in the regulation of specific membrane trafficking steps along the endocytic pathway.

A defining feature of TRP-ML1 is that it is exclusively localized to lysosomes and late endosomes. Little information existed regarding how this protein is delivered to lysosomes. In Chapter 2, I described the machinery and intracellular pathway involved in TRP-ML1 lysosomal targeting. This work was the first to identify the trafficking

itinerary of TRP-ML1 along the biosynthetic pathway and was subsequently validated by two other groups (202, 259). Lysosomal targeting of TRP-ML1 is mediated by both the E_{11}TERLL$_{16}$ and E_{573}EHLL$_{578}$ motifs present within the N- and C-terminal cytosolic tail, respectively (Figure 4.1). Direct lysosomal targeting of TRP-ML1 is mediated by the N-terminal sorting motif that facilitates the AP-1-dependnt Golgi export of TRP-ML1 (170), while C-terminal sorting information mediates AP-2-dependent internalization of TRP-ML1 from the plasma membrane (259). In addition, I have also demonstrated that cysteine residues within both cytosolic tails of TRP-ML1 are subject to palmitoylation (Figure 4.1) and others have shown that palmitoylation of the C-terminal tail serves to increase the efficiency of TRP-ML1 internalization from the cell surface (259). Finally, I have demonstrated that TRP-ML1 is subject to proteolytic processing along the biosynthetic pathway. I determined that cleavage occurs within a 40 amino acid region present between the second and third N-glycosylation sites of TRP-ML1 (Figure 4.1). This finding is largely consistent with observations made by others (121) who further suggested that cleavage serves to negatively regulate TRP-ML1 channel activity.

Chapter 3 was dedicated to examining the role of TRP-ML1 in regulation of membrane trafficking steps along the endocytic pathway. The goal was to evaluate models of MLIV pathogenesis, as it is debated whether TRP-ML1 functions to regulate membrane trafficking directly through late endosome-lysosome interactions (the 'biogenesis' model), or by helping to maintain lysosomal ion homeostasis that is essential for efficient lipid catabolism (the 'metabolic model'). Previous work has documented trafficking defects in TRP-ML1-deficient cells (14, 44, 202, 248). However, these observations were made using MLIV fibroblasts as a model system. Thus, the

possibility arose that potential abnormalities in trafficking may be the result of chronic lipid accumulation (a secondary effect), and not due specifically to the loss of TRP-ML1. I addressed this question by examining endocytic membrane trafficking steps in both MLIV fibroblasts and in cells treated with specific siRNAs to acutely down-regulate TRP-ML1 expression. This enabled me to directly compare trafficking in cells that lacked TRP-ML1, but had not yet accumulated large amounts of undigested lipid material. These studies revealed that the lysosomal delivery of multiple protein and lipid markers was not perturbed in MLIV fibroblasts or TRP-ML1 siRNA-treated cells.

I also examined the lysosomal hydrolysis kinetics of both the lipid (cholesterol) and protein (apoB) components of the LDL complex in TRP-ML1-deficient cells. I found that degradation of the cholesterol component of LDL was impaired in MLIV fibroblasts. Surprisingly, I did not observe this deficiency in TRP-ML1 siRNA-treated cells despite a documented increase in lysosomal acidity. Overall, my data suggest that TRP-ML1 does not function to directly regulate specific endocytic membrane trafficking events that mediate the delivery of lipids and proteins to lysosomes. These studies are more consistent with TRP-ML1 involvement in the maintenance of lysosomal ion homeostasis that is necessary for the efficient metabolism of internalized lipid substrates as is predicted in the metabolic model. In the remainder of this section, I will discuss potential mechanisms through which defects in lysosomal ion homeostasis may contribute to MLIV pathogenesis.

```
1   MTAPAGPRGS ETERLLTPNP GYGTQAGPSP APPTPPEEED LRRRLKYFFM SPCDKFRAKG
61  RKPCKLMLQV VKILVVTVQL ILFGLSNQLA VTFREENTIA FRHLFLLGYS DGADDTFAAY
121 TREQLYQAIF HAVDQYLALP DVSLGRYAYV RGGGDPWTNG SGLALCQRYY HRGHVDPAND
181 TFDIDPMVVT DCIQVDPPER PPPPPSDDLT LLESSSSYKN LTLKFHKLVN VTIHFRLKTI
241 NLQSLINNEI PDCYTFSVLI TFDNKAHSGR IPISLETQAH IQECKHPSVF QHGDNSFRLL
301 FDVVVILTCS LSFLLCARSL LRGFLLQNEF VGFMWRQRGR VISLWERLEF VNGWYILLVT
361 SDVLTISGTI MKIGIEAKNL ASYDVCSILL GTSTLLVWVG VIRYLTFFHN YNILIATLRV
421 ALPSVMRFCC CVAVIYLGYC FCGWIVLGPY HVKFRSLSMV SECLFSLING DDMFVTFAAM
481 QAQQGRSSLV WLFSQLYLYS FISLFIYMVL SLFIALITGA YDTIKHPGGA GAEESELQAY
541 IAQCQDSPTS GKFRRGSGSA CSLLCCCGRD PSEEHSLLVN
```

TM domains:
Sorting information:
Palmitoylation sites:
Phosphorylation sites:
N-glycosylation sites:

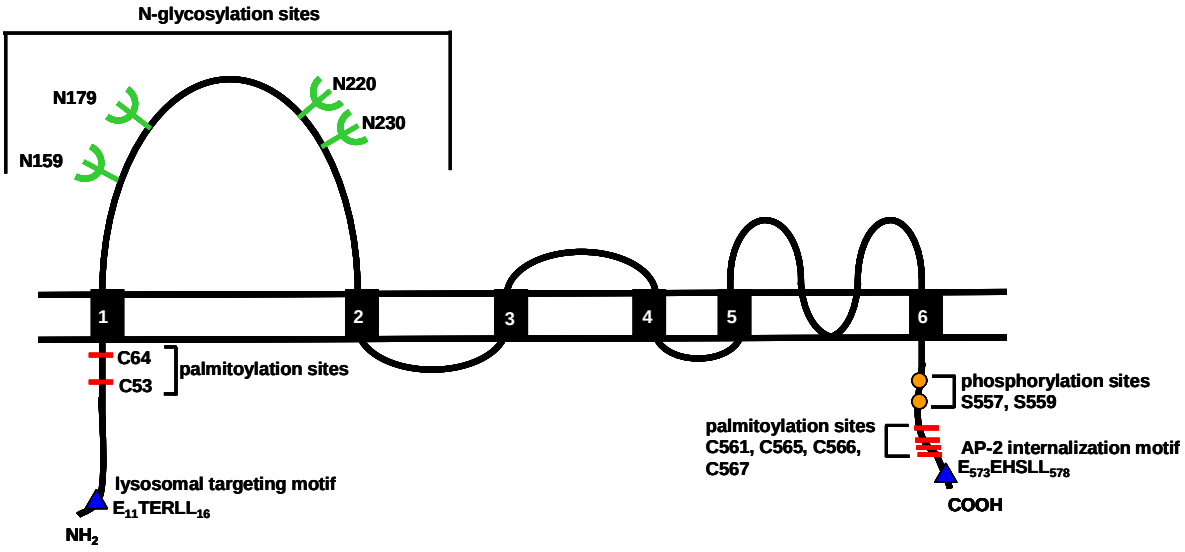

Figure 4.1 Amino acid sequence and predicted topology of TRP-ML1.

(Top panel) Amino acid sequence of human TRP-ML1. Key features of this sequence are highlighted as described in the legend to identify important TRP-ML1 features including transmembrane (TM) segments, trafficking motifs, and sites of post-translational modification. (Bottom panel) Predicted topology of TRP-ML1 with the same features highlighted as described above.

4.1 TRP-ML1 AND REGULATION OF THE LYSOSOMAL MICROENVIRONMENT

The results of my thesis research suggest that MLIV pathogenesis is linked to defects in lysosomal ion homeostasis caused by the loss of functional TRP-ML1. Although the ion permeability characteristics of this channel are still debated, it is clear that both H^+ and Ca^{2+} ions have important roles in the coordination of endocytic events (149, 264). In my studies, lysosomal pH in cells treated with TRP-ML1-specific siRNA was found to be lower than values obtained for control cells. In TRP-ML1-deficient cells, I estimated lysosomal pH to be ~4.0 (compared to 5.0 in control cells). Other groups have demonstrated that the optimal pH for lysosomal acid lipase (LAL) activity is 4.0-5.0 (81). LAL is responsible for the de-esterification of LDL-derived cholesterol. Therefore, a seemingly 'optimal' environment for LAL activity has been created in TRP-ML1 siRNA-treated cells, and indeed, I found no defect in cholesterol metabolism in these cells. However, I did observe significant impairment of cholesterol hydrolysis in MLIV fibroblasts. What leads to impairment of cholesterol hydrolysis in MLIV fibroblasts?

One explanation may be the relationship between increased lysosomal acidity and the regulation of lipase stability. Hydrolases that reside within the lysosomal lumen are subjected to proteolytic degradation. The half-lives of certain proteases have been shown to be significantly increased by binding to a Cathepsin A-containing protective scaffold (99, 186). To date, no such protective mechanism has been described for lysosomal lipases. At increased levels of lysosomal acidity, lipases may be more prone to increased proteolysis while some proteases may be able to avoid this processing through such a protective interaction. Therefore, increased lysosomal acidity may result in significantly reduced levels of specific lipases, causing downstream effects on lipid

handling. In Appendix A, I demonstrate that LAL protein levels in TRP-ML1 siRNA-treated cells are significantly reduced compared to control cells (Figure A.4). However, I find no concurrent abnormality in cholesterol hydrolysis in these cells. How is this observation explained? Although decreased, the LAL that remains may actually be working in a more optimal environment created by increased lysosomal acidity. Therefore, reduced levels of LAL may be able to sufficiently compensate and process cholesterol normally.

My data demonstrate that cholesterol hydrolysis is impaired in MLIV fibroblasts. I also compared LAL levels in control and MLIV fibroblasts (Figure A.4) and I did not find a significant decrease in overall LAL levels. However, I did observe the increased presence of an apparent proteolytic LAL fragment, suggesting that abnormal processing of this enzyme may contribute to the defect in cholesterol metabolism. Thus, LAL-mediated cholesterol metabolism may be maintained temporarily, but ultimately impaired LAL proteolytic processing and/or regulation of stability may culminate in defective cholesterol hydrolysis over time. It would be useful to formally evaluate LAL activity in TRP-ML1-deficient cells, as reports regarding its activity in MLIV fibroblasts are conflicting (105, 231). It would also be beneficial to examine whether the half-life of LAL is altered in TRP-ML1-deficient cells, as a dramatic decrease may suggest an up-regulation of LAL proteolysis. It should also be noted that abnormal lysosomal proteolysis in TRP-ML1-deficient cells may not be strictly limited to LAL. I have observed reduced levels of cathepsin B in TRP-ML1-deficient cells, suggesting that there may be a negative effect on the processing of this hydrolase to its active form (Figures A.1 and A.2). Similar reports regarding abnormalities in enzyme processing

have been described using HT-29 cells (a colon cancer epithelial cell line), showing that abnormal sialic acid metabolism alters the lysosomal processing of Cathepsin D (250).

Another compounding issue involving the LDLR-mediated pathway and cholesterol homeostasis comes from recent work in which gene expression profiling was performed in MLIV fibroblasts (29). It was shown in these studies that mRNA levels of several LDL pathway genes were more abundantly expressed in MLIV fibroblasts including *LDLR, SREBP1,* and*, SREBP2.* The elevated expression of these gene products would result in the increased uptake of LDL which may facilitate the 'swamping out' of an already disabled cholesterol-metabolizing system. Thus, ionic imbalance within the lysosome created by pH dysregulation may cause initial defects in LDL metabolism which intensify over time, creating an overall imbalance in cellular cholesterol homeostasis. This initial insult may subsequently induce the accumulation of other lipid species, as cholesterol and glycosphingolipid homeostasis are integrally related (204, 226).

Currently, I am unable to assess if defects in cholesterol metabolism are directly attributed to changes in lysosomal pH because of difficulties in reliably determining values in MLIV fibroblasts. This is a critical issue because results describing lysosomal pH in MLIV fibroblasts are conflicting (7, 126, 202, 231). My preliminary studies suggest that lysosomal pH in MLIV fibroblasts is not significantly different than values obtained in control cells. This observation has also been made by others (202). Thus, another question that arises is to explain why lysosomal pH is lower in cells treated with TRP-ML1 siRNA compared to MLIV fibroblasts? As described in Chapter 3, one of the main differences between TRP-ML1 siRNA-treated cells and MLIV fibroblasts is that the

former have not yet undergone the chronic accumulation of undigested lipid material that is characteristic of MLIV cells. Thus, overall lipid storage content may influence lysosomal pH. Numerous LSD cell lines have been previously shown to have elevated lysosomal pH (7). With respect to TRP-ML1 siRNA-treated cells, the decrease in lysosomal pH I observed may be an 'early-onset' phenotype that is eventually alleviated as storage content accumulates over time. This preliminary decrease in lysosomal pH may still have an important role in generating dysfunction of the lysosomal microenvironment that initiates downstream effects on cholesterol handling and/or lipid metabolism. Assuming that lysosomal pH in MLIV fibroblasts is normal it would be interesting to determine how long this initial decrease in lysosomal acidity persists. My data suggest that cholesterol metabolism in TRP-ML1 siRNA-treated cells is normal after 12 days of siRNA treatment and during this time there is not a significant increase in the total number of lipid inclusions present in these cells (Figure 3.2). Therefore, it is necessary to determine if lysosomal pH increases concurrently with the increased build-up of stored lipid material in siRNA-treated cells.

Ionic imbalance within the lysosomal lumen may also be created via mechanisms that are not directly the result of abnormal pH. The release of Ca^{2+} is necessary for the efficient fusion of late endosomes and lysosomes (200). The transporters and channels involved in the regulation of lumenal ionic composition are only beginning to be identified. With respect to Ca^{2+}, the lysosomal NAADP (nicotinic acid-adenine dinucleotide phosphate)-regulated Ca^{2+} channel (the NAADP receptor) is also a likely candidate to play a role in regulation of the lumenal concentration of lysosomal Ca^{2+} (173, 275, 276). Recent unpublished findings by Peterneva and Llyod-Evans (University

of Oxford, UK) implicate a role for TRP-ML1 in the regulation of NAADP receptor function in the process of late endosome-lysosome fusion.

It was demonstrated that MLIV lysosomes have both normal pH and intralumenal Ca^{2+} concentrations (202, 231). However, in spite of normal Ca^{2+} levels, it is suggested that MLIV lysosomes are susceptible to multiple, spastic Ca^{2+}-release events whereas normal lysosomes are not. Intriguingly, inhibition of the NAADP receptor was shown to alleviate abnormal Ca^{2+}-release events observed in MLIV cells. This imbalance of lysosomal ion homeostasis induced by changes in lumenal Ca^{2+} concentrations was associated with the increased presence of hybrid late endosome-lysosome structures and subsequent glycosphingolipid storage. These results suggest that TRP-ML1 is involved in maintaining proper lysosomal ionic balance, potentially through regulation of the NAADP receptor.

Lastly, the above examples are not meant to exclude the possibility that defects in Ca^{2+} and H^{+} homeostasis in TRP-ML1-deficient cells are dependent on one another. Studies in mouse macrophage lysosomes show that the intralumenal concentration of Ca^{2+} is significant (400-600 µM), and changes in pH can have a dramatic impact on lysosomal Ca^{2+} levels (49). After treatment with bafilomycin A_1, lysosomal pH increased from 4 to 7 and lysosomal Ca^{2+} concentration decreased from 0.6 mM to 285 nM, indicating that Ca^{2+} levels are maintained in part by the pH gradient across the lysosomal membrane. Regarding lysosome biogenesis, reformation of mature (dense core) lysosomes is also dependent upon the release of lumenal Ca^{2+} (149, 200), and it has been shown that this release can be inhibited by treatment with either membrane permeable Ca^{2+}-chelators or Bafilomycin A_1.

4.2 ALTERNATIVE MEMBRANE TRAFFICKING DEFECTS IN TRP-ML1-DEFICIENT CELLS

MLIV is considered a disease whose pathology is rooted in endocytic membrane transport defects. It has been suggested that TRP-ML1 functions to regulate membrane interactions that are required for the lysosomal delivery and degradation of internalized proteins and lipids. My experimental results largely argue against this hypothesis. However, a possible role for TRP-ML1 function in the *exit* of lipids and proteins from late endocytic compartments has recently emerged that is consistent with my results (245). Using an siRNA-based approach, I demonstrated that the lysosomal delivery of internalized LacCer is normal. Despite unimpaired delivery, I found that subsequent Golgi-localization of this lipid is impaired. Moreover, I could reverse this phenotype upon expression of an siRNA-resistant TRP-ML1 construct. Similar results have also been obtained in MLIV fibroblasts demonstrating that TRP-ML1 channel activity is required for LacCer Golgi targeting (202).

Similarly, using an siRNA-based approach in a mouse macrophage cell line, Thompson et al. (245) recently concluded that TRP-ML1 is required for the efficient exit of lipids and proteins out of hybrid LE-lysosome organelles. In agreement with previous work that characterized the real-time dynamics of hybrid organelle formation (30), these studies also observed tubular intermediates that emanate from hybrid organelles. TRP-ML1 localized to both the parent compartment and the tubular intermediates. Tubular intermediates also contained various endocytic markers including dextran, BSA, LacCer, and the Major Histocompatibilty Complex II (MHC II). Reduction of TRP-ML1 levels resulted in abnormal transport of LacCer to the Golgi, transport of BSA to

lysosomes, and transport of MHC II to the plasma membrane. It was suggested that TRP-ML mediates the scission of tubules from the hybrid organelle, analogous to the process of lysosome re-formation previously described in a *C. elegans* model system (248). In their model, TRP-ML1 is located in a pre-lysosomal compartment that serves as a hub for molecules destined for transport to a variety of intracellular locations. Thus, the process of lysosome biogenesis also includes sorting from the hybrid organelle in addition to the re-formation of individual late endosomes and lysosomes.

Comparing these results to my data it is clear that the Golgi targeting of GSLs such as LacCer is impaired in TRP-ML1-deficient cells. However it is not clear from which intracellular compartment this defect originates. While the model described above suggests lipid transport is impaired from a pre-lysosomal compartment, my data are more consistent with defects in post-lysosomal lipid transport. Are defects in LacCer Golgi targeting the result of impaired trafficking from lysosomes, or are they result of impaired lysosome re-formation?

It is uncertain whether TRP-ML1 activity affects LacCer trafficking directly. Moreover, the function of TRP-ML1-positive tubular intermediates is not clearly characterized. Do these intermediates participate in lysosome biogenesis, or do they strictly mediate sorting of various molecules from hybrids? Pryor et al. have demonstrated that Golgi targeting of LacCer in MLIV fibroblasts requires TRP-ML1 channel activity. Expression of a TRP-ML1 cDNA encoding a mutation in the pore region of the channel was unable to restore proper localization of this lipid (202). How might TRP-ML1 activity be involved in lipid transport? One potential explanation is that TRP-ML1 has a direct role in the formation and/or scission of transport intermediates

derived from hybrid organelles or lysosomes. The release of lumenal Ca^{2+} can affect *trans*-SNARE complex formation in endosomal fusion (152). For example, Hrs (hepatocyte growth factor-regulated tyrosine kinase substrate) is a Ca^{2+}-sensitive protein that directly interacts with SNARE proteins, preventing early endosome fusion (241). Hrs interacts with the Q-SNARE SNAP-25, preventing *trans*-SNARE complex formation with its cognate R-SNARE VAMP2. The release of lumenal Ca^{2+} has been demonstrated to alleviate the Hrs-SNAP-25 interaction, allowing for *trans*-SNARE complex formation and subsequent endosomal fusion (268). Therefore, the release of a similar inhibitory interaction may be required for transport from hybrid organelles and/or lysosomes. TRP-ML1 may function to directly mediate the release of intralumenal Ca^{2+}, promoting membrane interactions required for lipid transport. Alternatively, TRP-ML1 may also function in a manner that does not directly affect lipid trafficking. Rather, TRP-ML1 activity may contribute to the processing of lipids such as LacCer through regulation of the lumenal ionic conditions required for efficient hydrolysis. Chen et al. have shown that the activity of LacCer-hydrolyzing enzymes is normal in MLIV fibroblasts, suggesting that enzymatic activity is unperturbed (44). However, neither my work nor the studies performed by Thompson et al. specifically examined the activity of these enzymes and/or LacCer processing in TRP-ML1 siRNA-treated cells. Finally, the abnormal accumulation of LacCer occurs in numerous LSDs (157, 204). Therefore, it must also be considered that the accumulation of lipid species such as LacCer is not unique to lack of functional TRP-ML1. GSL accumulation may be a more general feature of LSDs. As described in Section 1.3.2, GSL accumulation occurs in storage disease cell lines that do not have specific defects in GSL-hydrolyzing enzymes. The

relationship between cholesterol and GSL homeostasis within cells is complex, where abnormalities in one substrate can affect the processing and/or transport of the other. My data demonstrate that LDL-derived cholesterol hydrolysis is impaired in MLIV fibroblasts; however, it is unimpaired in cells where TRP-ML1 has been acutely down-regulated. I concluded that MLIV pathogenesis is cumulative, resulting in a lag period before defects in cholesterol metabolism are apparent. Interestingly, I find that LacCer Golgi transport is affected under both conditions, suggesting that abnormalities may be independent of defects in cholesterol metabolism. Thus, defects in lipid transport may arise due to abnormalities in trafficking from lysosomes.

Currently, there is little information regarding intracellular trafficking from lysosomes. What is the machinery involved in post-lysosomal trafficking to the Golgi? How are SNARE components retrieved back to their respective compartments during lysosome re-formation? Pagano et al. (188, 189) found that LacCer transport from late endosomes is dependent on Rab9. Rab9 is implicated as a tethering factor that facilitates budding of vesicles derived from endosomal compartments (11, 146). Similarly, the mammalian retromer complex may have a role in the retrieval of SNARE components during lysosome biogenesis. The retromer, originally described in yeast, functions in the retrograde transport of the CI-MPR from endosomes to the TGN, and is associated with both vacuolar and tubular aspects of the endosomal network (26). Thus, the retromer resides in an optimal position to participate in either the transport of lipids to the Golgi, or the retrieval of SNARE components that are required for lysosome re-formation. TRP-ML1 is localized to tubular extensions that emanate from hybrid late endosome-lysosome organelles (245). Thus, TRP-ML1 and the retromer may function

together to facilitate the trafficking of tubular intermediates required for lipid transport or recycling of SNARE components. Tubule-based endosomal trafficking is an exciting new area of interest and details of this process are only beginning to emerge. It would be novel if a link between TRP-ML1 and the retromer complex is established. How might TRP-ML1 participate in retromer-mediated trafficking steps? It is necessary to determine whether TRP-ML1 activity serves to recruit and/or activate retromer components, maintain the proper ionic environment within tubular compartments to promote the proper assembly of trafficking machinery, or mediate the scission of these intermediates from the endosomal compartment. Defects in these processes may result in the abnormal exit of lipids from lysosomes, or negatively affect the retrieval of SNARE components required for LE-lysosome interaction. In either case, these deficiencies would disrupt normal lipid transport and/or metabolism, contributing to lipid storage.

4.3 MLIV AND AUTOPHAGIC DEFECTS

Autophagy is a process that mediates the sequesteration of macromolecules into specialized cytosolic vesicles for delivery and degradation in lysosomes. Autophagic activity is required for the degradation of aged cytosolic proteins and organelle turnover (132, 159). There are three primary autophagic pathways: macroautophagy, microautophagy, and chaperone-mediated autophagy (CMA). Autophagic deficiencies have been documented in a number of storage diseases (220), as autophagy is dependent upon lysosome function. One of the most difficult issues in studying LSDs is identifying the underlying mechanisms that link lysosomal function and autophagy. More

importantly, it is not well characterized how an upset in this balance results in cell death. It is increasingly more relevant to determine if autophagic defects can trigger such events because of the interconnected relationships of these two pathways. Recent evidence suggests that there are indeed autophagic defects in TRP-ML1-deficient cells (108, 257), specifically with regards to macroautophagy and CMA. These studies are of considerable importance because they may provide insight into the general mechanism that leads to cell death in LSDs.

Macroautophagy is the primary pathway by which cellular components such as organelles are turned over. In macroautophagy, sequesteration of organelles requires the formation of an intermediate vesicle termed an autophagosome. Efficient transduction of this pathway requires fusion of autophagosomes with lysosomes (reviewed in Section 1.2.1). Therefore, autophagy has been examined in MLIV fibroblasts because of the proposed role for TRP-ML1 in regulation of late endosome-lysosome interaction. Basal levels of autophagy were found to be increased in TRP-ML1-deficient cells and it was shown that the majority of phagosomes contained aggregates of ubiquitinated proteins (257). It was also demonstrated that the increased numbers of autophagosomes in MLIV cells were caused by both delayed fusion with lysosomes and increased levels of autophagosome formation (257).

Recent work has also shed light on a potential mechanism relating overall lysosomal function to defects in autophagy, providing a model for the basis of cell death in MLIV (108, 122, 123). Lysosomes are essential for the completion of autophagy-mediated organelle degradation. It was recently found that MLIV fibroblasts displayed an increased accumulation of fragmented mitochondria with impaired Ca^{2+}-buffering

capacity (108). Without, the optimal Ca^{2+}-buffering capacity of the mitochondria, MLIV cells were shown to be increasingly susceptible to caspase-dependent apoptotic cell death pathways which are triggered by rises in cytosolic Ca^{2+} (122, 123). Therefore, chronic disruption of lysosomal function apparently leads to disrupted autophagic turnover of mitochondria. Accumulation of impaired mitochondria reduces the ability to buffer against a potent pro-apoptotic signal, resulting in increased cell death. Intriguingly, studies performed in *cup5*$^{-/-}$ *C. elegans* have suggested that lethality in these animals is due in part to cellular starvation caused by decreased levels of ATP (216). This deficit culminates in apoptotic cell death via a CED-3 (caspase)-mediated pathway. Unfortunately, mitochondrial abnormalities were not examined in these studies, but it is tempting to speculate that ATP levels could have been negatively affected in a mechanism similar to what has been described above.

Lastly, there is evidence for a potential connection between the lysosomal dysfunction caused by lack of TRP-ML1 and the process of chaperone-mediated autophagy (CMA). CMA is a selective mechanism for the degradation of soluble cytosolic proteins in lysosomes. The limiting step in this autophagic pathway is the binding of substrates to LAMP-2A, which facilitates the selective import of cytosolic proteins for lysosomal degradation (119). Specifically, the pool of LAMP-2A responsible for protein import was found to be concentrated within discrete detergent resistant fractions of the lysosomal membrane. Overloading lysosomes with cholesterol caused a marked decrease in CMA activity. Thus, both the dynamic lysosomal distribution of LAMP-2A and lysosomal cholesterol homeostasis are implicated in regulation of CMA activity. Interestingly, my data suggest that there are increased levels of LAMP-1 and

impairments in cellular cholesterol homeostasis in cells lacking TRP-ML1 (Figures A.1 and A.2; Figure 3.9). This presents the possibility that the observed defects in cholesterol metabolism in MLIV cells may also alter the lysosomal distribution and/or levels of LAMP proteins, causing downstream alterations in CMA. These preliminary findings only hint at CMA being affected in MLIV cells. There is no published report documenting CMA-related defects in MLIV fibroblasts. Specific experiments would need to be performed to demonstrate abnormal CMA activity in these cells. Furthermore, I do not know if LAMP-2A levels are affected in a similar manner to LAMP-1. However, I observe elevated levels of LAMP-1 in cells treated with TRP-ML1-specific siRNA, suggesting that the change occurs rapidly upon down-regulation of TRP-ML1. As a result, defects in CMA may occur in parallel with changes in LAMP-1 levels, suggesting that auotophagic defects and cell death occur early on in MLIV progression. It has also recently been documented (256) that there is a direct interaction between TRP-ML1 and the cytosolic chaperone hsc70. This protein is a known component of the chaperone machinery that is responsible for protein transport into the lysosome during CMA. Therefore, TRP-ML1 may also function to facilitate the import of proteins in concert with LAMP-2A during CMA.

APPENDIX A

PROTEIN PROFILING IN TRP-ML1-DEFICIENT CELLS

Prevailing models of MLIV pathogenesis suggest that TRP-ML1 directly regulates the postendocytic delivery of internalized lipids and proteins by mediating the transient interactions between late endosomal and lysosomal compartments (202, 248). My work in Chapter 3 argues against this model for TRP-ML1 function (169). My results suggest that the lysosomal delivery and degradation of various lipids and proteins is unperturbed. However, cholesterol ester hydrolysis in MLIV patient fibroblasts was found to be selectively impaired. From these results I hypothesize that the loss of functional TRP-ML1 negatively alters hydrolytic activity and has a cumulative effect on lysosome function. Therefore, I suggest that TRP-ML1 may have a role in maintaining overall lysosomal ion homeostasis. My present studies are aimed at identifying specific lysosomal proteins whose levels and/or activities may be affected by TRP-ML1 loss. Toward this end, I have employed quantitative Western analysis of cell extracts prepared from TRP-ML1-deficient cells and control cells to examine whether the levels and/or processing of certain lysosomal proteins are altered in cells lacking TRP-ML1. In addition, recent data suggest that TRP-ML1 may function as a proton-leak pathway to

prevent over-acidification of the lysosomal lumen. Furthermore, my data suggest that in cells treated with TRP-ML1-specific siRNA, lysosomal pH is lower when compared to that of control cells. I want to examine whether the expression of a lysosomally-tagged version of the influenza A M2 protein, a known H^+-permeable channel (195, 221, 261), is able to alleviate this effect. Toward this end, I have begun to examine the intracellular distribution of lysosomally-targeted versions of M2.

A.1 MATERIALS AND METHODS

Western analysis of whole cell extracts. To compare the total levels of various lysosomal proteins, whole cell extracts were examined by quantitative Western analysis. Cell extracts were prepared by gently trypsinizing either fibroblasts or siRNA-treated HeLa SS6 cells, resuspending the resultant cell pellet in ice cold PBS supplemented with protease inhibitors (Roche), and subjecting them to 3 cycles of freeze-thaw in liquid nitrogen and pulse sonication to disrupt cellular membranes. Lysates were then briefly centrifuged at 4ºC to pellet remaining cellular debris, and protein concentrations of individual extracts were determined by Bradford assay against a BSA standard curve. 50 µg (unless otherwise stated) of lysate was loaded in duplicate for each sample, subjected to SDS-PAGE, and Western analysis to detect endogenous levels of LAMP-1 (BD Biosciences; 1:500), cathepsin D (EMD Biosciences; 1:500), cathepsin B (EMD Biosciences; 1:500), lysosomal acid lipase (Abnova; 1:250). β-actin (Sigma; 1:5000) was used as a loading control. Protein levels were quantified using the BioRad Versa Doc system Quantity One software for densitometry analysis. One-Way ANOVA

analysis using the Holm-Sidak method was employed to assess statistical differences between groups.

Generation of HA-M2$_{LAMP1}$. A modified version of the Quikchange (Stratagene) protocol previously described by Wang and Malcolm (263) and in Chapter 2 was used to insert both the HA epitope and the C-terminal tail of LAMP-1 that contains lysosomal targeting information (RKRSHAGYQTI) into the cytosolic tail of the influenza A M2 protein. The following primers were used for the PCR reaction: (Forward) 5'-ATAGAGCTGGAGATGTACCCATACGATGTTCCAGATTACGCTAGGAAGAGGAGTC ACGCAGGCTACCAGACTATCTAAGGATCCCGGGT-3' and (Reverse) 5'-ACCCGGGATCCTTAGATAGTCTGGTAGCCTGCGTGACTCCTCTTCCTAGCGTAATC TGGAACATCGTATGGGTACATCTCCAGCTCTAT-3'. Following HA-M2$_{LAMP1}$ synthesis, the construct was transiently transfected into HeLa SS6 cells and standard immunofluorescence staining procedures (as described in Chapter 2) were used to detect the intracellular distribution of the HA epitope and compare it to the localization of the endogenous lysosomal marker LAMP-1.

A.2 RESULTS

A.2.1 Comparison of lysosomal protein levels in control and MLIV fibroblast cell lines.

To date, only one large-scale study has been performed comparing gene expression profiles in control and MLIV fibroblasts (29). My goal was to begin protein profiling in control and MLIV fibroblasts to examine if the levels and/or processing of lysosomal membrane proteins or soluble hydrolases are affected. I employed quantitative Western analysis to examine levels of these proteins. Thus far, I have examined the levels of three lysosomal proteins: LAMP-1, cathepsin D, and cathepsin B in four control fibroblast cell lines (F93, F94, M1 and WG987; WG987 is a heterozygous parental control cell line) and one MLIV fibroblast cell line (WG909). The results of these studies are presented in Figure A.1. 50 µg of cell extract was prepared from each cell line and subjected to Western and densitometry analysis to detect endogenous levels of actin (loading control), LAMP-1, cathepsin D, and cathepsin B. As shown in Figure A.1A, levels of LAMP-1 in MLIV fibroblast extracts were significantly increased (~30% higher compared to levels obtained in WG987 extracts; a heterozygous parental control) compared to control cell lines. I observed no significant difference in the levels of cathepsin D among control and MLIV cell lines (Fig. A.1B). However, I did find a dramatic decrease in the overall levels of the active form of cathepsin B in MLIV extracts (~60% less than WG987) (Fig. A.1C). Figure A.1D displays a representative Western of one of these experiments. Comparisons between WG987 and WG909 were

each performed 6 times and analysis with other control cell lines (F93, F94, and M1) was performed 4 times.

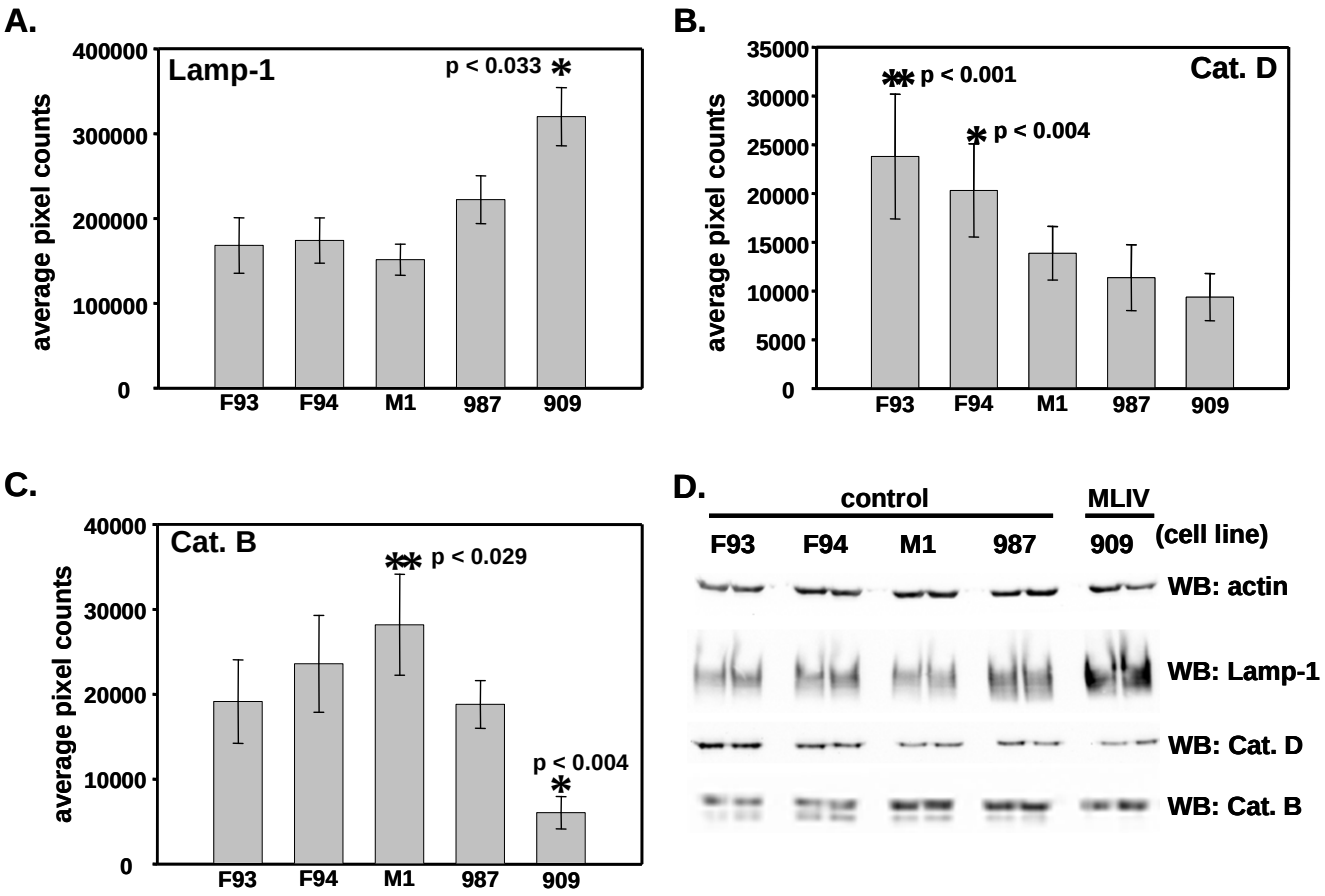

Figure A.1 Comparison of lysosomal protein levels in control and MLIV fibroblast cell lines.

(A-C) 50 ug cell lysate was prepared from each cell line, loaded in duplicate samples, and subjected to SDS-PAGE and Western analysis to detect endogenous levels of actin (loading control), Lamp-1, cathepsin D, and cathepsin B. Levels of these proteins were quantified using the BioRad Versa Doc system and Quantity One software. Levels of proteins are expressed as the average raw pixel counts for the total number of experiments. For the F93, F94, and M1 cell lines experiments were repeated 4 times. For 987 and 909, experiments were repeated 6 times. (D) Representative Western blot of the cell lines tested. One-Way ANOVA analysis using the Holm-Sidak method was employed to assess statistical differences between groups.

A.2.2 Comparison of lysosomal protein levels in control and TRP-ML1 siRNA-treated cells.

I have also examined the levels of the lysosomal proteins LAMP-1 and cathepsin B in cells treated with control or TRP-ML1-specific siRNAs for 5 d. Overall, I find similar results compared to studies performed using fibroblast extracts. The results of these studies are shown in Figure A.2. For LAMP-1, I observe a significant increase in the levels in extracts prepared from cells treated with TRP-ML1-specific siRNA (Fig. A.2A and A.2B). These results are consistent with results obtained in MLIV fibroblasts. In addition, analysis of lysosomes purified from control and MLIV fibroblasts display similar findings (Fig. A.2D).

While I have not been able to directly quantitate levels in control and TRP-ML1 siRNA-treated cells, I have observed qualitative differences in cathepsin B levels that suggest differential processing of this lysosomal cysteine protease. cathepsin B is synthesized as an inactive preproenzyme (40 kDa) which is further processed to a still inactive proenzyme (37 kDa) within the lysosomal compartment (174). Removal of the propeptide (63 amino acid residues) results in the conversion of the inactive proenzyme into the single chain active form of 30 kDa. However, cathepsin B may also undergo further hydrolysis within the lysosome, converting it to a second active form consisting of a heavy (25 kDa) and light (5 kDa) chain components that remain associated through a cysteine disulfide bond (174). I find that in control siRNA-treated cells there is the presence of two distinct molecular weight forms of cathepsin B, a higher molecular weight form that migrates at ~30 kDa, and a slightly smaller form that is ~25 kDa (Fig. A.2C). However, in extracts prepared from cells treated with TRP-ML1 specific siRNA, I

observe an almost complete absence of the 25 kDa fragment, while finding an increased presence of the 30 kDa single chain active form (Fig. A.2C). These results are consistent with results obtained in MLIV fibroblast extracts where a significant reduction in the amount of the 25 kDa form of cathepsin B was also found (Fig A.1D). Combined with the results obtained in MLIV fibroblasts, my results suggest that levels of the active form of cathepsin B are reduced and/or abnormally processed. Analysis of isolated lysosomes from control and MLIV fibroblasts indicate that there are increased levels of the single chain active form of cathepsin B in MLIV fibroblasts (Fig. A.2D). However, I was unable to detect the heavy chain 25 kDa fragment in lysosomes isolated from either cell type. These results are consistent with abnormal processing and/or conversion of the active forms of cathepsin B in cells lacking functional TRP-ML1. However, it is necessary to determine if cathepsin B activity is impaired in cells lacking TRP-ML1.

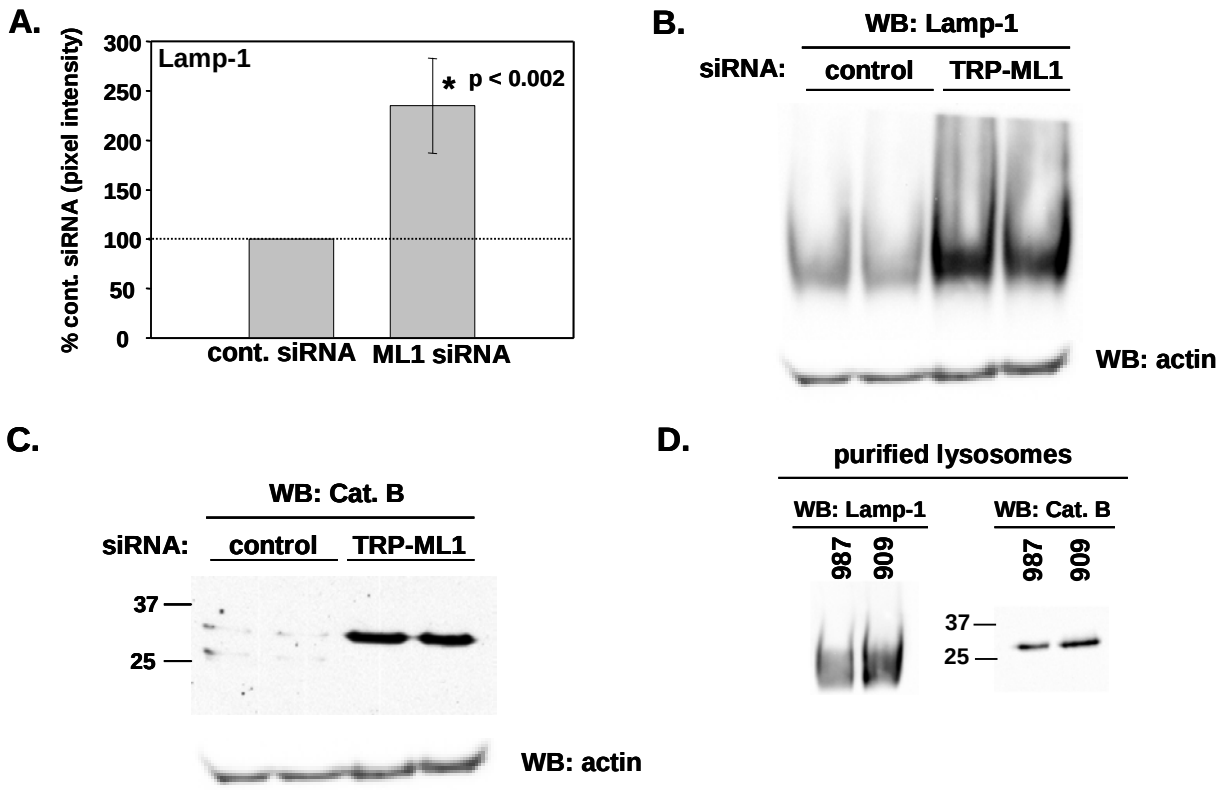

Figure A.2 Comparison of lysosomal protein levels in control and ML1 siRNA treated HeLa cells. (A and B) Levels of Lamp-1 were quantified as described in Figure A.1 for both control and ML1 siRNA treated cells. The data here represent 3 independent experiments and are represented as % of levels (pixel intensity) obtained in control cells. Statistical significance was determined by using the Student's t-test. Panel B is a representative Western blot from one of the experiments. (C) Representative Western blot detecting endogenous cathepsin B in control and ML1 siRNA treated cells. (D) Representative Western blot detecting endogenous LAMP-1 (left) and Cathepsin B (right) in lysosomes isolated from control (987) or MLIV (909) fibroblasts.

A.2.3 Examination of lysosomal acid lipase in TRP-ML1-deficient cells

Lysosomal acid lipase (LAL) is the primary enzyme responsible for the degradation of cholesterol esters and triglycerols that are delivered to lysosomes via the LDLR-mediated pathway (81). The free cholesterol created by LAL activity is important to overall intracellular cholesterol homeostasis (36, 103). Deficiency in LAL results in two genetic diseases, Wolman's disease and cholesteryl ester storage disease (CESD) (103, 161). Reports regarding LAL function in MLIV are conflicting as earlier reports suggest that LAL activity is normal in MLIV fibroblasts (105), while more recent work suggests that acid lipase activity is hindered in MLIV patient cells (231). Work presented in Chapter 3 (169) also suggests that there is an impairment in hydrolysis of LDL-derived cholesterol in MLIV fibroblasts. Interestingly, I only observed this defect in MLIV fibroblasts, and not in cells where TRP-ML1 had been acutely down-regulated with siRNA treatment. Therefore, my goal in these studies was to examine LAL both in MLIV fibroblasts as well as in siRNA-treated cells, and to determine if overall levels and/or processing of LAL were altered.

Previous work has demonstrated that LAL undergoes proteolytic processing resulting in 56 kDa and 41 kDa forms (278). Therefore, it has been suggested that the 56 kDa form of LAL may serve as a preproprotein form of LAL (2, 278). I first examined LAL by Western analysis in extracts prepared from control and MLIV fibroblasts, and found increased levels of a smaller LAL fragment that migrated at ~50 kDa in MLIV fibroblasts compared to a higher ~55 kDa form of LAL whose levels stayed consistent between control and MLIV cell lines (Fig. A1.3A). In addition, I also examined LAL by Western analysis in control and TRP-ML1 siRNA-treated cells. In both instances, I only

found the 55 kDa form of LAL (Fig. A1.3B). However, upon quantification of this band, I did observe that levels of this LAL form were significantly reduced (50% of control) in TRP-ML1 siRNA-treated cells, suggesting that LAL levels may be affected by loss of TRP-ML1 (Fig. A1.3C). Taken together, these studies suggest that both the overall levels and processing of LAL may be negatively affected in TRP-ML1-deficient cells. A summary of my protein profiling studies in TRP-ML1-deficient cells is found in Table A.1.

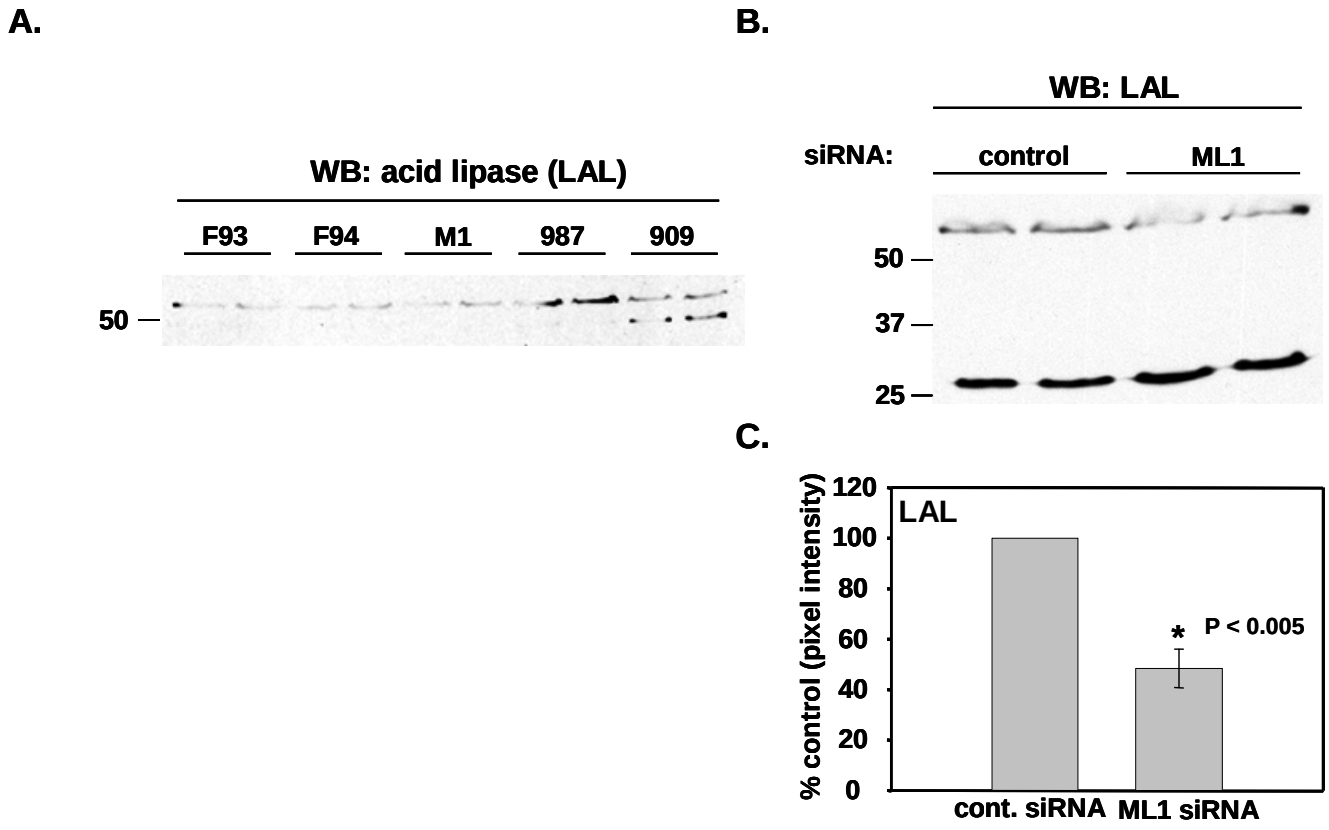

Figure A.3 Examination of lysosomal acid lipase (LAL) levels in control and ML1-deficient cells. (A and B) Representative Western blot of LAL in fibroblast cell lines (A) and in siRNA-treated HeLa cells (B). Full length LAL is 55 kDa. (C) Quantitation of Western analysis in siRNA treated cells using Quantity One software. These data are presented as % of levels (pixel intensity) obtained in control cells. This graph represents 3 independent experiments. Statistical significance was assessed by using the Student's t-test.

Table A.1 Summary table of protein profiling in TRP-ML1-deficient cells.

Protein examined / Cell Type	LAMP-1	Cathepsin B	LAL
Control Fibroblasts (WG987)	- 150 kDa band	- 30 kDa and 25 kDa bands	- 55 kDa band
MLIV Fibroblasts (WG909)	- 150 kDa band - levels increased by 30% compared to WG987	- 30 kDa and 25 kDa bands - no change in levels of 30 kDa form - decrease in levels of 25 kDa band	- 55 kDa and 50 kDa bands
Control siRNA	- 150 kDa band	- 30 kDa and 25 kDa bands	- 50 kDa band
TRP-ML1 siRNA	- 150 kDa band - levels increased by 37% compared to control	- 30 kDa and 25 kDa bands -Increase in levels of 30 kDa form - decrease in levels of 25 kDa form	-50 kDa band -Levels of 50 kDa band decreased by 50%

A.2.4 Localization of a lysosomally targeted version of the influenza A M2 protein

Recent work suggests that TRP-ML1 may function to regulate lysosomal pH by preventing the over-acidification of the lysosome via a proton-leak mechanism (231). Data presented in Chapter 3 suggests that lysosomal pH is more acidic compared to control cells (169). Therefore, I wanted to examine whether expression of lysosomally targeted version of a known H^+-leak channel is able to reverse any of the defects found in TRP-ML1-deficient cells.

The influenza A M2 protein is an acid-activated, H^+-permeable channel (195, 221). The M2 protein is a 97 amino acid type III integral membrane protein that contains 23 N-terminal extracellular amino acids, a highly conserved 19 amino acid transmembrane segment, and a 54 amino acid C-terminal cytosolic tail (134, 135). M2 has been demonstrated to function both at the cell surface and the TGN, and has H^+-permeability that is inhibited by the antiviral drug amantadine (261). M2 channel activity is regulated by changes in pH. Specifically, M2 is activated at the low pH found within the lumenal compartments of endosomes and the TGN (135). Previous work has employed M2 channel to selectively alter the pH of a subset of acidified organelles and examine various steps in apical protein transport in polarized epithelial cells (93-96).

My goal in these studies was to successfully generate a lysosomally-targeted version of M2. My approach was to incorporate the lysosomal targeting information of LAMP-1 and the HA epitope tag into the M2 C-terminal (cytoplasmic) tail. I then used immunofluorescence to examine the intracellular distribution of HA-$M2_{LAMP1}$ and compare it to that of the endogenous lysosomal marker LAMP-1. The results of these studies are shown in Figure A1.4. The distribution of HA-$M2_{LAMP1}$ (green) was found in

numerous punctuate cytoplasmic structures that frequently overlapped with LAMP-1-positive vesicles (red). These results suggest that a significant portion of HA-$M2_{LAMP1}$ reaches the lysosomal compartment. Future studies will be aimed at determining whether expression of this construct in TRP-ML1-deficient cells is able to reduce the presence of lipid inclusions and/or rescue observed defects in lysosomal pH.

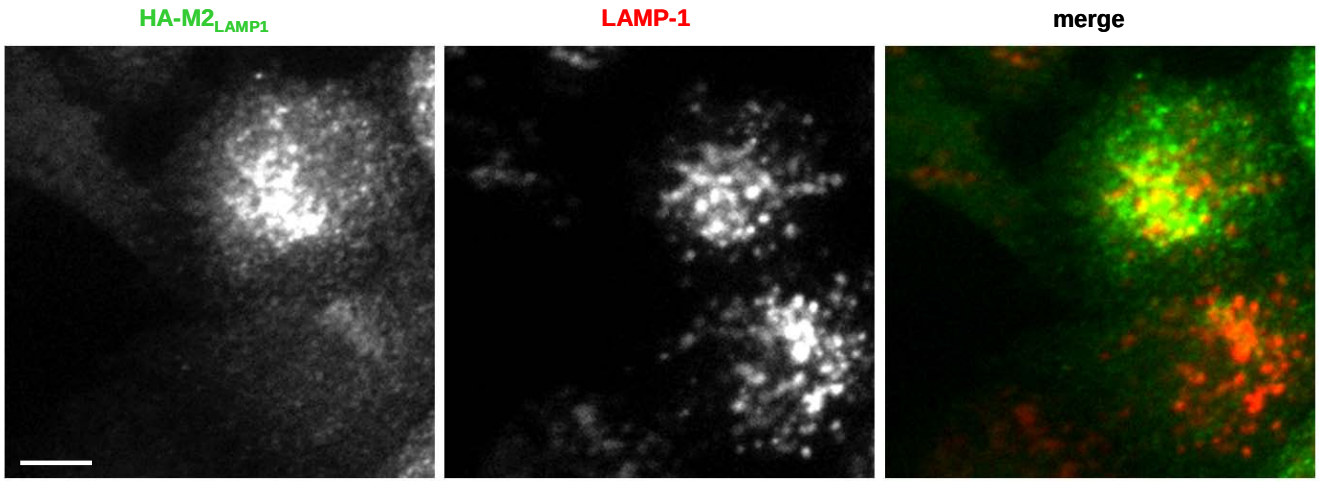

Figure A.4 Subcellular localization of HA-M2$_{LAMP1}$.

HeLa cells were transiently transfected with a cDNA encoding HA-M2$_{LAMP1}$. The following day cells were processed for immunofluorescence to detect the HA epitope (M2) and the lysosomal marker protein LAMP-1. Scale bar; 10 µm.

BIBLIOGRAPHY

1. **Altarescu, G., M. Sun, D. F. Moore, J. A. Smith, E. A. Wiggs, B. I. Solomon, N. J. Patronas, K. P. Frei, S. Gupta, C. R. Kaneski, O. W. Quarrell, S. A. Slaugenhaupt, E. Goldin, and R. Schiffmann.** 2002. The neurogenetics of mucolipidosis type IV. Neurology **59:**306-13.
2. **Ameis, D., M. Merkel, C. Eckerskorn, and H. Greten.** 1994. Purification, characterization and molecular cloning of human hepatic lysosomal acid lipase. Eur J Biochem **219:**905-14.
3. **Amir, N., J. Zlotogora, and G. Bach.** 1987. Mucolipidosis type IV: clinical spectrum and natural history. Pediatrics **79:**953-9.
4. **Antonin, W., C. Holroyd, D. Fasshauer, S. Pabst, G. F. Von Mollard, and R. Jahn.** 2000. A SNARE complex mediating fusion of late endosomes defines conserved properties of SNARE structure and function. Embo J **19:**6453-64.
5. **Bach, G.** 2001. Mucolipidosis type IV. Mol Genet Metab **73:**197-203.
6. **Bach, G.** 2005. Mucolipin 1: endocytosis and cation channel--a review. Pflugers Arch **451:**313-7.
7. **Bach, G., C. S. Chen, and R. E. Pagano.** 1999. Elevated lysosomal pH in Mucolipidosis type IV cells. Clin Chim Acta **280:**173-9.
8. **Bach, G., M. Zeigler, T. Schaap, and G. Kohn.** 1979. Mucolipidosis type IV: ganglioside sialidase deficiency. Biochem Biophys Res Commun **90:**1341-7.
9. **Bagshaw, R. D., D. J. Mahuran, and J. W. Callahan.** 2005. Lysosomal membrane proteomics and biogenesis of lysosomes. Mol Neurobiol **32:**27-41.
10. **Bagshaw, R. D., D. J. Mahuran, and J. W. Callahan.** 2005. A proteomic analysis of lysosomal integral membrane proteins reveals the diverse composition of the organelle. Mol Cell Proteomics **4:**133-43.
11. **Barbero, P., L. Bittova, and S. R. Pfeffer.** 2002. Visualization of Rab9-mediated vesicle transport from endosomes to the trans-Golgi in living cells. J Cell Biol **156:**511-8.
12. **Bargal, R., N. Avidan, E. Ben-Asher, Z. Olender, M. Zeigler, A. Frumkin, A. Raas-Rothschild, G. Glusman, D. Lancet, and G. Bach.** 2000. Identification of the gene causing mucolipidosis type IV. Nat Genet **26:**118-23.
13. **Bargal, R., N. Avidan, T. Olender, E. Ben Asher, M. Zeigler, A. Raas-Rothschild, A. Frumkin, O. Ben-Yoseph, Y. Friedlender, D. Lancet, and G. Bach.** 2001. Mucolipidosis type IV: novel MCOLN1 mutations in Jewish and non-

Jewish patients and the frequency of the disease in the Ashkenazi Jewish population. Hum Mutat **17:**397-402.
14. **Bargal, R., and G. Bach.** 1997. Mucolipidosis type IV: abnormal transport of lipids to lysosomes. J Inherit Metab Dis **20:**625-32.
15. **Bargal, R., and G. Bach.** 1989. Phosphatidylcholine storage in mucolipidosis IV. Clin Chim Acta **181:**167-74.
16. **Bargal, R., and G. Bach.** 1988. Phospholipids accumulation in mucolipidosis IV cultured fibroblasts. J Inherit Metab Dis **11:**144-50.
17. **Bargal, R., H. H. Goebel, E. Latta, and G. Bach.** 2002. Mucolipidosis IV: novel mutation and diverse ultrastructural spectrum in the skin. Neuropediatrics **33:**199-202.
18. **Barriere, H., C. Nemes, D. Lechardeur, M. Khan-Mohammad, K. Fruh, and G. L. Lukacs.** 2006. Molecular basis of oligoubiquitin-dependent internalization of membrane proteins in Mammalian cells. Traffic **7:**282-97.
19. **Bassi, M. T., M. Manzoni, E. Monti, M. T. Pizzo, A. Ballabio, and G. Borsani.** 2000. Cloning of the gene encoding a novel integral membrane protein, mucolipidin-and identification of the two major founder mutations causing mucolipidosis type IV. Am J Hum Genet **67:**1110-20.
20. **Bayer, N., D. Schober, E. Prchla, R. F. Murphy, D. Blaas, and R. Fuchs.** 1998. Effect of bafilomycin A1 and nocodazole on endocytic transport in HeLa cells: implications for viral uncoating and infection. J Virol **72:**9645-55.
21. **Berger, A. C., G. Salazar, M. L. Styers, K. A. Newell-Litwa, E. Werner, R. A. Maue, A. H. Corbett, and V. Faundez.** 2007. The subcellular localization of the Niemann-Pick Type C proteins depends on the adaptor complex AP-3. J Cell Sci **120:**3640-52.
22. **Bernacchi, S., G. Mueller, J. Langowski, and W. Waldeck.** 2004. Characterization of simian virus 40 on its infectious entry pathway in cells using fluorescence correlation spectroscopy. Biochem Soc Trans **32:**746-9.
23. **Bonifacino, J. S., and E. C. Dell'Angelica.** 1999. Molecular bases for the recognition of tyrosine-based sorting signals. J Cell Biol **145:**923-6.
24. **Bonifacino, J. S., and B. S. Glick.** 2004. The mechanisms of vesicle budding and fusion. Cell **116:**153-66.
25. **Bonifacino, J. S., and J. Lippincott-Schwartz.** 2003. Coat proteins: shaping membrane transport. Nat Rev Mol Cell Biol **4:**409-14.
26. **Bonifacino, J. S., and R. Rojas.** 2006. Retrograde transport from endosomes to the trans-Golgi network. Nat Rev Mol Cell Biol **7:**568-79.
27. **Bonifacino, J. S., and L. M. Traub.** 2003. Signals for sorting of transmembrane proteins to endosomes and lysosomes. Annu Rev Biochem **72:**395-447.
28. **Bonifacino, J. S., and A. M. Weissman.** 1998. Ubiquitin and the control of protein fate in the secretory and endocytic pathways. Annu Rev Cell Dev Biol **14:**19-57.
29. **Bozzato, A., S. Barlati, and G. Borsani.** 2008. Gene expression profiling of mucolipidosis type IV fibroblasts reveals deregulation of genes with relevant functions in lysosome physiology. Biochim Biophys Acta **1782:**250-8.

30. **Bright, N. A., M. J. Gratian, and J. P. Luzio.** 2005. Endocytic delivery to lysosomes mediated by concurrent fusion and kissing events in living cells. Curr Biol **15:**360-5.
31. **Bright, N. A., B. J. Reaves, B. M. Mullock, and J. P. Luzio.** 1997. Dense core lysosomes can fuse with late endosomes and are re-formed from the resultant hybrid organelles. J Cell Sci **110 (Pt 17):**2027-40.
32. **Brodsky, F. M., C. Y. Chen, C. Knuehl, M. C. Towler, and D. E. Wakeham.** 2001. Biological basket weaving: formation and function of clathrin-coated vesicles. Annu Rev Cell Dev Biol **17:**517-68.
33. **Brown, D. A., and E. London.** 2000. Structure and function of sphingolipid- and cholesterol-rich membrane rafts. J Biol Chem **275:**17221-4.
34. **Brown, M. S., S. E. Dana, and J. L. Goldstein.** 1975. Receptor-dependent hydrolysis of cholesteryl esters contained in plasma low density lipoprotein. Proc Natl Acad Sci U S A **72:**2925-9.
35. **Brown, M. S., and J. L. Goldstein.** 1979. Receptor-mediated endocytosis: insights from the lipoprotein receptor system. Proc Natl Acad Sci U S A **76:**3330-7.
36. **Brown, M. S., and J. L. Goldstein.** 1986. A receptor-mediated pathway for cholesterol homeostasis. Science **232:**34-47.
37. **Brown, R. E.** 1998. Sphingolipid organization in biomembranes: what physical studies of model membranes reveal. J Cell Sci **111 (Pt 1):**1-9.
38. **Bucci, C., P. Thomsen, P. Nicoziani, J. McCarthy, and B. van Deurs.** 2000. Rab7: a key to lysosome biogenesis. Mol Biol Cell **11:**467-80.
39. **Buchholz, T., G. Molitor, K. E. Lukong, M. Praun, O. Genzel-Boroviczeny, M. Freund, A. V. Pshezhetsky, and A. Schulze.** 2001. Clinical presentation of congenital sialidosis in a patient with a neuraminidase gene frameshift mutation. Eur J Pediatr **160:**26-30.
40. **Cantiello, H. F., N. Montalbetti, W. H. Goldmann, M. K. Raychowdhury, S. Gonzalez-Perrett, G. A. Timpanaro, and B. Chasan.** 2005. Cation channel activity of mucolipin-1: the effect of calcium. Pflugers Arch **451:**304-12.
41. **Caplan, S., L. M. Hartnell, R. C. Aguilar, N. Naslavsky, and J. S. Bonifacino.** 2001. Human Vam6p promotes lysosome clustering and fusion in vivo. J Cell Biol **154:**109-22.
42. **Casteels, I., D. S. Taylor, B. D. Lake, D. J. Spalton, and G. Bach.** 1992. Mucolipidosis type IV. Presentation of a mild variant. Ophthalmic Paediatr Genet **13:**205-10.
43. **Chapuy, B., R. Tikkanen, C. Muhlhausen, D. Wenzel, K. von Figura, and S. Honing.** 2008. AP-1 and AP-3 Mediate Sorting of Melanosomal and Lysosomal Membrane Proteins into Distinct Post-Golgi Trafficking Pathways. Traffic.
44. **Chen, C. S., G. Bach, and R. E. Pagano.** 1998. Abnormal transport along the lysosomal pathway in mucolipidosis, type IV disease. Proc Natl Acad Sci U S A **95:**6373-8.
45. **Chen, H. J., J. Yuan, and P. Lobel.** 1997. Systematic mutational analysis of the cation-independent mannose 6-phosphate/insulin-like growth factor II receptor cytoplasmic domain. An acidic cluster containing a key aspartate is important for function in lysosomal enzyme sorting. J Biol Chem **272:**7003-12.

46. **Cheng, Z. J., R. D. Singh, D. L. Marks, and R. E. Pagano.** 2006. Membrane microdomains, caveolae, and caveolar endocytosis of sphingolipids. Mol Membr Biol **23:**101-10.
47. **Chiang, H. L., S. R. Terlecky, C. P. Plant, and J. F. Dice.** 1989. A role for a 70-kilodalton heat shock protein in lysosomal degradation of intracellular proteins. Science **246:**382-5.
48. **Chitayat, D., C. M. Meunier, K. A. Hodgkinson, K. Silver, M. Flanders, I. J. Anderson, J. M. Little, D. A. Whiteman, and S. Carpenter.** 1991. Mucolipidosis type IV: clinical manifestations and natural history. Am J Med Genet **41:**313-8.
49. **Christensen, K. A., J. T. Myers, and J. A. Swanson.** 2002. pH-dependent regulation of lysosomal calcium in macrophages. J Cell Sci **115:**599-607.
50. **Ciechanover, A., A. L. Schwartz, A. Dautry-Varsat, and H. F. Lodish.** 1983. Kinetics of internalization and recycling of transferrin and the transferrin receptor in a human hepatoma cell line. Effect of lysosomotropic agents. J Biol Chem **258:**9681-9.
51. **Clapham, D. E., L. W. Runnels, and C. Strubing.** 2001. The TRP ion channel family. Nat Rev Neurosci **2:**387-96.
52. **Conner, S. D., and S. L. Schmid.** 2003. Differential requirements for AP-2 in clathrin-mediated endocytosis. J Cell Biol **162:**773-9.
53. **Conner, S. D., and S. L. Schmid.** 2003. Regulated portals of entry into the cell. Nature **422:**37-44.
54. **Cuervo, A. M., and J. F. Dice.** 1996. A receptor for the selective uptake and degradation of proteins by lysosomes. Science **273:**501-3.
55. **Dahms, N. M., and S. Kornfeld.** 1989. The cation-dependent mannose 6-phosphate receptor. Structural requirements for mannose 6-phosphate binding and oligomerization. J Biol Chem **264:**11458-67.
56. **Dahms, N. M., P. Lobel, and S. Kornfeld.** 1989. Mannose 6-phosphate receptors and lysosomal enzyme targeting. J Biol Chem **264:**12115-8.
57. **Danon, M. J., S. J. Oh, S. DiMauro, J. R. Manaligod, A. Eastwood, S. Naidu, and L. H. Schliselfeld.** 1981. Lysosomal glycogen storage disease with normal acid maltase. Neurology **31:**51-7.
58. **Dautry-Varsat, A., A. Ciechanover, and H. F. Lodish.** 1983. pH and the recycling of transferrin during receptor-mediated endocytosis. Proc Natl Acad Sci U S A **80:**2258-62.
59. **De Duve, C., B. C. Pressman, R. Gianetto, R. Wattiaux, and F. Appelmans.** 1955. Tissue fractionation studies. 6. Intracellular distribution patterns of enzymes in rat-liver tissue. Biochem J **60:**604-17.
60. **Degroote, S., J. Wolthoorn, and G. van Meer.** 2004. The cell biology of glycosphingolipids. Semin Cell Dev Biol **15:**375-87.
61. **Dell'Angelica, E. C., V. Shotelersuk, R. C. Aguilar, W. A. Gahl, and J. S. Bonifacino.** 1999. Altered trafficking of lysosomal proteins in Hermansky-Pudlak syndrome due to mutations in the beta 3A subunit of the AP-3 adaptor. Mol Cell **3:**11-21.
62. **Di, A., M. E. Brown, L. V. Deriy, C. Li, F. L. Szeto, Y. Chen, P. Huang, J. Tong, A. P. Naren, V. Bindokas, H. C. Palfrey, and D. J. Nelson.** 2006. CFTR

regulates phagosome acidification in macrophages and alters bactericidal activity. Nat Cell Biol **8:**933-44.
63. **Di Fiore, P. P., and P. De Camilli.** 2001. Endocytosis and signaling. an inseparable partnership. Cell **106:**1-4.
64. **Di Palma, F., I. A. Belyantseva, H. J. Kim, T. F. Vogt, B. Kachar, and K. Noben-Trauth.** 2002. Mutations in Mcoln3 associated with deafness and pigmentation defects in varitint-waddler (Va) mice. Proc Natl Acad Sci U S A **99:**14994-9.
65. **Diaz, E., and S. R. Pfeffer.** 1998. TIP47: a cargo selection device for mannose 6-phosphate receptor trafficking. Cell **93:**433-43.
66. **Dice, J. F.** 1990. Peptide sequences that target cytosolic proteins for lysosomal proteolysis. Trends Biochem Sci **15:**305-9.
67. **Du, H., and G. A. Grabowski.** 2004. Lysosomal acid lipase and atherosclerosis. Curr Opin Lipidol **15:**539-44.
68. **Eskelinen, E. L., Y. Tanaka, and P. Saftig.** 2003. At the acidic edge: emerging functions for lysosomal membrane proteins. Trends Cell Biol **13:**137-45.
69. **Fares, H., and I. Greenwald.** 2001. Genetic analysis of endocytosis in Caenorhabditis elegans: coelomocyte uptake defective mutants. Genetics **159:**133-45.
70. **Fares, H., and I. Greenwald.** 2001. Regulation of endocytosis by CUP-5, the Caenorhabditis elegans mucolipin-1 homolog. Nat Genet **28:**64-8.
71. **Faust, P. L., D. A. Wall, E. Perara, V. R. Lingappa, and S. Kornfeld.** 1987. Expression of human cathepsin D in Xenopus oocytes: phosphorylation and intracellular targeting. J Cell Biol **105:**1937-45.
72. **Fidzianska, A., E. Walczak, and M. Walski.** 2007. Abnormal chaperone-mediated autophagy (CMA) in cardiomyocytes of a boy with Danon disease. Folia Neuropathol **45:**133-9.
73. **Folkerth, R. D., J. Alroy, I. Lomakina, E. Skutelsky, S. S. Raghavan, and E. H. Kolodny.** 1995. Mucolipidosis IV: morphology and histochemistry of an autopsy case. J Neuropathol Exp Neurol **54:**154-64.
74. **Futai, M., T. Oka, G. Sun-Wada, Y. Moriyama, H. Kanazawa, and Y. Wada.** 2000. Luminal acidification of diverse organelles by V-ATPase in animal cells. J Exp Biol **203:**107-16.
75. **Futerman, A. H., and G. van Meer.** 2004. The cell biology of lysosomal storage disorders. Nat Rev Mol Cell Biol **5:**554-65.
76. **Gent, J., and I. Braakman.** 2004. Low-density lipoprotein receptor structure and folding. Cell Mol Life Sci **61:**2461-70.
77. **Geuze, H. J., W. Stoorvogel, G. J. Strous, J. W. Slot, J. E. Bleekemolen, and I. Mellman.** 1988. Sorting of mannose 6-phosphate receptors and lysosomal membrane proteins in endocytic vesicles. J Cell Biol **107:**2491-501.
78. **Ghosh, P., J. Griffith, H. J. Geuze, and S. Kornfeld.** 2003. Mammalian GGAs act together to sort mannose 6-phosphate receptors. J Cell Biol **163:**755-66.
79. **Girao, H., M. I. Geli, and F. Z. Idrissi.** 2008. Actin in the endocytic pathway: From yeast to mammals. FEBS Lett **582:**2112-2119.

80. **Goldin, E., E. J. Blanchette-Mackie, N. K. Dwyer, P. G. Pentchev, and R. O. Brady.** 1995. Cultured skin fibroblasts derived from patients with mucolipidosis 4 are auto-fluorescent. Pediatr Res **37:**687-92.
81. **Goldstein, J. L., S. E. Dana, J. R. Faust, A. L. Beaudet, and M. S. Brown.** 1975. Role of lysosomal acid lipase in the metabolism of plasma low density lipoprotein. Observations in cultured fibroblasts from a patient with cholesteryl ester storage disease. J Biol Chem **250:**8487-95.
82. **Gonzalez-Perrett, S., K. Kim, C. Ibarra, A. E. Damiano, E. Zotta, M. Batelli, P. C. Harris, I. L. Reisin, M. A. Arnaout, and H. F. Cantiello.** 2001. Polycystin-2, the protein mutated in autosomal dominant polycystic kidney disease (ADPKD), is a Ca2+-permeable nonselective cation channel. Proc Natl Acad Sci U S A **98:**1182-7.
83. **Gonzalez-Polo, R. A., P. Boya, A. L. Pauleau, A. Jalil, N. Larochette, S. Souquere, E. L. Eskelinen, G. Pierron, P. Saftig, and G. Kroemer.** 2005. The apoptosis/autophagy paradox: autophagic vacuolization before apoptotic death. J Cell Sci **118:**3091-102.
84. **Grabe, M., and G. Oster.** 2001. Regulation of organelle acidity. J Gen Physiol **117:**329-44.
85. **Graves, A. R., P. K. Curran, C. L. Smith, and J. A. Mindell.** 2008. The Cl(-)/H(+) antiporter ClC-7 is the primary chloride permeation pathway in lysosomes. Nature.
86. **Grimm, C., M. P. Cuajungco, A. F. van Aken, M. Schnee, S. Jors, C. J. Kros, A. J. Ricci, and S. Heller.** 2007. A helix-breaking mutation in TRPML3 leads to constitutive activity underlying deafness in the varitint-waddler mouse. Proc Natl Acad Sci U S A **104:**19583-8.
87. **Groener, J. E., W. Bax, and B. J. Poorthuis.** 1996. Metabolic fate of oleic acid derived from lysosomal degradation of cholesteryl oleate in human fibroblasts. J Lipid Res **37:**2271-9.
88. **Gruenberg, J., and F. R. Maxfield.** 1995. Membrane transport in the endocytic pathway. Curr Opin Cell Biol **7:**552-63.
89. **Gruenberg, J., and F. G. van der Goot.** 2006. Mechanisms of pathogen entry through the endosomal compartments. Nat Rev Mol Cell Biol **7:**495-504.
90. **Gundelfinger, E. D., M. M. Kessels, and B. Qualmann.** 2003. Temporal and spatial coordination of exocytosis and endocytosis. Nat Rev Mol Cell Biol **4:**127-39.
91. **Hardie, R. C., and B. Minke.** 1992. The trp gene is essential for a light-activated Ca2+ channel in Drosophila photoreceptors. Neuron **8:**643-51.
92. **Haucke, V.** 2005. Phosphoinositide regulation of clathrin-mediated endocytosis. Biochem Soc Trans **33:**1285-9.
93. **Henkel, J. R., G. Apodaca, Y. Altschuler, S. Hardy, and O. A. Weisz.** 1998. Selective perturbation of apical membrane traffic by expression of influenza M2, an acid-activated ion channel, in polarized madin-darby canine kidney cells. Mol Biol Cell **9:**2477-90.
94. **Henkel, J. R., G. A. Gibson, P. A. Poland, M. A. Ellis, R. P. Hughey, and O. A. Weisz.** 2000. Influenza M2 proton channel activity selectively inhibits trans-Golgi

network release of apical membrane and secreted proteins in polarized Madin-Darby canine kidney cells. J Cell Biol **148:**495-504.

95. **Henkel, J. R., J. L. Popovich, G. A. Gibson, S. C. Watkins, and O. A. Weisz.** 1999. Selective perturbation of early endosome and/or trans-Golgi network pH but not lysosome pH by dose-dependent expression of influenza M2 protein. J Biol Chem **274:**9854-60.
96. **Henkel, J. R., and O. A. Weisz.** 1998. Influenza virus M2 protein slows traffic along the secretory pathway. pH perturbation of acidified compartments affects early Golgi transport steps. J Biol Chem **273:**6518-24.
97. **Hill, E., O. Olusanya, J. van der Kaay, C. P. Downes, P. D. Andrews, J. R. Swedlow, and E. Smythe.** 2001. Regulation of clathrin-coated vesicle formation. Biochem Soc Trans **29:**375-7.
98. **Hill, E., J. van Der Kaay, C. P. Downes, and E. Smythe.** 2001. The role of dynamin and its binding partners in coated pit invagination and scission. J Cell Biol **152:**309-23.
99. **Hiraiwa, M.** 1999. Cathepsin A/protective protein: an unusual lysosomal multifunctional protein. Cell Mol Life Sci **56:**894-907.
100. **Holopainen, J. M., J. Saarikoski, P. K. Kinnunen, and I. Jarvela.** 2001. Elevated lysosomal pH in neuronal ceroid lipofuscinoses (NCLs). Eur J Biochem **268:**5851-6.
101. **Hong, W.** 1998. Protein transport from the endoplasmic reticulum to the Golgi apparatus. J Cell Sci **111 (Pt 19):**2831-9.
102. **Huang, C. L.** 2004. The transient receptor potential superfamily of ion channels. J Am Soc Nephrol **15:**1690-9.
103. **Ikonen, E.** 2006. Mechanisms for cellular cholesterol transport: defects and human disease. Physiol Rev **86:**1237-61.
104. **Jager, S., C. Bucci, I. Tanida, T. Ueno, E. Kominami, P. Saftig, and E. L. Eskelinen.** 2004. Role for Rab7 in maturation of late autophagic vacuoles. J Cell Sci **117:**4837-48.
105. **Jansen, S. M., J. E. Groener, W. Bax, and B. J. Poorthuis.** 2001. Delayed lysosomal metabolism of lipids in mucolipidosis type IV fibroblasts after LDL-receptor-mediated endocytosis. J Inherit Metab Dis **24:**577-86.
106. **Janvier, K., and J. S. Bonifacino.** 2005. Role of the endocytic machinery in the sorting of lysosome-associated membrane proteins. Mol Biol Cell **16:**4231-42.
107. **Jarvela, I., M. Sainio, T. Rantamaki, V. M. Olkkonen, O. Carpen, L. Peltonen, and A. Jalanko.** 1998. Biosynthesis and intracellular targeting of the CLN3 protein defective in Batten disease. Hum Mol Genet **7:**85-90.
108. **Jennings, J. J., Jr., J. H. Zhu, Y. Rbaibi, X. Luo, C. T. Chu, and K. Kiselyov.** 2006. Mitochondrial aberrations in mucolipidosis Type IV. J Biol Chem **281:**39041-50.
109. **Jentsch, T. J.** 2007. Chloride and the endosomal-lysosomal pathway: emerging roles of CLC chloride transporters. J Physiol **578:**633-40.
110. **Jentsch, T. J., I. Neagoe, and O. Scheel.** 2005. CLC chloride channels and transporters. Curr Opin Neurobiol **15:**319-25.

111. **Jentsch, T. J., M. Poet, J. C. Fuhrmann, and A. A. Zdebik.** 2005. Physiological functions of CLC Cl- channels gleaned from human genetic disease and mouse models. Annu Rev Physiol **67:**779-807.
112. **Jeon, H., and S. C. Blacklow.** 2005. Structure and physiologic function of the low-density lipoprotein receptor. Annu Rev Biochem **74:**535-62.
113. **Jeyakumar, M., R. A. Dwek, T. D. Butters, and F. M. Platt.** 2005. Storage solutions: treating lysosomal disorders of the brain. Nat Rev Neurosci **6:**713-25.
114. **Journet, A., A. Chapel, S. Kieffer, F. Roux, and J. Garin.** 2002. Proteomic analysis of human lysosomes: application to monocytic and breast cancer cells. Proteomics **2:**1026-40.
115. **Kalatzis, V., and C. Antignac.** 2003. New aspects of the pathogenesis of cystinosis. Pediatr Nephrol **18:**207-15.
116. **Karacsonyi, C., A. S. Miguel, and R. Puertollano.** 2007. Mucolipin-2 localizes to the Arf6-associated pathway and regulates recycling of GPI-APs. Traffic **8:**1404-14.
117. **Kasper, D., R. Planells-Cases, J. C. Fuhrmann, O. Scheel, O. Zeitz, K. Ruether, A. Schmitt, M. Poet, R. Steinfeld, M. Schweizer, U. Kornak, and T. J. Jentsch.** 2005. Loss of the chloride channel ClC-7 leads to lysosomal storage disease and neurodegeneration. Embo J **24:**1079-91.
118. **Kaushik, S., and A. M. Cuervo.** 2008. Chaperone-mediated autophagy. Methods Mol Biol **445:**227-44.
119. **Kaushik, S., A. C. Massey, and A. M. Cuervo.** 2006. Lysosome membrane lipid microdomains: novel regulators of chaperone-mediated autophagy. Embo J **25:**3921-33.
120. **Kida, E., W. Kaczmarski, A. A. Golabek, A. Kaczmarski, M. Michalewski, and K. E. Wisniewski.** 1999. Analysis of intracellular distribution and trafficking of the CLN3 protein in fusion with the green fluorescent protein in vitro. Mol Genet Metab **66:**265-71.
121. **Kiselyov, K., J. Chen, Y. Rbaibi, D. Oberdick, S. Tjon-Kon-Sang, N. Shcheynikov, S. Muallem, and A. Soyombo.** 2005. TRP-ML1 is a lysosomal monovalent cation channel that undergoes proteolytic cleavage. J Biol Chem **280:**43218-23.
122. **Kiselyov, K., J. J. Jennigs, Jr., Y. Rbaibi, and C. T. Chu.** 2007. Autophagy, mitochondria and cell death in lysosomal storage diseases. Autophagy **3:**259-62.
123. **Kiselyov, K., and S. Muallem.** 2008. Mitochondrial Ca(2+) homeostasis in lysosomal storage diseases. Cell Calcium **44:**103-11.
124. **Kiselyov, K., A. Soyombo, and S. Muallem.** 2007. TRPpathies. J Physiol **578:**641-53.
125. **Klausner, R. D., J. Van Renswoude, G. Ashwell, C. Kempf, A. N. Schechter, A. Dean, and K. R. Bridges.** 1983. Receptor-mediated endocytosis of transferrin in K562 cells. J Biol Chem **258:**4715-24.
126. **Kopitz, J., C. Gerhard, P. Hofler, and M. Cantz.** 1994. [14C]Methylamine accumulation in cultured human skin fibroblasts--a biochemical test for lysosomal storage and lysosomal diseases. Clin Chim Acta **227:**121-33.

127. **Kornak, U., D. Kasper, M. R. Bosl, E. Kaiser, M. Schweizer, A. Schulz, W. Friedrich, G. Delling, and T. J. Jentsch.** 2001. Loss of the ClC-7 chloride channel leads to osteopetrosis in mice and man. Cell **104:**205-15.
128. **Kornfeld, S.** 1990. Lysosomal enzyme targeting. Biochem Soc Trans **18:**367-74.
129. **Kornfeld, S.** 1992. Structure and function of the mannose 6-phosphate/insulinlike growth factor II receptors. Annu Rev Biochem **61:**307-30.
130. **Kornfeld, S., and I. Mellman.** 1989. The biogenesis of lysosomes. Annu Rev Cell Biol **5:**483-525.
131. **Kudo, M., M. S. Brem, and W. M. Canfield.** 2006. Mucolipidosis II (I-cell disease) and mucolipidosis IIIA (classical pseudo-hurler polydystrophy) are caused by mutations in the GlcNAc-phosphotransferase alpha / beta -subunits precursor gene. Am J Hum Genet **78:**451-63.
132. **Kundu, M., and C. B. Thompson.** 2008. Autophagy: basic principles and relevance to disease. Annu Rev Pathol **3:**427-55.
133. **Kyttala, A., U. Lahtinen, T. Braulke, and S. L. Hofmann.** 2006. Functional biology of the neuronal ceroid lipofuscinoses (NCL) proteins. Biochim Biophys Acta **1762:**920-33.
134. **Lamb, R. A., C. J. Lai, and P. W. Choppin.** 1981. Sequences of mRNAs derived from genome RNA segment 7 of influenza virus: colinear and interrupted mRNAs code for overlapping proteins. Proc Natl Acad Sci U S A **78:**4170-4.
135. **Lamb, R. A., S. L. Zebedee, and C. D. Richardson.** 1985. Influenza virus M2 protein is an integral membrane protein expressed on the infected-cell surface. Cell **40:**627-33.
136. **LaPlante, J. M., J. Falardeau, M. Sun, M. Kanazirska, E. M. Brown, S. A. Slaugenhaupt, and P. M. Vassilev.** 2002. Identification and characterization of the single channel function of human mucolipin-1 implicated in mucolipidosis type IV, a disorder affecting the lysosomal pathway. FEBS Lett **532:**183-7.
137. **Laplante, J. M., M. Sun, J. Falardeau, D. Dai, E. M. Brown, S. A. Slaugenhaupt, and P. M. Vassilev.** 2006. Lysosomal exocytosis is impaired in mucolipidosis type IV. Mol Genet Metab **89:**339-348.
138. **LaPlante, J. M., C. P. Ye, S. J. Quinn, E. Goldin, E. M. Brown, S. A. Slaugenhaupt, and P. M. Vassilev.** 2004. Functional links between mucolipin-1 and Ca2+-dependent membrane trafficking in mucolipidosis IV. Biochem Biophys Res Commun **322:**1384-91.
139. **Laude, A. J., and I. A. Prior.** 2004. Plasma membrane microdomains: organization, function and trafficking. Mol Membr Biol **21:**193-205.
140. **Le Borgne, R., A. Alconada, U. Bauer, and B. Hoflack.** 1998. The mammalian AP-3 adaptor-like complex mediates the intracellular transport of lysosomal membrane glycoproteins. J Biol Chem **273:**29451-61.
141. **Le Borgne, R., G. Griffiths, and B. Hoflack.** 1996. Mannose 6-phosphate receptors and ADP-ribosylation factors cooperate for high affinity interaction of the AP-1 Golgi assembly proteins with membranes. J Biol Chem **271:**2162-70.
142. **Le Borgne, R., and B. Hoflack.** 1997. Mannose 6-phosphate receptors regulate the formation of clathrin-coated vesicles in the TGN. J Cell Biol **137:**335-45.
143. **Levine, B., and D. J. Klionsky.** 2004. Development by self-digestion: molecular mechanisms and biological functions of autophagy. Dev Cell **6:**463-77.

144. **Lieser, M., E. Harms, H. Kern, G. Bach, and M. Cantz.** 1989. Ganglioside GM3 sialidase activity in fibroblasts of normal individuals and of patients with sialidosis and mucolipidosis IV. Subcellular distribution and and some properties. Biochem J **260:**69-74.
145. **Lok, C. N., and T. T. Loh.** 1998. Regulation of transferrin function and expression: review and update. Biol Signals Recept **7:**157-78.
146. **Lombardi, D., T. Soldati, M. A. Riederer, Y. Goda, M. Zerial, and S. R. Pfeffer.** 1993. Rab9 functions in transport between late endosomes and the trans Golgi network. Embo J **12:**677-82.
147. **Lubensky, I. A., R. Schiffmann, E. Goldin, and M. Tsokos.** 1999. Lysosomal inclusions in gastric parietal cells in mucolipidosis type IV: a novel cause of achlorhydria and hypergastrinemia. Am J Surg Pathol **23:**1527-31.
148. **Lukong, K. E., K. Landry, M. A. Elsliger, Y. Chang, S. Lefrancois, C. R. Morales, and A. V. Pshezhetsky.** 2001. Mutations in sialidosis impair sialidase binding to the lysosomal multienzyme complex. J Biol Chem **276:**17286-90.
149. **Luzio, J. P., N. A. Bright, and P. R. Pryor.** 2007. The role of calcium and other ions in sorting and delivery in the late endocytic pathway. Biochem Soc Trans **35:**1088-91.
150. **Luzio, J. P., B. M. Mullock, P. R. Pryor, M. R. Lindsay, D. E. James, and R. C. Piper.** 2001. Relationship between endosomes and lysosomes. Biochem Soc Trans **29:**476-80.
151. **Luzio, J. P., V. Poupon, M. R. Lindsay, B. M. Mullock, R. C. Piper, and P. R. Pryor.** 2003. Membrane dynamics and the biogenesis of lysosomes. Mol Membr Biol **20:**141-54.
152. **Luzio, J. P., P. R. Pryor, and N. A. Bright.** 2007. Lysosomes: fusion and function. Nat Rev Mol Cell Biol **8:**622-32.
153. **Luzio, J. P., P. R. Pryor, S. R. Gray, M. J. Gratian, R. C. Piper, and N. A. Bright.** 2005. Membrane traffic to and from lysosomes. Biochem Soc Symp**:**77-86.
154. **Luzio, J. P., B. A. Rous, N. A. Bright, P. R. Pryor, B. M. Mullock, and R. C. Piper.** 2000. Lysosome-endosome fusion and lysosome biogenesis. J Cell Sci **113 (Pt 9):**1515-24.
155. **Machamer, C. E., R. Z. Florkiewicz, and J. K. Rose.** 1985. A single N-linked oligosaccharide at either of the two normal sites is sufficient for transport of vesicular stomatitis virus G protein to the cell surface. Mol Cell Biol **5:**3074-83.
156. **Manzoni, M., E. Monti, R. Bresciani, A. Bozzato, S. Barlati, M. T. Bassi, and G. Borsani.** 2004. Overexpression of wild-type and mutant mucolipin proteins in mammalian cells: effects on the late endocytic compartment organization. FEBS Lett **567:**219-24.
157. **Marks, D. L., and R. E. Pagano.** 2002. Endocytosis and sorting of glycosphingolipids in sphingolipid storage disease. Trends Cell Biol **12:**605-13.
158. **Martin, O. C., M. E. Comly, E. J. Blanchette-Mackie, P. G. Pentchev, and R. E. Pagano.** 1993. Cholesterol deprivation affects the fluorescence properties of a ceramide analog at the Golgi apparatus of living cells. Proc Natl Acad Sci U S A **90:**2661-5.

159. **Massey, A., R. Kiffin, and A. M. Cuervo.** 2004. Pathophysiology of chaperone-mediated autophagy. Int J Biochem Cell Biol **36:**2420-34.
160. **Maxfield, F. R., and T. E. McGraw.** 2004. Endocytic recycling. Nat Rev Mol Cell Biol **5:**121-32.
161. **Maxfield, F. R., and I. Tabas.** 2005. Role of cholesterol and lipid organization in disease. Nature **438:**612-21.
162. **Maxfield, F. R., and D. Wustner.** 2002. Intracellular cholesterol transport. J Clin Invest **110:**891-8.
163. **Medigeshi, G. R., and P. Schu.** 2003. Characterization of the in vitro retrograde transport of MPR46. Traffic **4:**802-11.
164. **Meikle, P. J., J. J. Hopwood, A. E. Clague, and W. F. Carey.** 1999. Prevalence of lysosomal storage disorders. Jama **281:**249-54.
165. **Mellman, I.** 1996. Endocytosis and molecular sorting. Annu Rev Cell Dev Biol **12:**575-625.
166. **Mellman, I.** 1992. The importance of being acid: the role of acidification in intracellular membrane traffic. J Exp Biol **172:**39-45.
167. **Mellman, I., and G. Warren.** 2000. The road taken: past and future foundations of membrane traffic. Cell **100:**99-112.
168. **Messner, D. J., G. Griffiths, and S. Kornfeld.** 1989. Isolation and characterization of membranes from bovine liver which are highly enriched in mannose 6-phosphate receptors. J Cell Biol **108:**2149-62.
169. **Miedel, M. T., Y. Rbaibi, C. J. Guerriero, G. Colletti, K. M. Weixel, O. A. Weisz, and K. Kiselyov.** 2008. Membrane traffic and turnover in TRP-ML1-deficient cells: a revised model for mucolipidosis type IV pathogenesis. J Exp Med.
170. **Miedel, M. T., K. M. Weixel, J. R. Bruns, L. M. Traub, and O. A. Weisz.** 2006. Posttranslational cleavage and adaptor protein complex-dependent trafficking of mucolipin-1. J Biol Chem **281:**12751-9.
171. **Mittnacht, A. J., C. Moung, and W. W. Lai.** 2007. Massive cardiac hypertrophy in a patient with Danon disease: an intraoperative transesophageal echocardiographic evaluation. Anesth Analg **105:**963-5.
172. **Montell, C.** 2005. The TRP superfamily of cation channels. Sci STKE **2005:**re3.
173. **Morgan, A. J., and A. Galione.** 2007. NAADP induces pH changes in the lumen of acidic Ca2+ stores. Biochem J **402:**301-10.
174. **Mort, J. S., and D. J. Buttle.** 1997. Cathepsin B. Int J Biochem Cell Biol **29:**715-20.
175. **Mukherjee, S., R. N. Ghosh, and F. R. Maxfield.** 1997. Endocytosis. Physiol Rev **77:**759-803.
176. **Mukherjee, S., and F. R. Maxfield.** 2004. Lipid and cholesterol trafficking in NPC. Biochim Biophys Acta **1685:**28-37.
177. **Mullins, C., and J. S. Bonifacino.** 2001. The molecular machinery for lysosome biogenesis. Bioessays **23:**333-43.
178. **Mullock, B. M., N. A. Bright, C. W. Fearon, S. R. Gray, and J. P. Luzio.** 1998. Fusion of lysosomes with late endosomes produces a hybrid organelle of intermediate density and is NSF dependent. J Cell Biol **140:**591-601.

179. **Mullock, B. M., J. H. Perez, T. Kuwana, S. R. Gray, and J. P. Luzio.** 1994. Lysosomes can fuse with a late endosomal compartment in a cell-free system from rat liver. J Cell Biol **126:**1173-82.
180. **Nabi, I. R., and P. U. Le.** 2003. Caveolae/raft-dependent endocytosis. J Cell Biol **161:**673-7.
181. **Nelson, N., N. Perzov, A. Cohen, K. Hagai, V. Padler, and H. Nelson.** 2000. The cellular biology of proton-motive force generation by V-ATPases. J Exp Biol **203:**89-95.
182. **Nichols, B.** 2003. Caveosomes and endocytosis of lipid rafts. J Cell Sci **116:**4707-14.
183. **Nilius, B., T. Voets, and J. Peters.** 2005. TRP channels in disease. Sci STKE **2005:**re8.
184. **Ohno, H., R. C. Aguilar, D. Yeh, D. Taura, T. Saito, and J. S. Bonifacino.** 1998. The medium subunits of adaptor complexes recognize distinct but overlapping sets of tyrosine-based sorting signals. J Biol Chem **273:**25915-21.
185. **Ohno, H., M. C. Fournier, G. Poy, and J. S. Bonifacino.** 1996. Structural determinants of interaction of tyrosine-based sorting signals with the adaptor medium chains. J Biol Chem **271:**29009-15.
186. **Ostrowska, H., K. Krukowska, J. Kalinowska, M. Orlowska, and I. Lengiewicz.** 2003. Lysosomal high molecular weight multienzyme complex. Cell Mol Biol Lett **8:**19-24.
187. **Padinjat, R., and S. Andrews.** 2004. TRP channels at a glance. J Cell Sci **117:**5707-9.
188. **Pagano, R. E.** 2003. Endocytic trafficking of glycosphingolipids in sphingolipid storage diseases. Philos Trans R Soc Lond B Biol Sci **358:**885-91.
189. **Pagano, R. E., V. Puri, M. Dominguez, and D. L. Marks.** 2000. Membrane traffic in sphingolipid storage diseases. Traffic **1:**807-15.
190. **Parton, R. G.** 2003. Caveolae--from ultrastructure to molecular mechanisms. Nat Rev Mol Cell Biol **4:**162-7.
191. **Parton, R. G., and A. A. Richards.** 2003. Lipid rafts and caveolae as portals for endocytosis: new insights and common mechanisms. Traffic **4:**724-38.
192. **Pedersen, S. F., G. Owsianik, and B. Nilius.** 2005. TRP channels: an overview. Cell Calcium **38:**233-52.
193. **Perrais, D., and C. J. Merrifield.** 2005. Dynamics of endocytic vesicle creation. Dev Cell **9:**581-92.
194. **Pillay, C. S., E. Elliott, and C. Dennison.** 2002. Endolysosomal proteolysis and its regulation. Biochem J **363:**417-29.
195. **Pinto, L. H., L. J. Holsinger, and R. A. Lamb.** 1992. Influenza virus M2 protein has ion channel activity. Cell **69:**517-28.
196. **Piper, R. C., and J. P. Luzio.** 2004. CUPpling calcium to lysosomal biogenesis. Trends Cell Biol **14:**471-3.
197. **Piwon, N., W. Gunther, M. Schwake, M. R. Bosl, and T. J. Jentsch.** 2000. ClC-5 Cl- -channel disruption impairs endocytosis in a mouse model for Dent's disease. Nature **408:**369-73.
198. **Poet, M., U. Kornak, M. Schweizer, A. A. Zdebik, O. Scheel, S. Hoelter, W. Wurst, A. Schmitt, J. C. Fuhrmann, R. Planells-Cases, S. E. Mole, C. A.**

Hubner, and T. J. Jentsch. 2006. Lysosomal storage disease upon disruption of the neuronal chloride transport protein ClC-6. Proc Natl Acad Sci U S A **103:**13854-9.
199. **Poupon, V., A. Stewart, S. R. Gray, R. C. Piper, and J. P. Luzio.** 2003. The role of mVps18p in clustering, fusion, and intracellular localization of late endocytic organelles. Mol Biol Cell **14:**4015-27.
200. **Pryor, P. R., B. M. Mullock, N. A. Bright, S. R. Gray, and J. P. Luzio.** 2000. The role of intraorganellar Ca(2+) in late endosome-lysosome heterotypic fusion and in the reformation of lysosomes from hybrid organelles. J Cell Biol **149:**1053-62.
201. **Pryor, P. R., B. M. Mullock, N. A. Bright, M. R. Lindsay, S. R. Gray, S. C. Richardson, A. Stewart, D. E. James, R. C. Piper, and J. P. Luzio.** 2004. Combinatorial SNARE complexes with VAMP7 or VAMP8 define different late endocytic fusion events. EMBO Rep **5:**590-5.
202. **Pryor, P. R., F. Reimann, F. M. Gribble, and J. P. Luzio.** 2006. Mucolipin-1 is a lysosomal membrane protein required for intracellular lactosylceramide traffic. Traffic **7:**1388-98.
203. **Puri, V., J. R. Jefferson, R. D. Singh, C. L. Wheatley, D. L. Marks, and R. E. Pagano.** 2003. Sphingolipid storage induces accumulation of intracellular cholesterol by stimulating SREBP-1 cleavage. J Biol Chem **278:**20961-70.
204. **Puri, V., R. Watanabe, M. Dominguez, X. Sun, C. L. Wheatley, D. L. Marks, and R. E. Pagano.** 1999. Cholesterol modulates membrane traffic along the endocytic pathway in sphingolipid-storage diseases. Nat Cell Biol **1:**386-8.
205. **Puri, V., R. Watanabe, R. D. Singh, M. Dominguez, J. C. Brown, C. L. Wheatley, D. L. Marks, and R. E. Pagano.** 2001. Clathrin-dependent and -independent internalization of plasma membrane sphingolipids initiates two Golgi targeting pathways. J Cell Biol **154:**535-47.
206. **Qian, F., and K. Noben-Trauth.** 2005. Cellular and molecular function of mucolipins (TRPML) and polycystin 2 (TRPP2). Pflugers Arch **451:**277-85.
207. **Raghavan, S., E. Leshinsky, and E. H. Kolodny.** 1999. G(M2)-ganglioside metabolism in situ in mucolipidosis IV fibroblasts. Neurochem Res **24:**475-9.
208. **Raychowdhury, M. K., S. Gonzalez-Perrett, N. Montalbetti, G. A. Timpanaro, B. Chasan, W. H. Goldmann, S. Stahl, A. Cooney, E. Goldin, and H. F. Cantiello.** 2004. Molecular pathophysiology of mucolipidosis type IV: pH dysregulation of the mucolipin-1 cation channel. Hum Mol Genet **13:**617-27.
209. **Reis, S., R. N. Sheffer, S. Merin, A. S. Luder, and G. Bach.** 1993. Mucolipidosis type IV: a mild form with late onset. Am J Med Genet **47:**392-4.
210. **Renlund, M., F. Tietze, and W. A. Gahl.** 1986. Defective sialic acid egress from isolated fibroblast lysosomes of patients with Salla disease. Science **232:**759-62.
211. **Riedel, K. G., J. Zwaan, K. R. Kenyon, E. H. Kolodny, L. Hanninen, and D. M. Albert.** 1985. Ocular abnormalities in mucolipidosis IV. Am J Ophthalmol **99:**125-36.
212. **Rouille, Y., W. Rohn, and B. Hoflack.** 2000. Targeting of lysosomal proteins. Semin Cell Dev Biol **11:**165-71.
213. **Sahagian, G. G., J. Distler, and G. W. Jourdian.** 1981. Characterization of a membrane-associated receptor from bovine liver that binds phosphomannosyl

residues of bovine testicular beta-galactosidase. Proc Natl Acad Sci U S A **78:**4289-93.
214. **Sandhoff, K., and T. Kolter.** 1997. Biochemistry of glycosphingolipid degradation. Clin Chim Acta **266:**51-61.
215. **Sandoval, I. V., and O. Bakke.** 1994. Targeting of membrane proteins to endosomes and lysosomes. Trends Cell Biol **4:**292-7.
216. **Schaheen, L., H. Dang, and H. Fares.** 2006. Basis of lethality in C. elegans lacking CUP-5, the Mucolipidosis Type IV orthologue. Dev Biol **293:**382-91.
217. **Scheel, O., A. A. Zdebik, S. Lourdel, and T. J. Jentsch.** 2005. Voltage-dependent electrogenic chloride/proton exchange by endosomal CLC proteins. Nature **436:**424-7.
218. **Schiffmann, R., N. K. Dwyer, I. A. Lubensky, M. Tsokos, V. E. Sutliff, J. S. Latimer, K. P. Frei, R. O. Brady, N. W. Barton, E. J. Blanchette-Mackie, and E. Goldin.** 1998. Constitutive achlorhydria in mucolipidosis type IV. Proc Natl Acad Sci U S A **95:**1207-12.
219. **Schroder, B., C. Wrocklage, C. Pan, R. Jager, B. Kosters, H. Schafer, H. P. Elsasser, M. Mann, and A. Hasilik.** 2007. Integral and associated lysosomal membrane proteins. Traffic **8:**1676-86.
220. **Settembre, C., A. Fraldi, L. Jahreiss, C. Spampanato, C. Venturi, D. Medina, R. de Pablo, C. Tacchetti, D. C. Rubinsztein, and A. Ballabio.** 2008. A block of autophagy in lysosomal storage disorders. Hum Mol Genet **17:**119-29.
221. **Shimbo, K., D. L. Brassard, R. A. Lamb, and L. H. Pinto.** 1996. Ion selectivity and activation of the M2 ion channel of influenza virus. Biophys J **70:**1335-46.
222. **Shintani, T., and D. J. Klionsky.** 2004. Autophagy in health and disease: a double-edged sword. Science **306:**990-5.
223. **Siegel, H., K. Frei, J. Greenfield, R. Schiffmann, and S. Sato.** 1998. Electroencephalographic findings in patients with mucolipidosis type IV. Electroencephalogr Clin Neurophysiol **106:**400-3.
224. **Sillence, D. J., and F. M. Platt.** 2003. Storage diseases: new insights into sphingolipid functions. Trends Cell Biol **13:**195-203.
225. **Sillence, D. J., V. Puri, D. L. Marks, T. D. Butters, R. A. Dwek, R. E. Pagano, and F. M. Platt.** 2002. Glucosylceramide modulates membrane traffic along the endocytic pathway. J Lipid Res **43:**1837-45.
226. **Simons, K., and J. Gruenberg.** 2000. Jamming the endosomal system: lipid rafts and lysosomal storage diseases. Trends Cell Biol **10:**459-62.
227. **Slaugenhaupt, S. A.** 2002. The molecular basis of mucolipidosis type IV. Curr Mol Med **2:**445-50.
228. **Slaugenhaupt, S. A., J. S. Acierno, Jr., L. A. Helbling, C. Bove, E. Goldin, G. Bach, R. Schiffmann, and J. F. Gusella.** 1999. Mapping of the mucolipidosis type IV gene to chromosome 19p and definition of founder haplotypes. Am J Hum Genet **65:**773-8.
229. **Sleat, D. E., and P. Lobel.** 1997. Ligand binding specificities of the two mannose 6-phosphate receptors. J Biol Chem **272:**731-8.
230. **Sonnichsen, B., S. De Renzis, E. Nielsen, J. Rietdorf, and M. Zerial.** 2000. Distinct membrane domains on endosomes in the recycling pathway visualized by multicolor imaging of Rab4, Rab5, and Rab11. J Cell Biol **149:**901-14.

231. **Soyombo, A. A., S. Tjon-Kon-Sang, Y. Rbaibi, E. Bashllari, J. Bisceglia, S. Muallem, and K. Kiselyov.** 2006. TRP-ML1 regulates lysosomal pH and acidic lysosomal lipid hydrolytic activity. J Biol Chem **281:**7294-301.
232. **Spranger, J. W., and H. R. Wiedemann.** 1970. The genetic mucolipidoses. Diagnosis and differential diagnosis. Humangenetik **9:**113-39.
233. **Stahl, P. D., and M. A. Barbieri.** 2002. Multivesicular bodies and multivesicular endosomes: the "ins and outs" of endosomal traffic. Sci STKE **2002:**PE32.
234. **Steel, K. P.** 2002. Varitint-waddler: a double whammy for hearing. Proc Natl Acad Sci U S A **99:**14613-5.
235. **Stinchcombe, J., G. Bossi, and G. M. Griffiths.** 2004. Linking albinism and immunity: the secrets of secretory lysosomes. Science **305:**55-9.
236. **Storrie, B., and M. Desjardins.** 1996. The biogenesis of lysosomes: is it a kiss and run, continuous fusion and fission process? Bioessays **18:**895-903.
237. **Strehle, E. M.** 2003. Sialic acid storage disease and related disorders. Genet Test **7:**113-21.
238. **Strous, G. J., P. van Kerkhof, R. Govers, A. Ciechanover, and A. L. Schwartz.** 1996. The ubiquitin conjugation system is required for ligand-induced endocytosis and degradation of the growth hormone receptor. Embo J **15:**3806-12.
239. **Sudhof, T. C.** 2004. The synaptic vesicle cycle. Annu Rev Neurosci **27:**509-47.
240. **Sun, M., E. Goldin, S. Stahl, J. L. Falardeau, J. C. Kennedy, J. S. Acierno, Jr., C. Bove, C. R. Kaneski, J. Nagle, M. C. Bromley, M. Colman, R. Schiffmann, and S. A. Slaugenhaupt.** 2000. Mucolipidosis type IV is caused by mutations in a gene encoding a novel transient receptor potential channel. Hum Mol Genet **9:**2471-8.
241. **Sun, W., Q. Yan, T. A. Vida, and A. J. Bean.** 2003. Hrs regulates early endosome fusion by inhibiting formation of an endosomal SNARE complex. J Cell Biol **162:**125-37.
242. **Tardy, C., N. Andrieu-Abadie, R. Salvayre, and T. Levade.** 2004. Lysosomal storage diseases: is impaired apoptosis a pathogenic mechanism? Neurochem Res **29:**871-80.
243. **Terpstra, A. H., R. J. Nicolosi, and P. N. Herbert.** 1989. In vitro incorporation of radiolabeled cholesteryl esters into high and low density lipoproteins. J Lipid Res **30:**1663-71.
244. **Tettamanti, G.** 2004. Ganglioside/glycosphingolipid turnover: new concepts. Glycoconj J **20:**301-17.
245. **Thompson, E. G., L. Schaheen, H. Dang, and H. Fares.** 2007. Lysosomal trafficking functions of mucolipin-1 in murine macrophages. BMC Cell Biol **8:**54.
246. **Traub, L. M.** 2005. Common principles in clathrin-mediated sorting at the Golgi and the plasma membrane. Biochim Biophys Acta **1744:**415-37.
247. **Traub, L. M., S. Kornfeld, and E. Ungewickell.** 1995. Different domains of the AP-1 adaptor complex are required for Golgi membrane binding and clathrin recruitment. J Biol Chem **270:**4933-42.
248. **Treusch, S., S. Knuth, S. A. Slaugenhaupt, E. Goldin, B. D. Grant, and H. Fares.** 2004. Caenorhabditis elegans functional orthologue of human protein h-

mucolipin-1 is required for lysosome biogenesis. Proc Natl Acad Sci U S A **101:**4483-8.
249. **Turk, V., B. Turk, and D. Turk.** 2001. Lysosomal cysteine proteases: facts and opportunities. Embo J **20:**4629-33.
250. **Ulloa, F., C. Franci, and F. X. Real.** 2000. GalNAc-alpha -O-benzyl inhibits sialylation of de Novo synthesized apical but not basolateral sialoglycoproteins and blocks lysosomal enzyme processing in a post-trans-Golgi network compartment. J Biol Chem **275:**18785-93.
251. **Ungewickell, E. J., and L. Hinrichsen.** 2007. Endocytosis: clathrin-mediated membrane budding. Curr Opin Cell Biol **19:**417-25.
252. **van der Goot, F. G., and J. Gruenberg.** 2006. Intra-endosomal membrane traffic. Trends Cell Biol **16:**514-21.
253. **van Weert, A. W., K. W. Dunn, H. J. Gueze, F. R. Maxfield, and W. Stoorvogel.** 1995. Transport from late endosomes to lysosomes, but not sorting of integral membrane proteins in endosomes, depends on the vacuolar proton pump. J Cell Biol **130:**821-34.
254. **Venkatachalam, K., T. Hofmann, and C. Montell.** 2006. Lysosomal localization of TRPML3 depends on TRPML2 and the mucolipidosis-associated protein TRPML1. J Biol Chem **281:**17517-27.
255. **Venkatachalam, K., and C. Montell.** 2007. TRP channels. Annu Rev Biochem **76:**387-417.
256. **Venugopal, B., M. F. Browning, C. Curcio-Morelli, A. Varro, N. Michaud, N. Nanthakumar, S. U. Walkley, J. Pickel, and S. A. Slaugenhaupt.** 2007. Neurologic, gastric, and opthalmologic pathologies in a murine model of mucolipidosis type IV. Am J Hum Genet **81:**1070-83.
257. **Vergarajauregui, S., P. S. Connelly, M. P. Daniels, and R. Puertollano.** 2008. Autophagic Dysfunction In Mucolipidosis Type Iv Patients. Hum Mol Genet.
258. **Vergarajauregui, S., R. Oberdick, K. Kiselyov, and R. Puertollano.** 2007. Mucolipin-1 channel activity is regulated by protein kinase A mediated phosphorylation. Biochem J.
259. **Vergarajauregui, S., and R. Puertollano.** 2006. Two di-leucine motifs regulate trafficking of mucolipin-1 to lysosomes. Traffic **7:**337-53.
260. **Vieitez, I., S. Teijeira, S. Miranda, B. San Millan, and C. Navarro.** 2008. Gene symbol: LAMP2. Disease: Glycogen storage disease 2b. Hum Genet **123:**113.
261. **Wang, C., K. Takeuchi, L. H. Pinto, and R. A. Lamb.** 1993. Ion channel activity of influenza A virus M2 protein: characterization of the amantadine block. J Virol **67:**5585-94.
262. **Wang, T., and C. Montell.** 2007. Phototransduction and retinal degeneration in Drosophila. Pflugers Arch **454:**821-47.
263. **Wang, W., and B. A. Malcolm.** 1999. Two-stage PCR protocol allowing introduction of multiple mutations, deletions and insertions using QuikChange Site-Directed Mutagenesis. Biotechniques **26:**680-2.
264. **Weisz, O. A.** 2003. Acidification and protein traffic. Int Rev Cytol **226:**259-319.
265. **Weisz, O. A.** 2003. Organelle acidification and disease. Traffic **4:**57-64.
266. **Xie, Z., and D. J. Klionsky.** 2007. Autophagosome formation: core machinery and adaptations. Nat Cell Biol **9:**1102-9.

267. **Xu, H., M. Delling, L. Li, X. Dong, and D. E. Clapham.** 2007. Activating mutation in a mucolipin transient receptor potential channel leads to melanocyte loss in varitint-waddler mice. Proc Natl Acad Sci U S A **104:**18321-6.
268. **Yan, Q., W. Sun, J. A. McNew, T. A. Vida, and A. J. Bean.** 2004. Ca2+ and N-ethylmaleimide-sensitive factor differentially regulate disassembly of SNARE complexes on early endosomes. J Biol Chem **279:**18270-6.
269. **Yang, W., C. Li, D. M. Ward, J. Kaplan, and S. L. Mansour.** 2000. Defective organellar membrane protein trafficking in Ap3b1-deficient cells. J Cell Sci **113 (Pt 22):**4077-86.
270. **Yang, Z., and M. Vatta.** 2007. Danon disease as a cause of autophagic vacuolar myopathy. Congenit Heart Dis **2:**404-9.
271. **Yoshikawa, M., S. Uchida, J. Ezaki, T. Rai, A. Hayama, K. Kobayashi, Y. Kida, M. Noda, M. Koike, Y. Uchiyama, F. Marumo, E. Kominami, and S. Sasaki.** 2002. CLC-3 deficiency leads to phenotypes similar to human neuronal ceroid lipofuscinosis. Genes Cells **7:**597-605.
272. **Zeevi, D. A., A. Frumkin, and G. Bach.** 2007. TRPML and lysosomal function. Biochim Biophys Acta **1772:**851-8.
273. **Zeigler, M., and G. Bach.** 1986. Internalization of exogenous gangliosides in cultured skin fibroblasts for the diagnosis of mucolipidosis IV. Clin Chim Acta **157:**183-9.
274. **Zerial, M., and H. McBride.** 2001. Rab proteins as membrane organizers. Nat Rev Mol Cell Biol **2:**107-17.
275. **Zhang, F., and P. L. Li.** 2007. Reconstitution and characterization of a nicotinic acid adenine dinucleotide phosphate (NAADP)-sensitive Ca2+ release channel from liver lysosomes of rats. J Biol Chem **282:**25259-69.
276. **Zhang, F., G. Zhang, A. Y. Zhang, M. J. Koeberl, E. Wallander, and P. L. Li.** 2006. Production of NAADP and its role in Ca2+ mobilization associated with lysosomes in coronary arterial myocytes. Am J Physiol Heart Circ Physiol **291:**H274-82.
277. **Zhu, Y., B. Doray, A. Poussu, V. P. Lehto, and S. Kornfeld.** 2001. Binding of GGA2 to the lysosomal enzyme sorting motif of the mannose 6-phosphate receptor. Science **292:**1716-8.
278. **Zschenker, O., D. Oezden, and D. Ameis.** 2004. Lysosomal acid lipase as a preproprotein. J Biochem **136:**65-72.